PACIFIC EARTHQUAKE ENGINEERING
RESEARCH CENTER

NGA-West2 Equations for Predicting Response Spectral Accelerations for Shallow Crustal Earthquakes

David M. Boore
US Geological Survey
Menlo Park, CA

Jonathan P. Stewart
Emel Seyhan
Department of Civil and Environmental Engineering
University of California, Los Angeles

Gail M. Atkinson
Western University
Ontario, Canada

PEER 2013/05
MAY 2013

NGA-West2 Equations for Predicting Response Spectral Accelerations for Shallow Crustal Earthquakes

David M. Boore
US Geological Survey
Menlo Park, California

Jonathan P. Stewart
Emel Seyhan
Department of Civil and Environmental Engineering
University of California, Los Angeles

Gail M. Atkinson
Western University
Ontario, Canada

PEER Report 2013/05
Pacific Earthquake Engineering Research Center
Headquarters, University of California, Berkeley

May 2013

ABSTRACT

We provide ground-motion prediction equations (GMPEs) for the computation of median peak ground motions and response spectra for shallow crustal earthquakes in active tectonic regions. The equations were developed as part of the NGA-West 2 project and are based on a composite data set [Ancheta et al. 2013] that includes global events from 1935 to 2011 spanning a wide magnitude range, plus a large number of small-to-moderate magnitude events from California principally from 1998 to 2011. This data set comprises more than 21,000 records, of which we use a subset of ~16000 records in our analysis. The equations follow a philosophy, functional form, and regression method that is similar to the Boore and Atkinson [2008] (BA08) ground-motion model from the original NGA project (i.e., the "NGA-West 1" project). That approach, which is continued here, provides for what we refer to as base-case GMPEs accounting for ground motion scaling with magnitude, distance, and site condition.

Aside from updating the coefficients based on new data, a principal motivation for the revised regression is that the enhanced database enables improved evaluations of numerous factors, including: the distinction between mainshock and aftershock motions; the influence of depth to top of rupture; basin depth effects; and regional variations of site effects and distance attenuation. Of these, only basin depth and regional apparent anelastic attenuation were found to be statistically significant and were incorporated into the median model. We treat these additional variables as optional adjustment factors to the base-case GMPEs, which maintains the simplicity of the base-case GMPEs for general applications. The enhanced data also enables evaluation of the effects of magnitude, distance, and site condition on standard deviation terms, which are now incorporated into the GMPEs.

The predicted ground-motion amplitudes from this study are generally similar to those from BA08 for larger magnitudes. The most significant differences are for motions from $\mathbf{M} < 6$ earthquakes, where the new predicted motions are less than those from BA08 as modified by Atkinson and Boore [2011], particularly at distances within about 20 km. We were unable to identify significant differences between motions from a mainshock and its aftershocks, and hence we consider our equations applicable for both event types. We find that over the magnitude range of engineering interest ($\mathbf{M} > 5$) the equations are unbiased with respect to source depth, as represented by either depth to top-of-rupture or hypocentral depth. Hence, a depth term is not introduced. With regard to apparent anelastic attenuation, the base-case GMPEs are unbiased for data from California and Taiwan, but other regions exhibit faster (Italy and Japan) or slower (China and Turkey) attenuation rates for which adjustment factors are introduced. Our equations are found to be centered for basin-depths compatible with an empirical relationship between depth parameter z_1 and V_{S30}, to be negative for depths shallower than the mean of such models, and positive for depths greater than the mean. These changes in ground motions with depth occur for long period ground motions, and applicable adjustment factors are introduced.

As with BA08, the standard deviation is segregated into between-event and within-event components. However, unlike BA08, the between-event component is now **M**-dependent, decreasing as **M** increases beyond 5.5. The within-event component now has variable trends with **M** for different spectral periods (decreases for short periods, increases for long period), increases with distance for $R_{JB} > 80$ km, and is reduced for soft soil sites.

Our GMPEs are considered applicable over a magnitude range of 3 to 8.5 for strike-slip or reverse-slip events (**M** 3 to 7 for normal-slip events), distances up to 400 km, and site conditions ranging from V_{S30} = 150 to 1500 m/sec and $z_1 = 0.0$ to 3.0 km. The equations are useful for prediction of the ground-motion intensity measures (IMs) PGA, PGV, and PSA at periods $T = 0$ to 10 sec.

ACKNOWLEDGMENTS

This study was sponsored by the Pacific Earthquake Engineering Research Center (PEER) and funded by the California Earthquake Authority, the California Department of Transportation, and the Pacific Gas & Electric Company. Participation of the fourth author was funded by the Natural Sciences and Engineering Research Council of Canada. Any opinions, findings, and conclusions or recommendations expressed in this material are those of the authors and do not necessarily reflect those of the sponsoring agencies. This work described in this report benefitted from the constructive discussions among the NGA developers Norman A. Abrahamson, Yousef Bozorgnia, Kenneth W. Campbell, Brian Chiou, I. M. Idriss, Walter J. Silva, and Robert E. Youngs. Input from supporting researchers was also invaluable, including Timothy Ancheta, Jack Baker, Ann Marie Baltay, Jennifer Donahue, Christine Goulet, Thomas Hanks, Ronnie Kamai, Albert Kottke, Tadahiro Kishida, Katie Wooddell, Paul Spudich, and Jennie Watson-Lamprey. It was a pleasure to work with this most distinguished group of researchers in an open and collaborative manner. We thank Sinan Akkar, John Douglas, and Silvia Mazzoni for their useful reviews.

ERRATA
PEER Report No. 2013-05

NGA-West 2 Equations for Predicting Response Spectral Accelerations for Shallow Crustal Earthquakes

July 10, 2013

In the site amplification model presented in Section 4.2.2, we have a maximum velocity (denoted V_c) beyond which there is no scaling of ground motion with V_{S30}. The selection of V_c is based on plots of site amplification from data against V_{S30}, as shown in Figure 4.8 of the report. Upon further inspection of these plots, we have increased V_c for short periods. Updated plots of Figure 4.8 reflecting these changes are given below.

The increase of V_c also increases the amount of data used to constrain the V_{S30}-scaling parameter c. The resulting change in slope was small, but was consistently in the direction of stronger scaling (i.e., values of c became more negative). Updated plots of c vs. period are given below (Figure 4.9). Coefficient tables for these two parameters, originally presented I the appendix, are also updated as part of this erratum.

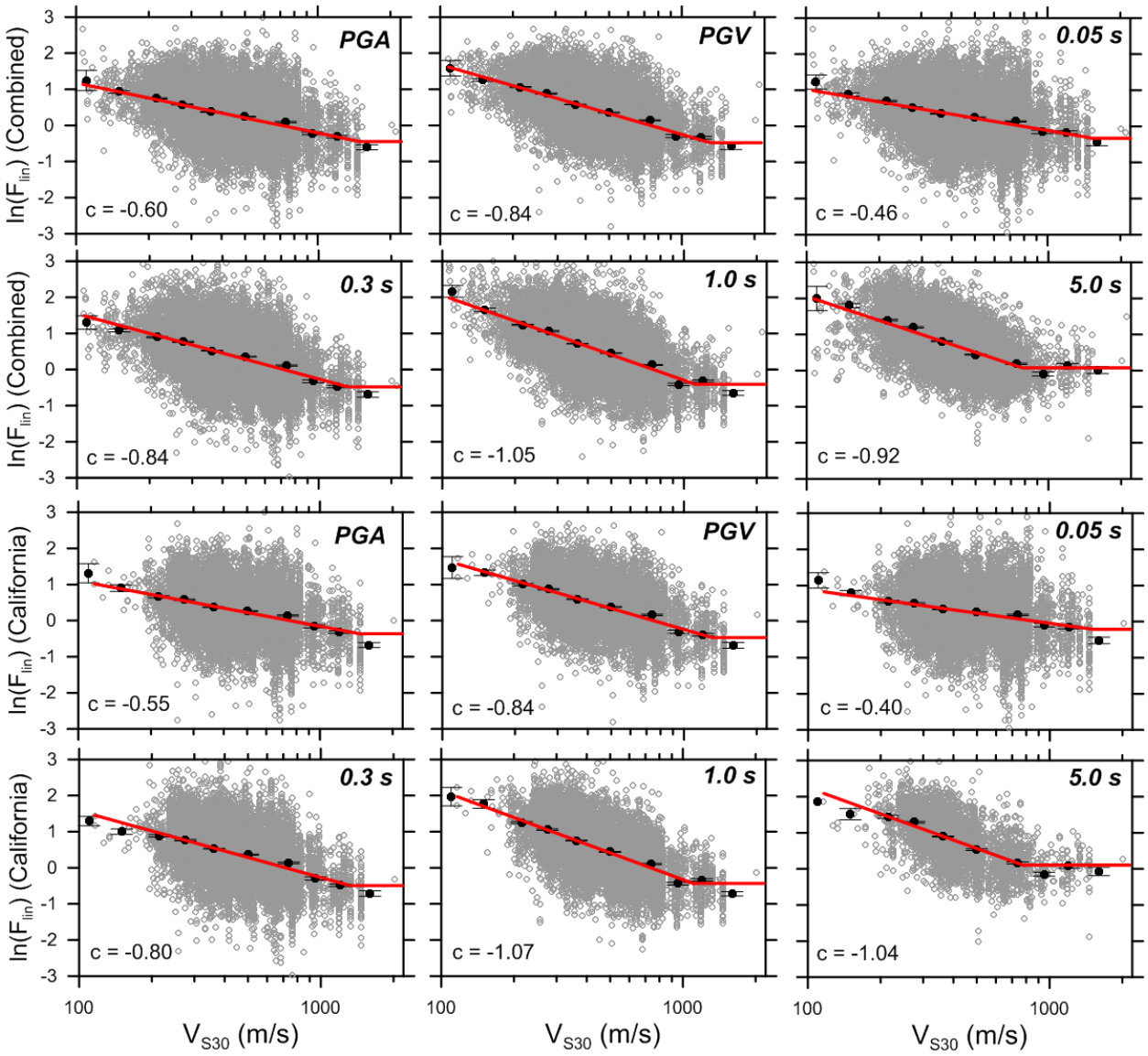

Figure 4.8a **Variation of linearized site amplification [Equation (4.3)] with V_{S30} for combined data set and subset from California. Red line indicates model prediction, black dots are binned means and their 95% confidence intervals.**

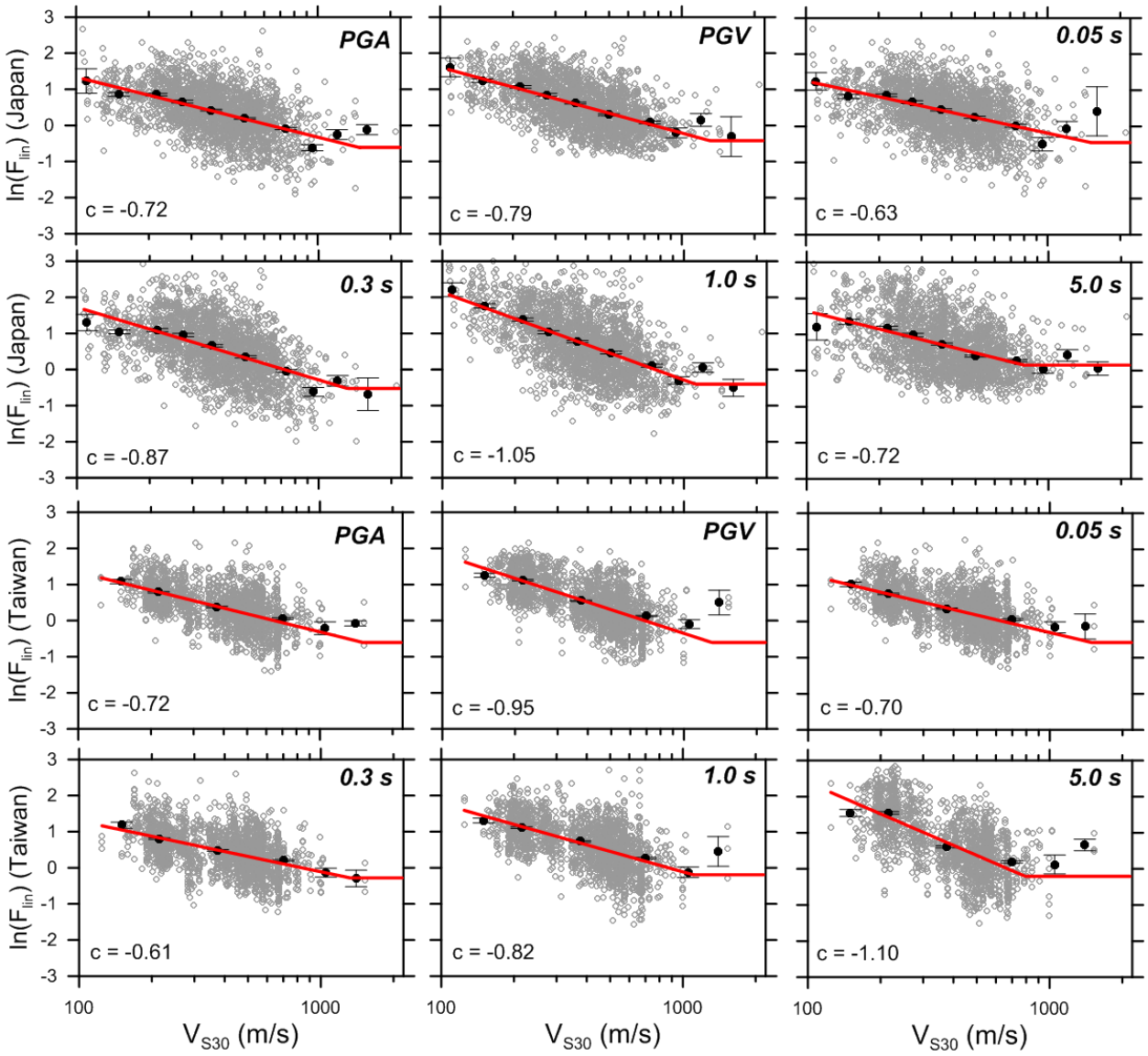

Figure 4.8b **Variation of linearized site amplification [Equation [4.3]) with V_{S30} for subset of data from Japan and Taiwan.**

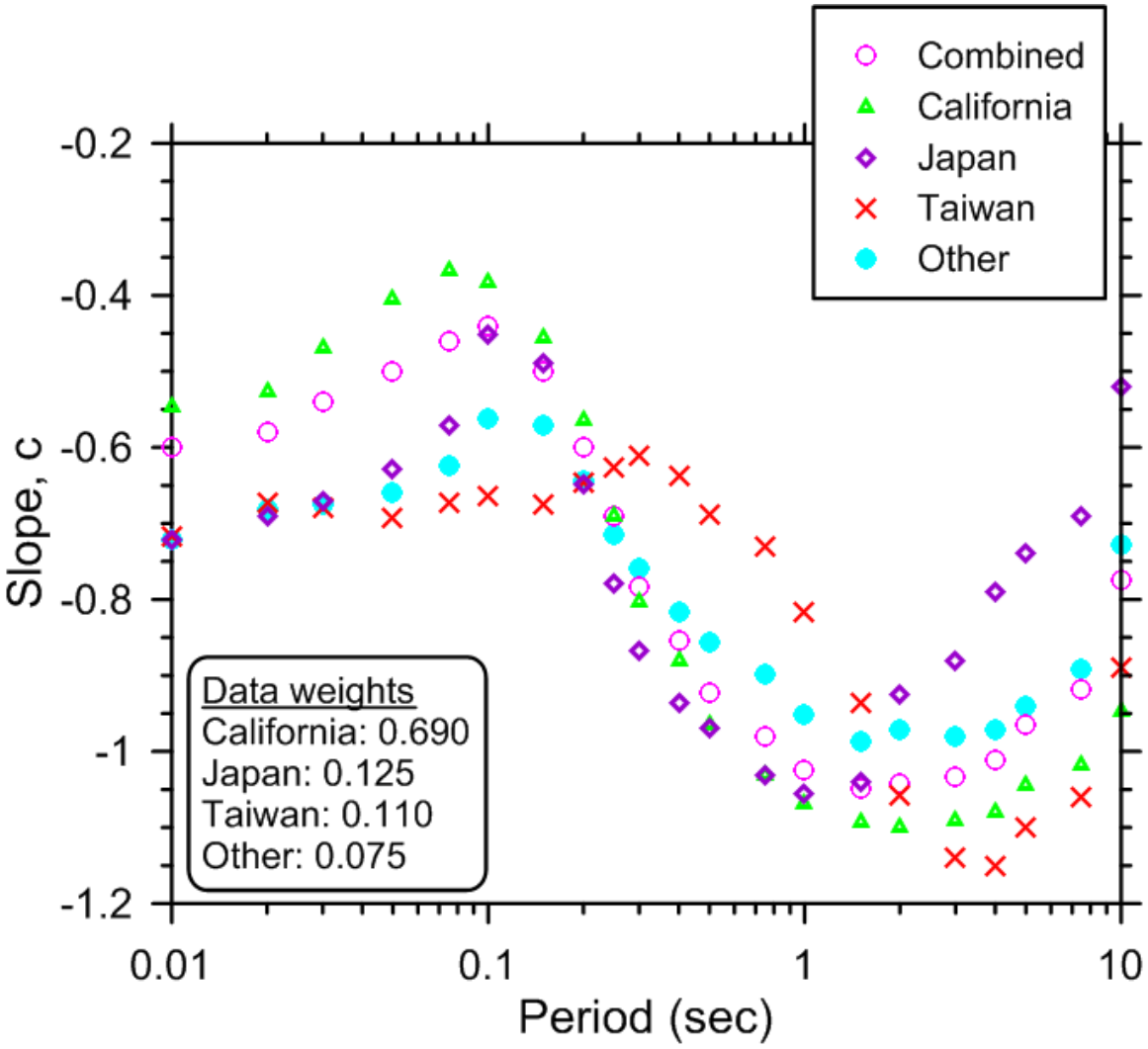

Figure 4.9 **Variation of slope (*c*) within spectral periods for combined data set and various regions. Data weights refer to the relative contributions to the 'combined' slope.**

Updated Coefficients

Period(sec)	c	V_c (m/s)
-1	-0.8400	1300.00
0	-0.6000	1500.00
0.01	-0.6037	1500.20
0.02	-0.5739	1500.36
0.022	-0.5668	1500.68
0.025	-0.5552	1501.04
0.029	-0.5385	1501.26
0.03	-0.5341	1502.95
0.032	-0.5253	1503.12
0.035	-0.5119	1503.24
0.036	-0.5075	1503.32
0.04	-0.4906	1503.35
0.042	-0.4829	1503.34
0.044	-0.4757	1503.13
0.045	-0.4724	1502.84
0.046	-0.4691	1502.47
0.048	-0.4632	1502.01
0.05	-0.4580	1501.42
0.055	-0.4479	1500.71
0.06	-0.4419	1499.83
0.065	-0.4395	1498.74
0.067	-0.4395	1497.42
0.07	-0.4404	1495.85
0.075	-0.4441	1494.00
0.08	-0.4502	1491.82
0.085	-0.4581	1489.29
0.09	-0.4673	1486.36
0.095	-0.4772	1482.98
0.1	-0.4872	1479.12
0.11	-0.5063	1474.74
0.12	-0.5244	1469.75
0.13	-0.5421	1464.09
0.133	-0.5475	1457.76
0.14	-0.5603	1450.71
0.15	-0.5796	1442.85
0.16	-0.6005	1434.22

0.17	-0.6225	1424.85
0.18	-0.6449	1414.77
0.19	-0.6668	1403.99
0.2	-0.6876	1392.61
0.22	-0.7243	1380.72
0.24	-0.7565	1368.51
0.25	-0.7718	1356.21
0.26	-0.7870	1343.89
0.28	-0.8161	1331.67
0.29	-0.8295	1319.83
0.3	-0.8417	1308.47
0.32	-0.8618	1297.65
0.34	-0.8773	1287.50
0.35	-0.8838	1278.06
0.36	-0.8896	1269.19
0.38	-0.9004	1260.74
0.4	-0.9109	1252.66
0.42	-0.9224	1244.80
0.44	-0.9346	1237.03
0.45	-0.9408	1229.23
0.46	-0.9469	1221.16
0.48	-0.9586	1212.74
0.5	-0.9693	1203.91
0.55	-0.9892	1194.59
0.6	-1.0012	1184.93
0.65	-1.0078	1175.19
0.667	-1.0093	1165.69
0.7	-1.0117	1156.46
0.75	-1.0154	1147.59
0.8	-1.0210	1139.21
0.85	-1.0282	1131.34
0.9	-1.0360	1123.91
0.95	-1.0436	1116.83
1	-1.0500	1109.95
1.1	-1.0573	1103.07
1.2	-1.0584	1096.04
1.3	-1.0554	1088.67
1.4	-1.0504	1080.77
1.5	-1.0454	1072.39
1.6	-1.0421	1061.77
1.7	-1.0404	1049.29

1.8	-1.0397	1036.42
1.9	-1.0395	1023.14
2	-1.0392	1009.49
2.2	-1.0368	995.52
2.4	-1.0323	981.33
2.5	-1.0294	966.94
2.6	-1.0262	952.34
2.8	-1.0190	937.52
3	-1.0112	922.43
3.2	-1.0032	908.79
3.4	-0.9951	896.15
3.5	-0.9910	883.16
3.6	-0.9868	870.05
3.8	-0.9783	857.07
4	-0.9694	844.48
4.2	-0.9601	832.45
4.4	-0.9505	821.18
4.6	-0.9405	810.79
4.8	-0.9302	801.41
5	-0.9195	793.13
5.5	-0.8918	785.73
6	-0.8629	779.91
6.5	-0.8335	775.60
7	-0.8046	772.68
7.5	-0.7766	771.01
8	-0.7503	760.81
8.5	-0.7254	764.50
9	-0.7016	768.07
9.5	-0.6785	771.55
10	-0.6558	775.00

CONTENTS

LIST OF FIGURES

LIST OF TABLES

1 Introduction

1.1 PROJECT OBJECTIVES AND SCOPE

Ground-motion prediction equations (GMPEs) are used in seismic hazard applications to specify the expected levels of shaking as a function of predictor variables such as earthquake magnitude and distance. GMPEs for active crustal regions are typically developed from an empirical regression of observed amplitudes against an available set of predictor variables. The complexity and sophistication of GMPEs has evolved over time as ground-motion databases and associated metadata concerning source and site conditions has grown. Early GMPEs were very simple equations giving peak ground acceleration as a function of magnitude and epicentral distance (e.g., Douglas [2003]). Modern GMPEs express peak motions and response spectra as functions of moment magnitude, distance to the rupture surface, and site condition variables such as the time-weighted average shear-wave velocity over the upper 30 m of the profile (V_{S30}); other predictor variables such as focal mechanism, depth to the top of the rupture, and depth to basement rock, may also be used (e.g., see NGA-West 1 equations, as described by Power et al., [2008] and references therein, as well as the compilation by Douglas [2011]). The larger and more comprehensive the available database, the greater the resolving power of empirical regression techniques to sort out the many effects that control ground motions.

In this study, we use a three-phase model building approach to the GMPE development (as described in Chapter 4); our aim is to take advantage of the rich NGA-West 2 database to develop a GMPE model for shallow crustal earthquakes in active tectonic regions that strikes a balance between accuracy of the prediction and simplicity of form and application. Our philosophy is as follows: The primary variables that control ground motion at a site are the earthquake magnitude (the primary source variable), distance to the fault (the primary path variable), and V_{S30} (the primary site variable). After constraining some variables based on an initial analysis of the data, in what we call Phase 1 of our study, we perform regressions to develop a base-case GMPE (for peak ground motions and response spectra) based on a simple functional form using just these variables, as well as fault type (Phase 2). We then refine the model as required, based on examination of the residuals (defined by the difference, in natural log units, between the observed and predicted amplitude of motion) of the regression against secondary predictor variables that are available as part of the NGA-West 2 metadata (Phase 3). These secondary parameters include the region in which the event occurs, whether the source is a mainshock or aftershock, the depth to the top of fault rupture, the depth to basement rock, etc. We assess the extent to which these additional variables improve the accuracy of the GMPE in a way that is both statistically significant and practically meaningful. We implement the inclusion of secondary variables, where warranted, as optional correction factors that may be applied to the

base-case GMPEs. In this way, we aim to ensure that our GMPE is centered for the general case of future events in regions for which site-specific fault rupture, path and site parameters may be unknown.

The scope of our GMPEs includes the prediction of horizontal-component peak ground acceleration (PGA), peak ground velocity (PGV) and response spectra (PSA, the 5% damped pseudo response spectral acceleration), for earthquakes of moment magnitude (**M**) 3.0 to 8.5, at distances from 0 to 400 km, at sites having V_{S30} in the range from 150 m/sec to 1500 m/sec, for periods between 0.01 sec and 10 sec. We consider regional variability in source, path and site, and selected secondary source and site effects, but do not address directivity effects.

1.2 PRIOR RELATED WORK

This study builds on the GMPEs of Boore and Atkinson [2008], which were part of the NGA-West 1 project [Power et al. 2008 and references therein]. The NGA-West 1 was founded on the development of a comprehensive and consistent database of ground-motion variables for shallow crustal earthquakes in active regions, including assembling associated metadata parameters, as described by Chiou et al. [2008]. The NGA-West 1 project involved a novel collaborative process in which several developer groups interacted in using various subsets of the same master database to derive alternative GMPEs. The process was highly successful in initiating significant improvements to the GMPEs available for seismic hazard applications. Based on the success of NGA-West 1, the NGA-West 2 project was formed to take advantage of new data available since NGA-West 1, address some weaknesses in the NGA-West 1 database, and allow the developers to reconsider their functional forms.

One improvement needed to the NGA-West 1 equations involved adding data at small-to-moderate magnitudes. The need to enrich the database at the low-magnitude end to ensure robust magnitude scaling was highlighted by several studies [Atkinson and Morrison 2009; Chiou et al. 2010; Atkinson and Boore 2011], and two of the NGA-West 1 developers provided amendments to improve their equation performance at low magnitudes [Chiou et al. 2010; Atkinson and Boore 2011]; the revised Boore and Atkinson GMPEs that account for this adjustment are referred to as BA08′. Studies by Atkinson and Morrison [2009] and Chiou et al. [2010] also pointed to the need to consider regional variability of path effects, as the attenuation of motions with distance is faster in some active regions than in others.

An important issue not addressed in NGA-West 1 was the regional variability of site effects; this issue stems from the inherent limitations of using V_{S30} as the primary site condition variable. In reality, site amplification depends not only on soil stiffness (V_{S30}), but also on soil depth and other factors. There are regional variations in the period at which site amplification peaks, due to regional differences in the depths of typical soil profiles; the site amplification function versus period for a given value of V_{S30} should thus be regionally dependent. In particular, peak site response occurs at shorter periods in Japan than in western North America, even for the same value of V_{S30} [Atkinson and Casey 2003; Ghofrani et al. 2013; Stewart et al. 2013; Anderson et al. 2013]. Thus we can potentially improve on the NGA-West 1 equations by allowing the site response function to vary with region, in addition to V_{S30}. We wish to note here that we recognize different variables could be used to characterize site effects, such as the

quarter-wavelength shear wave velocity [Joyner and Fumal 1984, 1985; Douglas et al. 2009] or V_{S30} in combination with peak response period. This option was not pursued in the present work because this level of site description is not yet part of the NGA-West database or used in common practice.

Other improvements to the treatment of site effects are also made possible by better data. Boore and Atkinson [2008] used empirical site amplification factors based on the work of Choi and Stewart [2005]. Stewart and Seyhan [2013] have updated this work based on additional data, which now allows a more robust description of linear and nonlinear site amplification effects over a wider range of V_{S30}.

Finally, the richer database available for NGA-West 2 allows us to improve on prior work by considering additional variables that could not previously be adequately resolved. However, as described in the next sections, we maintain the same basic functional form for the equations as used in Boore and Atkinson [2008].

2 Database

2.1 DATA SOURCES AND DATA EXCLUSION CRITERIA

We use the strong-ground motion database developed in the NGA-West 2 project (http://peer.berkeley.edu/ngawest2/). As described in Ancheta et al. [2013], the NGA-West 2 database consists of a site database containing metadata for all stations producing usable recordings; a source database containing magnitudes, locations, and geometries of earthquake sources producing recordings; and a flatfile that merges critical site and source information with distance parameters and computed ground-motion intensity measures (IMs). The flatfile was a continuously evolving file over the project duration, hence in referring to the flatfile, it becomes necessary to specify a date or version number. Since the development of GMPEs is a gradual process, many versions of the flatfile were used in this project, starting with one dated 12 July 2012 and concluding with one dated 14 March 2013. The changes in the flatfile over this time period were substantial, with the number of recordings increasing by almost a factor of three due to the inclusion of a large volume of small magnitude recordings from California (details in Ancheta et al. [2013]).

All of the GMPEs developed in the NGA-West 2 project (including the model presented in this report) used some version of the flatfile, but each developer team made different decisions regarding what portion of the database to use. As will be described further in Chapter 4, we use variable subsets of the data for different phases of the analysis. Consistent criteria (i.e., applied in all analysis phases) were applied with respect to the following considerations:

- Availability of critical metadata: We required the presence of magnitude, distance, and site metadata in order to include the record in analysis.
- Co-located stations: We do not use more than one record when multiple records are recorded at the same site (e.g. in a differential array or different sensors at the same site).
- Single-component motions: We only use records having two horizontal-component recordings.
- Inappropriate crustal conditions: We exclude recordings from earthquakes originating in oceanic crust or in stable continental regions.
- Soil-structure interaction (SSI): We exclude records thought to not reasonably reflect free-field conditions as a result of SSI that potentially significantly affects the ground motions at the instrument. The flatfile contains site parameters referred

to as the Geomatrix 1st letter, which indicate housing information for the recording stations as shown in Table 2.1. We recognize that the Geomatrix 1st letter criteria are not optimized with respect to the identification of possible SSI effects on the recorded ground motions [Stewart 2000], but they are the only available information at present. The selected stations are marked in bold (with highlighting) in Table 2.1.

- Proprietary data: Data not publicly available are not used.
- Problems with record: Based on visual inspection by an NGA Database Working Group, we exclude records with S-triggers, second trigger (i.e., two time series from the same event due to consecutive triggers), noisy records, or records with time step problems.
- Usable frequency range: We only use a given record within its usable frequency range (described further in Section 2.2).
- An earthquake is only considered if it has at least four recordings.
- Magnitude and distance-dependent screening criteria (details below and in Figure 2.1).

The phase of model development in which the base-case model is regressed (referred to as Phase 2 in Chapter 4), applies the following additional criteria:

- Class 2 events (commonly known as aftershocks; Wooddell and Abrahamson, [2012]) were excluded. We did not use Class 2 events because there is some concern that the magnitude scaling of these events differs from that of mainshocks (Class 1 events) (see Boore and Atkinson [1989] and Atkinson [1993]), although others have found aftershock and mainshock motions for similar magnitudes to not be significantly different [Douglas and Halldórsson 2010]. After some experimentation, we used a Centroid R_{JB} distance of 10 km to differentiate between Class 1 and 2 events. Excluding Class 2 events per this criterion cut the dataset for the regression substantially.
- Only recordings at a closest distance to the surface projection of the fault (R_{JB}) of 80 km and under were considered in the actual regression. This limit was found to be necessary to achieve reasonable magnitude-scaling results from the regression when a magnitude-dependent geometric spreading term is used. However, fixed apparent anelastic attenuation coefficients were used in the Phase 2 regressions in the hope that the resulting GMPEs would be applicable at greater distances. The accuracy of the GMPEs at greater distances is subsequently assessed through residual analysis.

Table 2.1 **Geomatrix 1st letter descriptions of station housing. Station types marked in bold were considered for use (some H recordings were used if they were from toe locations of small dams). Not all records having the indicated Geomatrix letters were used, as they could be excluded on the basis of lacking metadata, lacking ground-motion values, event class, etc.**

GMX 1st Letter	Description
I	Free-field instrument or instrument shelter. Instrument is located at or within several feet of the ground surface, and not adjacent to any structure.
A	One-story structure of lightweight construction. Instrument is located at the lowest level and within several feet of the ground surface.
B	Two- to four-story structure of lightweight construction, or tall one-story warehouse-type building. Instrument is located at the lowest level and within several feet of the ground surface.
A,B	Used for small generally lightweight structures for which we can not determine the number of stories from the available information. These sites generally have COSMOS site code 4 which defines a reference station described as either a 1- or 2-story, small, light building. This classification is mainly used in the small-moderate magnitude data set.
C	One- to four-story structure of lightweight construction. Instrument is located at the lowest level in a basement and below the ground surface.
D	Five or more story structure or heavy construction. Instrument is located at the lowest level and within several feet of the ground surface.
E	Five or more story structure or heavy construction. Instrument is located at the lowest level in a basement and below the ground surface.
F	Structure housing instrument is buried below the ground surface about 1-2 m, at a shallow depth. e.g. tunnel or seismic vault (e.g. U. S. Array design) but shallow embedment (use 'T' for deeper embedments or 'V' for deeply embedded vaults, both not considered "free-field")
I,F	These sites generally have COSMOS site code 3 for which the sensors have been buried/set in ground at shallow or near surface depths (e.g. the U. S. Array station design). This classification is mainly used in the small-moderate magnitude western and EUS data sets.
G	Structure of light or heavyweight construction, instrument not at lowest level.
H	Earth dam (station at toe of embankment or on abutment).
J	Concrete Dam (none in database).
K	Near a one-story structure of lightweight construction. Instrument is located outside on the ground surface, within approximately 3 m of the structure.
L	Near a two- to four-story structure of lightweight construction. Instrument is located outside on the ground surface, within approximately 6 m of the structure.
M	Near a two- to four-story structure of lightweight construction with basement. Instrument is located outside on the ground surface, within approximately 6 m of the structure.
N	Near a five- to eight-story structure. Instrument is located outside on the ground surface, within approximately 10 m of the structure.
O	Near a five- to eight-story structure with basement. Instrument is located outside on the ground surface, within approximately 10 m of the structure.
T	Associated with a deep tunnel, e.g. a) L'Aquila - Parking: Pleistocene terrace above a pedestrian tunnel on the edge'slope of the terrace, nearby structure to the station is a car park. b) Various BDSN stations (e.g. WDC, WENL, YBH).
V	Deeply embedded seismic vault
W	Structural response e.g roof, penstock, etc. (e.g. CSMIP 23732, San Bernardino - Devil's Canyon Penstock)
Z	Embedded in a borehole or missile silo
P	Castle of masonry construction, massive 1-3 stories (used for the L'Aquila earthquake sequence).
Q	Associated with a structure, size of structure is not known (used for the L'Aquila earthquake sequence).
S	Associated with a structure and in the basement, size of structure is not known (used for the L'Aquila earthquake sequence).
U	Il Moro is on an embankment between two roads and retaining walls (used for the L'Aquila earthquake sequence).

All phases of model development applied the magnitude and distance-dependent screening criteria shown in Figure 2.1. These criteria are intended to minimize potential sampling bias, which can occur at large fault distances where ground motions are generally weak; at large distances, instruments may only be triggered by stronger-than-average motions. The inclusion of such records would lead to a bias in the predicted distance decay of the ground motion—there would be a tendency for the predicted ground-motions to decay less rapidly with distance than the real data. Boore et al. [1997] (BJF) avoided this bias by excluding data for each earthquake beyond the closest distance to an operational, non-triggered station (most of the data used by BJF were obtained on triggered analog stations). Unfortunately, information is not available in the NGA-West 2 flatfile that would allow us to apply a similar distance cutoff, at least for the case of triggered analog recordings. Furthermore, a similar bias can also exist in non-triggered digital recordings because of the presence of long-period noise. The criteria in Figure 2.1, adapted from correspondence with N. Abrahamson [2012, *personal communication*], provides exclusion criteria that we used to avoid this potential bias.

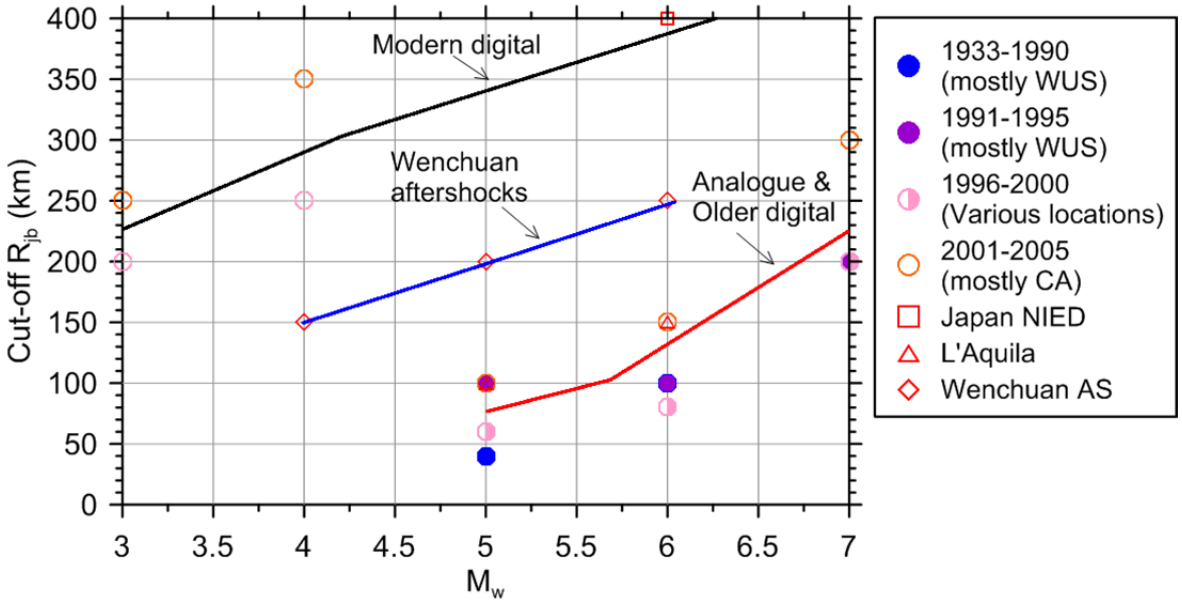

Figure 2.1 **Magnitude- and distance-dependent cutoff criteria for using records. The symbols in the figure represent judgment-based cutoffs of data reliability derived from discussions with N. Abrahamson [2012, *personal communication*].**

2.2 INTENSITY MEASURES CONSIDERED

The ground-motion parameters comprising the dependent variables of the GMPEs (also called ground-motion intensity measures, IMs) include PGA, PGV, and 5%-damped PSA all for the horizontal component. Unlike BA08′, we do not use response variables defined as the GMRotI50 parameter (effectively the median of all possible geometric means for various non-redundant horizontal rotation angles; Boore et al. [2006]) due to confusion among some engineers regarding its definition. Rather, we use the RotD50 parameter [Boore 2010], which is the median

single-component horizontal ground motion across all non-redundant azimuths—no geometric means are used in calculating RotD50. As shown in Figure 3 of Boore [2010], RotD50 is about a factor of 1.06 larger than GMRotI50 at a period of 10 sec, with the factor decreasing as period decreases; the standard deviation of RotD50 is about a factor of 1.05 larger than for GMRotI50 at short periods, and increasing to a factor of 1.08 at a period of 10 sec.

The GMPEs described in this report predict PGA, PGV, and 5%-damped PSA for periods between 0.01 sec and 10 sec. We do not include equations for peak ground displacement (PGD), which we believe to be too sensitive to the low-cut filters used in the data processing to be a stable measure of ground shaking. In addition there is some bias in the PGD values obtained in the NGA dataset from records for which the low-cut filtering was not performed as part of the NGA project. Appendix C of Boore and Atkinson [2007] contains a short discussion of these points. We recommend using response spectra at long periods instead of PGD.

The record processing procedures applied to all records in the flatfile include selection of record-specific corner frequencies to optimize the usable frequency range. The most important filter applied to the data is the low-cut filter, which removes low frequency noise. For each record the maximum usable period used in our analysis was taken as the inverse of the lowest usable frequency given by column EA in the NGA-West 2 flatfile. The lowest usable frequency is given by $\max(factor * f_{HP1}, factor * f_{HP2})$, where $factor$ usually equals 1.25, and f_{HP1} and f_{HP2} are the high-pass (equivalent to low-cut) corner frequencies used in the processing the two horizontal components.

2.3 PREDICTOR VARIABLES

The predictor variables (independent variables in the regression analysis) in the base model are moment magnitude **M**, R_{JB} distance (closest distance to the surface projection of the fault plane), and V_{S30} (time-weighted average shear-wave velocity over the top 30 m) for site characterization. Secondary parameters for which correction factors are developed through residuals analysis include depth to top of rupture Z_{tor} and basin depth z_1 (depth from the ground surface to the 1.0 km/sec shear-wave horizon).

We also considered the effect of fault type (i.e., normal, strike-slip, and reverse) and event type classified as Class 1 and 2 (CL1 and CL2). Each of these predictor variables was taken from the NGA-West 2 database. The fault type was specified by the plunge of the *P*- and *T*-axes, as shown in Table 2.2. This classification method provides the expected mechanism for the stress regime, as based on the orientation of the principal stress axes; it produces results that are similar to those based on the rake angle of the fault, but is more diagnostic for cases in which one of the two possible fault planes is shallowly dipping [Bommer et al. 2003].

Table 2.2 Fault-type definitions (*pl* is plunge angle, from horizontal).

P-axis plunge	T-axis plunge	Fault Type
$pl > 40°$	$pl \leq 40°$	Normal
$pl \leq 40°$	$pl > 40°$	Reverse
$pl \leq 40°$	$pl \leq 40°$	Strike-slip

2.4 DATA DISTRIBUTION

The distribution of data we used to develop our GMPEs is shown in Figure 2.2 by **M** and R_{JB}. For comparison, the distribution of data used in BA08 is also shown. Many more small magnitude data are used in the new GMPEs, as well as a few new large events such as the 2008 **M**7.9 Wenchuan, China, earthquake. Note that the data used to develop the base-case GMPE is a subset of the data shown in Figure 2.2 for mainshock events and distances under 80 km. The full data set shown in the figure was used in the Phase 3 analyses described subsequently.

The data distribution separated by fault type is shown in Figure 2.3. The distribution of the data by fault type, rake angle, and dip angle is shown in Figure 2.4. The widest range of available magnitudes is for strike-slip earthquakes, while the narrowest range is for normal-slip earthquakes (see Figure 2.3). This suggests that the magnitude scaling will be better determined for strike-slip than for normal-slip earthquakes—a problem that we circumvented by using a common magnitude scaling for all types of events, as discussed later.

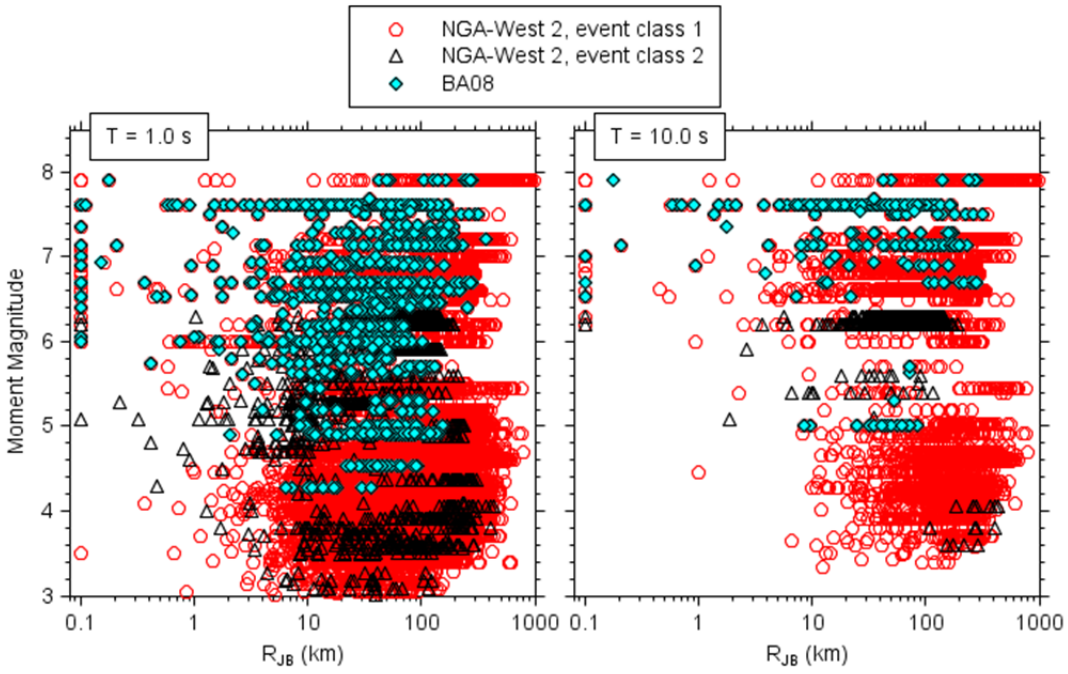

Figure 2.2 Distribution of data used to develop present GMPEs (BSSA13) compared to that used for BA08. The distributions for PGA and periods less than *T* = 1.0 sec are virtually ideintical to the distribution for *T* = 1 sec.

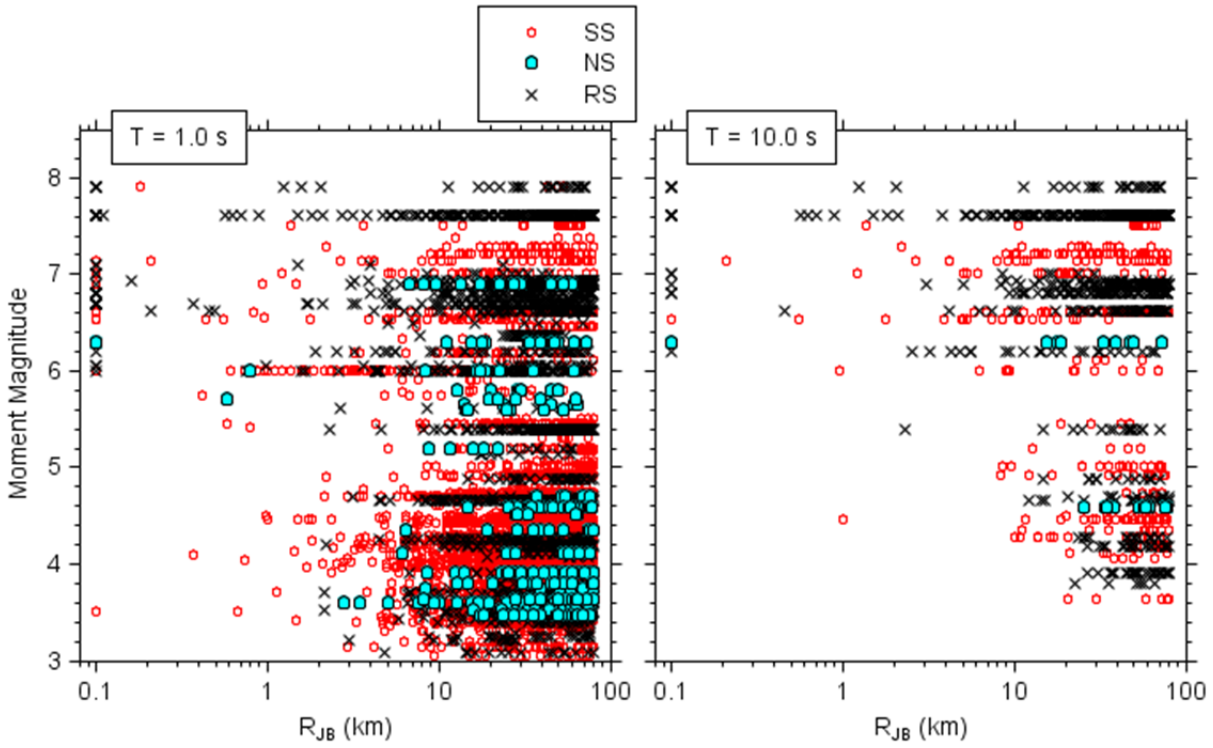

Figure 2.3(a) **Distribution of data, according to fault type, used to develop present base-case GMPEs. The data distribution shown here is that applied during the Phase 2 analysis. SS=strike-slip; NS=normal-slip; RS=reverse-slip.**

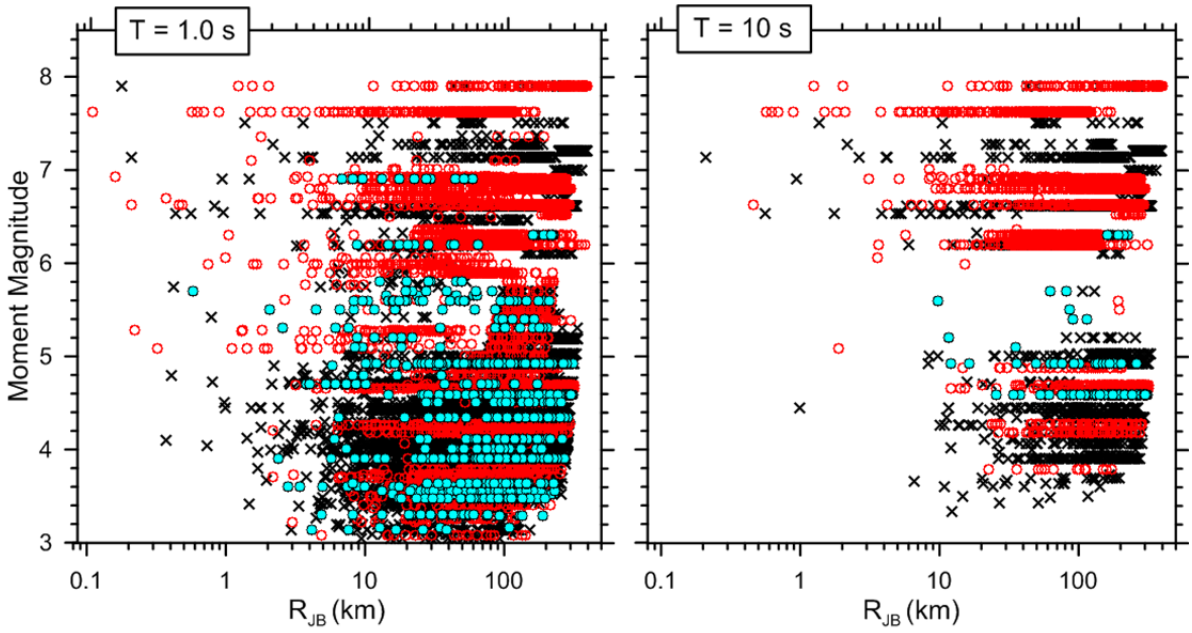

Figure 2.3(b) **Distribution of data used in residuals analysis of GMPE (Phase 3). Same legend as Figure 2.3(a).**

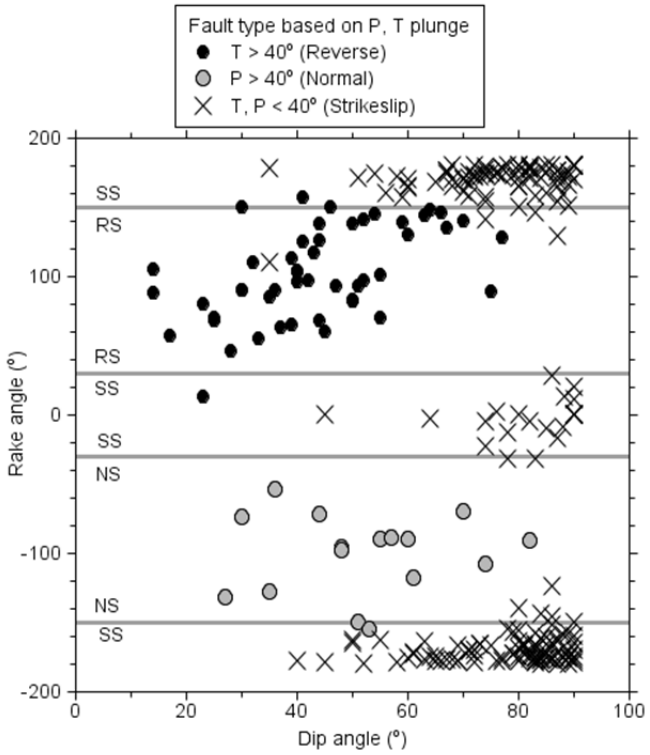

Figure 2.4 **Distribution of the data we used in rake-angle and dip-angle space. The horizontal gray lines indicate boundaries between fault types used by Boore et al. [1997], and the symbols and colors indicate our classification based on the plunges of the P- and T-axes (our classification scheme is indicated in the legend; see Appendix D in BA07).**

The number of recordings and earthquakes used in the base-case (Phase 2) regression analysis are shown in Figure 2.5. The numbers are differentiated by fault type. As in BA08, there is a rapid decrease in available data for periods longer than several seconds, but there are many more data available at the longest periods than were available in BA08. For example, there were no normal-slip (NS) records available in BA08 for T=10 sec, whereas 23 recordings were used in the analysis described in this report.

The distribution by V_{S30} is given in Figure 2.6. Also shown for convenience are the NEHRP site classes, although these were not used in the analyses. There are more rock sites (Class B) used for the residuals analysis (120 sites and 1022 recordings) than for the base-case model development (58 sites and 230 recordings).

The distributions of the data over the predictor variable space, as shown in Figures 2.2 to 2.6, necessarily influence the GMPEs. Note in particular the lack of data at close distances for small earthquakes. This means that the near-source ground motions for small events will not be constrained by observations. In addition, there are many fewer small magnitude data for long periods than for short periods, which means that the small-earthquake magnitude scaling will be less well determined for long oscillator periods than for short oscillator periods.

The distribution by site class (Figure 2.5) shows that very few data were from Class A sites (hard rock). The bulk of the data are from Class B to D sites, which range from firm rock to medium stiff soil. More detail can be found in Chapter 5, which provides recommendations to use in applying our equations at the limits of the V_{S30} range.

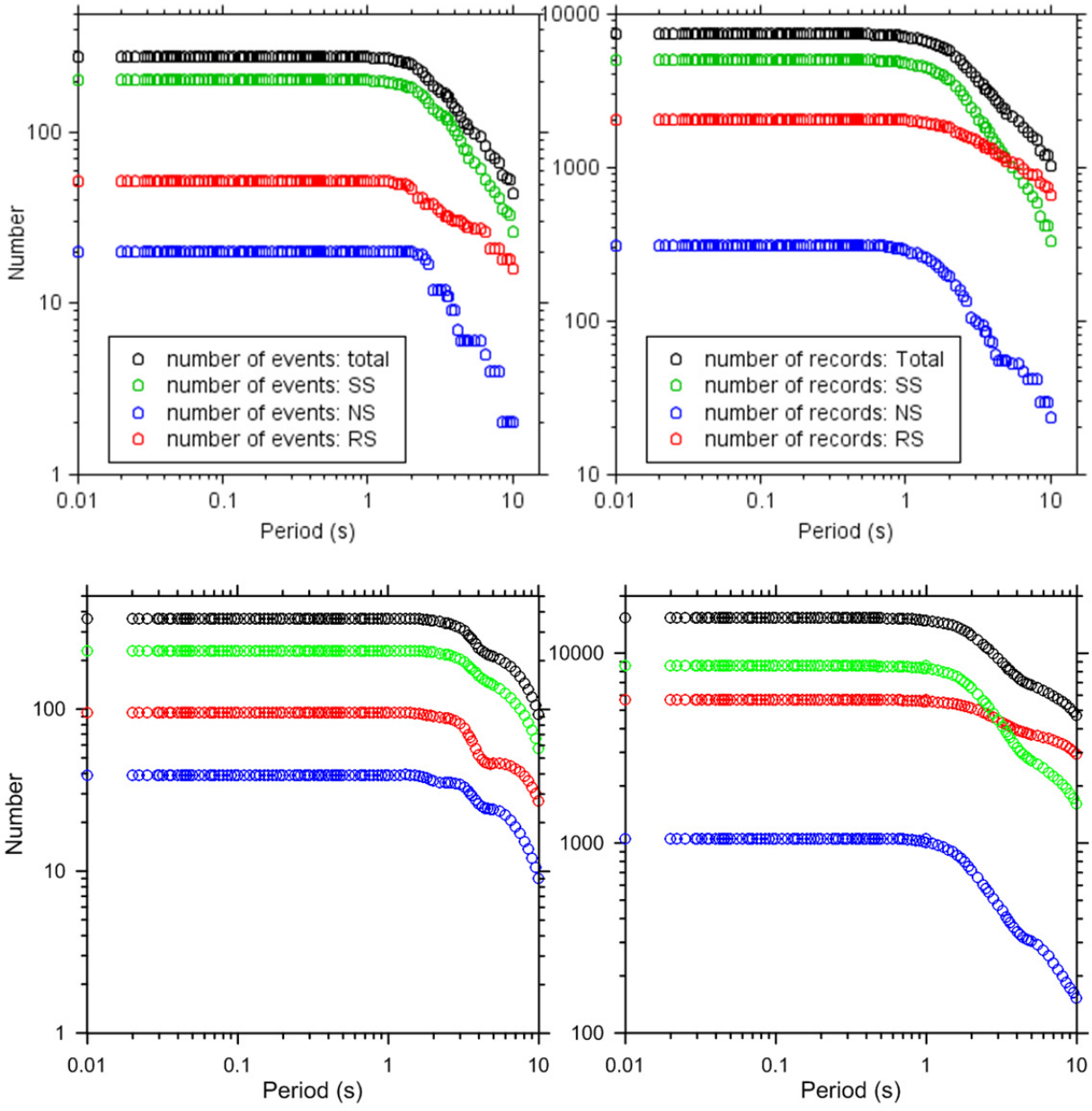

Figure 2.5 **Number of events (left) and recordings (right) used to develop Phase2 model (top) and Phase 3 residuals analysis (bottom). The numbers are differentiated by fault type. SS=strike-slip; NS=normal-slip; RS=reverse-slip.**

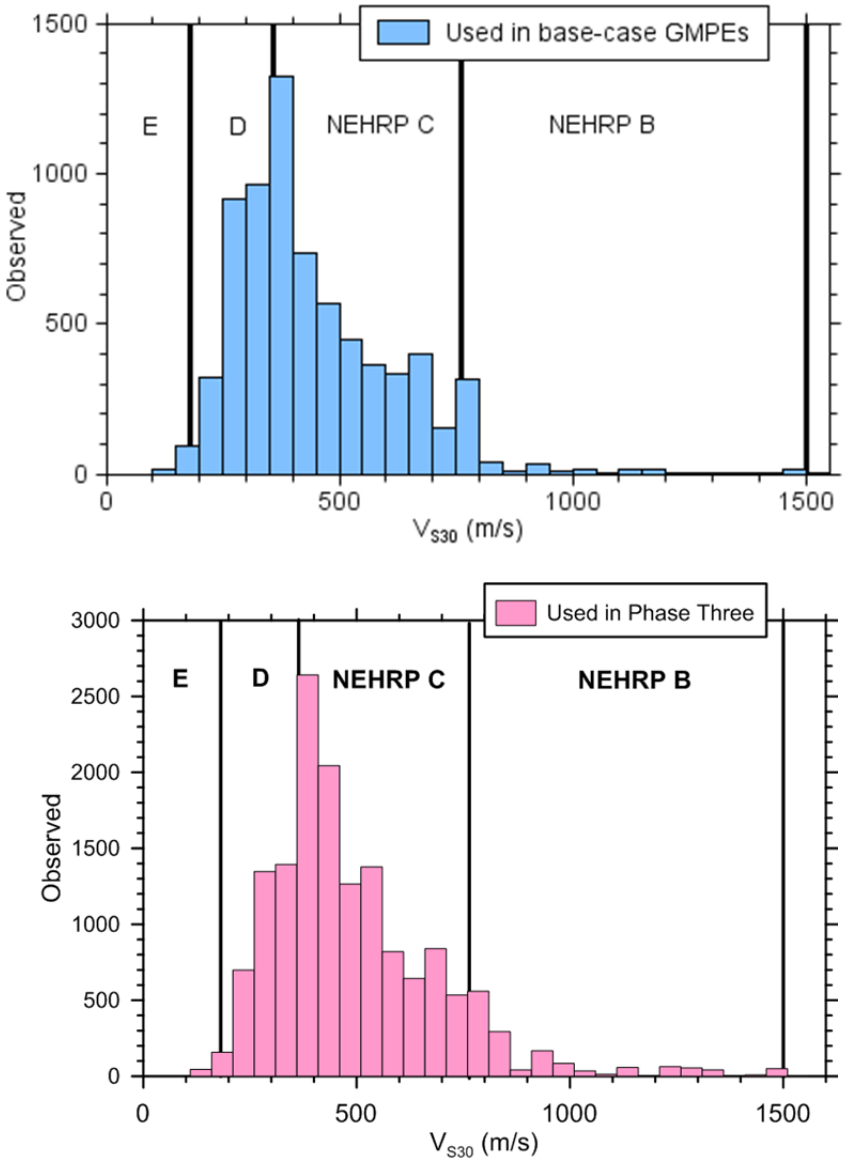

Figure 2.6 **Histogram of V_{S30} for records used in Phase 2 analysis (top) and Phase 3 residuals analysis (bottom), with NEHRP site classes indicated by the vertical lines. Only two records had a V_{S30} value (1526 m/sec and 2016 m/sec) corresponding to NEHRP class A, and thus the abscissa only extended slightly beyond 1500 m/sec.**

3 Form of the Equations

3.1 SOURCE AND PATH TERMS

We followed the philosophy of BJF97 and BA08 in seeking simple functional forms for our GMPEs, with the minimum required number of predictor variables. We call these the "base-case GMPEs". The selection of functional form was heavily guided by subjective inspection of nonparametric plots of data; many such plots were produced and studied before commencing the regression analysis. Figure 3.1 provides an example, in which the data (for strike-slip, CL1 events) are overlain to gain a sense of the general behavior. Close inspection of data-amplitude plots (such as Figure 3.1, and others not shown here) revealed several key features that the functional form must accommodate: magnitude-dependent geometric spreading; an apparent anelastic attenuation term to account for curvature in the decay of log ground motions versus log distance for distances beyond about 80 km; and strongly nonlinear (and period dependent) magnitude dependence of amplitude scaling at a fixed distance, with a tendency toward saturation (no magnitude dependence) with increasing magnitude for short periods and close distances. (Note: We add the modifier "apparent" to "anelastic attenuation" because the decay captured by this term represents an average over the propagation path of a number of processes; it includes scattering and other effects in addition to anelasticity.)

The functional forms of the equations used for the base-case GMPEs are the same as those used by BA08, except for the site response equations, which are discussed in Section 3.2. We investigate the statistical and practical utility of including adjustment factors involving additional predictor variables in an analysis of residuals from the base-case GMPEs in Section 4.4.

Our base-case equation for predicting ground motions is:

$$\ln Y = F_E\left(\mathbf{M},mech\right) + F_{P,B}\left(R_{JB},\mathbf{M}\right) + F_{S,B}\left(V_{S30},R_{JB},\mathbf{M}\right) + \varepsilon_n\sigma\left(\mathbf{M},R_{JB},V_{S30}\right) \tag{3.1}$$

where $\ln Y$ represents the natural logarithm of a ground-motion IM (PGA, PGV, or PSA); F_E, $F_{P,B}$, and $F_{S,B}$ represent the source-dependent function ("E" for "event"), path function ("P"), and site amplification function ("S"), respectively (subscript 'B' indicates base-case model; not used for event function since the same equations are used for the base-case and adjusted models). The predictor variables are **M**, *mech*, R_{JB}, and V_{S30}, which represent moment magnitude, fault type, Joyner-Boore distance (defined as the closest distance to the surface projection of the fault), and time-weighted average shear-wave velocity over the top 30 m of the site, respectively; ε_n is

the fractional number of standard deviations of a single predicted value of ln$Y$ away from the mean value of ln$Y$ (e.g., $\varepsilon_n = -1.5$ would be 1.5 standard deviations smaller than the mean value); σ is the total standard deviation of the model. The F_E, $F_{P,B}$, $F_{S,B}$, and σ functions are period dependent.

The total standard deviation σ is partitioned into components that represent between-event variability (τ) and within-event variability (ϕ) as follows:

$$\sigma(\mathbf{M}, R_{JB}, V_{S30}) = \sqrt{\phi^2(\mathbf{M}, R_{JB}, V_{S30}) + \tau^2(\mathbf{M})} \tag{3.2}$$

The dependence of ϕ and τ terms on the predictor variables of **M**, R_{JB}, and V_{S30} is presented in Section 4.4.4.

The base-case model in Equation (3.1) can be supplemented with the optional predictor variables accounting for regional apparent anelastic attenuation and basin depth z_1. The regional attenuation terms appear in the path function (Section 3.1.2). Parameter z_1 enters into the site amplification terms as described in Section 3.2.

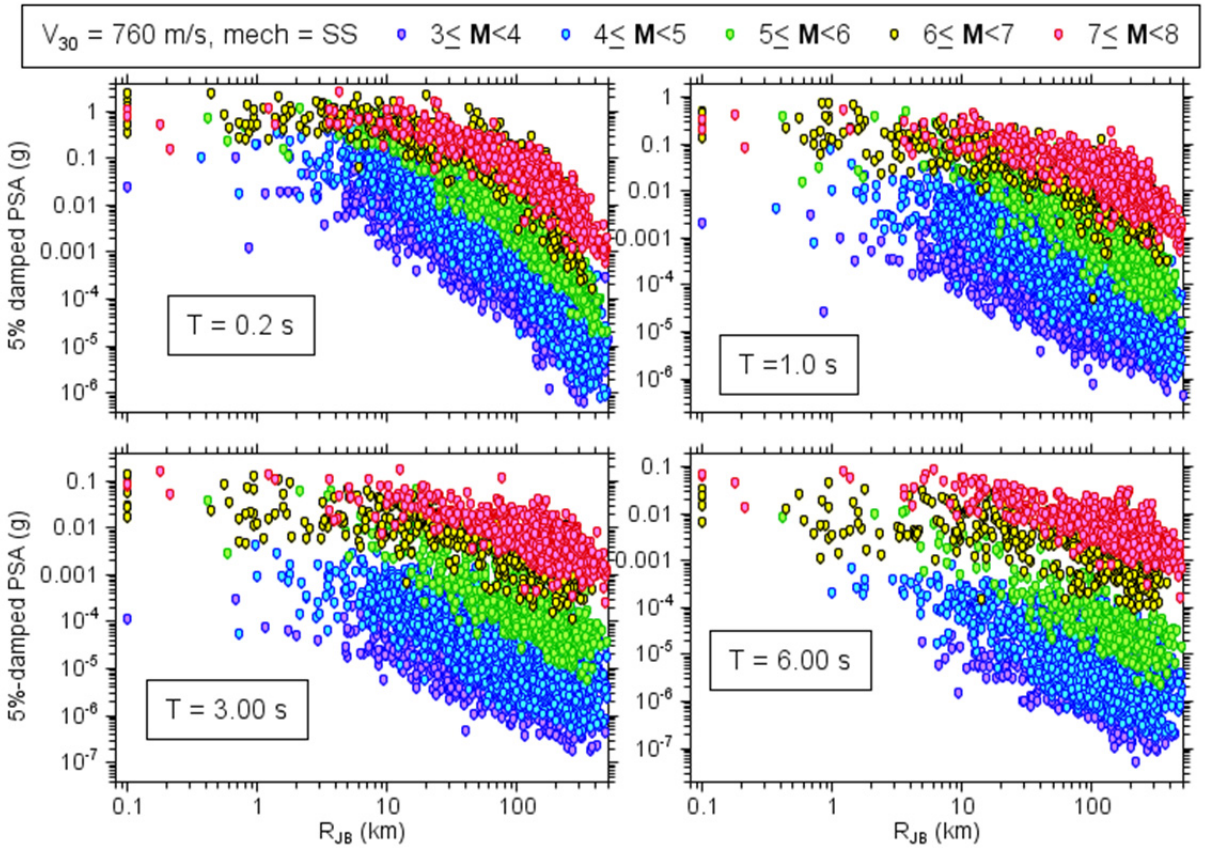

Figure 3.1 **PSA at four periods for strike-slip earthquakes. All amplitudes corrected to V_{S30} = 760 m/sec using the soil correction factors of this study.**

3.1.1 Path and Source Functions

The base-case path-dependent function is given by:

$$F_{P,B}\left(R_{JB},\mathbf{M}\right)=\left[c_1+c_2\left(\mathbf{M}-\mathbf{M}_{ref}\right)\right]\ln\left(R/R_{ref}\right)+c_3\left(R-R_{ref}\right) \tag{3.3}$$

where

$$R=\sqrt{{R_{JB}}^2+h^2} \tag{3.4}$$

and c_1, c_2, c_3, $\mathbf{M}_{ref}$, R_{ref}, and h are the coefficients determined by regression.

The event-specific function is given by:

$$F_E\left(\mathbf{M},mech\right)=\begin{cases}e_0U+e_1SS+e_2NS+e_3RS+e_4\left(\mathbf{M}-\mathbf{M}_h\right)+e_5\left(\mathbf{M}-\mathbf{M}_h\right)^2 & \mathbf{M}\le\mathbf{M}_h\\ e_0U+e_1SS+e_2NS+e_3RS+e_6\left(\mathbf{M}-\mathbf{M}_h\right) & \mathbf{M}>\mathbf{M}_h\end{cases} \tag{3.5}$$

where U, SS, NS, and RS are dummy variables (taking on values of 1 or 0, as indicated in Table 3.1) used to specify unspecified, strike-slip, normal-slip, and reverse-slip fault types, respectively; $\mathbf{M}_h$, the "hinge magnitude" for the shape of the magnitude scaling, is a coefficient to be set during the analysis. Unlike in BA08, $\mathbf{M}_h$ is period-dependent, as discussed below. The determination of the coefficients in the distance and magnitude functions is discussed in Chapter 4.

Adjustments to the base-case model for the effects of regional apparent aneleastic attenuation and basin depth are made on the basis of residuals analysis described in Section 4.4. With these adjustments, the main equation for the GMPE becomes:

$$\begin{aligned}\ln Y = {} & F_E\left(\mathbf{M},mech\right)+F_P\left(R_{JB},\mathbf{M},region\right)+F_S\left(V_{S30},R_{JB},\ \mathbf{M},z_1\right)+\\ & \varepsilon_n\sigma\left(\mathbf{M},R_{JB},V_{S30}\right)\end{aligned} \tag{3.6}$$

Note that the F_E term is unchanged, because residuals analysis did not support the addition of terms related to Class 2 events or source depth. We discuss the details of the path-specific adjustments in the next subsection; the site function is discussed in Section 3.2.

Table 3.1 Values of dummy variables for different fault types.

Fault Type	U	SS	NS	RS
Unspecified	1	0	0	0
Strike-slip	0	1	0	0
Normal-slip	0	0	1	0
Reverse-slip	0	0	0	1

3.1.2 Adjustments to Path Function

The adjusted path-dependent function is given in Equation (3.7), in which case Δc_3 can be region-dependent.

$$F_P\left(R_{JB}, \mathbf{M}, region\right) = F_{P,B}\left(R_{JB}, \mathbf{M}\right) + \Delta c_3\left(R - R_{ref}\right) \tag{3.7}$$

The tables of coefficients for our GMPEs include c_3 and Δc_3, with a different column of Δc_3 coefficients for each region.

3.2 SITE TERM

The nonlinear site amplification component of the base-case GMPE (introduced in Equation 3.1) is comprised of two additive terms representing V_{S30}-scaling and nonlinearity as follows:

$$F_{S,B} = \ln\left(F_{lin}\right) + \ln\left(F_{nl}\right) \tag{3.8}$$

where $F_{S,B}$ represents site amplification in natural logarithmic units; F_{lin} represents the linear component of site amplification, which is dependent on V_{S30}; and F_{nl} represents the nonlinear component of site amplification, which depends on V_{S30} and the amplitude of shaking on reference rock (taken as V_{S30} = 760 m/sec).

The linear component of the model (F_{lin}) describes the scaling of ground motion with V_{S30} for linear soil response conditions (i.e., small strains) as follows:

$$\ln\left(F_{lin}\right) = \begin{cases} c\ln\left(\dfrac{V_{S30}}{V_{ref}}\right) & V_{S30} \le V_c \\ c\ln\left(\dfrac{V_c}{V_{ref}}\right) & V_{S30} > V_c \end{cases} \tag{3.9}$$

where c describes the V_{S30}-scaling in the model, V_c is the limiting velocity beyond which ground motions no longer scale with V_{S30}, and V_{ref} is the site condition for which the amplification is unity (taken as 760 m/sec). Parameters c and V_c are period-dependent and are determined by regression as described in Section 4.2. Parameter c may be region-dependent, especially at long periods, but as discussed later, we do not allow c to be regionally dependent in this report.

The nonlinear term in the site amplification model (F_{nl}) modifies the linear site amplification so as to decrease amplification for strong shaking levels. The F_{nl} term is constructed so as to produce no change relative to the linear term for low PGA_r levels. The functional form for the F_{nl} term is as follows:

$$\ln(F_{nl}) = f_1 + f_2 \ln\left(\frac{PGA_r + f_3}{f_3}\right) \tag{3.10}$$

where f_1, f_2, and f_3 are coefficients in the model and PGA_r is the median peak horizontal acceleration for reference rock (taken as V_{S30}=760 m/sec). We take $f_1 = 0.0$ to force $\ln(F_{nl})$ to zero for $PGA_r << f_3$. We set $f_3 = 0.1\text{g}$, whereas f_2 is a function of period and V_{S30} as follows:

$$f_2 = f_4\left[\exp\left\{f_5\left(\min\left(V_{s30}, 760\right) - 360\right)\right\} - \exp\left\{f_5\left(760 - 360\right)\right\}\right] \tag{3.11}$$

This functional form for f_2 is the same as that used by Chiou and Youngs [2008].

In order to apply the site amplification function, we must first evaluate PGA_r for applicable magnitude and distance using Equation (3.1) for rock site conditions. Peak acceleration is used to represent the intensity of rock shaking in lieu of PSA at the period of interest. We are aware of the convenience of using PSA, but we retain the use of PGA for physical reasons. In particular, PGA is directly related to soil shear stress, which in turn is related to shear strain in an equivalent-linear sense.

The adjusted site amplification model used with Equation (3.6) is formulated as:

$$F_S\left(V_{S30}, \mathbf{M}, R_{JB}, z_1\right) = F_{S,B}\left(V_{S30}, \mathbf{M}, R_{JB}\right) + F_{\delta Z1}\left(\delta z_1\right) \tag{3.12}$$

where $F_{\delta z_1}$ is an adjustment to the base model to consider the effects of basin depth on ground-motion amplitude. This adjustment is based on residuals analysis described in Section 4.4. It is cast as follows:

$$F_{\delta Z1}\left(\delta z_1\right) = \begin{cases} 0 & T < 0.65 \\ f_6 \delta z_1 & T \geq 0.65 \;\&\; \delta z_1 \leq f_7 / f_6 \\ f_7 & T \geq 0.65 \;\&\; \delta z_1 > f_7 / f_6 \end{cases} \tag{3.13}$$

where f_6 and f_7 are estimated as described in Section 4.4, and the ratio f_7 / f_6 is in units of km. The parameter δz_1 is the difference between basin depth z_1 and the prediction of an empirical model relating z_1 to V_{S30} (given in Equation 4.9; Equation 4.9a for California, and Equation 4.9b for Japan). The adjustment factor $F_{\delta z_1}$ is an optional feature of the model. For many applications z_1 may be unknown; in such cases we recommend using the default value of $\delta z_1 = 0.0$, which turns off this adjustment factor (i.e., $F_{\delta z_1} = 0$). We believe this to be a reasonable default condition, because the remaining elements of the model are 'centered' on a condition of no $F_{\delta z_1}$ correction, as shown in Section 4.4.

4 Model Development

4.1 THREE-PHASE MODEL BUILDING PROCESS

In this chapter we describe the procedures used to build the GMPE. Model building occurred in three phases, which are described in detail in the following sections.

In Phase 1, we analyze subsets of data and simulation results to evaluate elements of the base-case model that would not be well-constrained if left as free parameters in the regression. Model elements evaluated in this way are c_3 (for apparent anelastic attenuation) and F_S (for site response). Phase 2 comprises the main regression for the base-case model shown in Equation (3.1). Phase 3 consists of mixed-effects regression analysis to check model performance and to develop adjustment factors for various secondary factors beyond **M**, *mech*, R_{JB}, and V_{S30}. The standard deviation model is also developed from Phase 3 analysis.

4.2 PHASE 1: SETTING OF FIXED PARAMETERS

There are several parameters that we "pre-set" before beginning the regression in order to ensure its stability and force behavior that we wish to constrain. In this section, we describe the parameters that are pre-set within the Phase 1 regression.

4.2.1 Apparent Anelastic Attenuation

Due to trade-offs between apparent geometric and apparent anelastic attenuation, regression cannot simultaneously determine both robustly; this arises because we cannot distinguish between the slope and the curvature of the distance decay from data with significant scatter. In this section, we describe regressions undertaken to constrain the apparent anelastic attenuation term, c_3, as part of Phase 1 model building.

In BA08, c_3 was constrained using four well-recorded small events (**M**4.3–6.0) in California. Much of the data used in that analysis was not contained in the NGA-West 1 flatfile. For the present analysis, we used the large inventory of data from small events ($\mathbf{M} \leq 5.0$) in California that are now available as part of the NGA-West 2 flatfile (this was a larger subset of data than used to derive the Phase 2 base-case GMPEs). Low-magnitude earthquakes were chosen to minimize possible complexities in the data associated with possible finite fault effects and nonlinear site effects. Using the model described in Section 4.2.2, we apply a site adjustment

to correct each observation to a reference V_{S30} of 760 m/sec. The data were then grouped into magnitude bins 0.5 in width (magnitude units), as shown in Figure 4.1, and regressed using an equation similar to Equation (3.3) but without the **M**-dependent geometric spreading term:

$$\ln Y_{ij} = \eta_i' + c_1' \ln\left(R/R_{ref}\right) + c_3\left(R - R_{ref}\right) \tag{4.1}$$

where η_i' is the event term for event i, j indicates a particular observation (and is implicitly contained in the distance R), $R_{ref} = 1.0$ km , and c_1' and c_3 are parameters fixed by the regression. The c_1' term represents the apparent geometric spreading for the magnitude bin; it would be expected to change with magnitude. The prime ($'$) is used on the event term and apparent geometric spreading term to indicate these are associated with the present analyses of binned data and are distinct from the Phase 2 regressions.

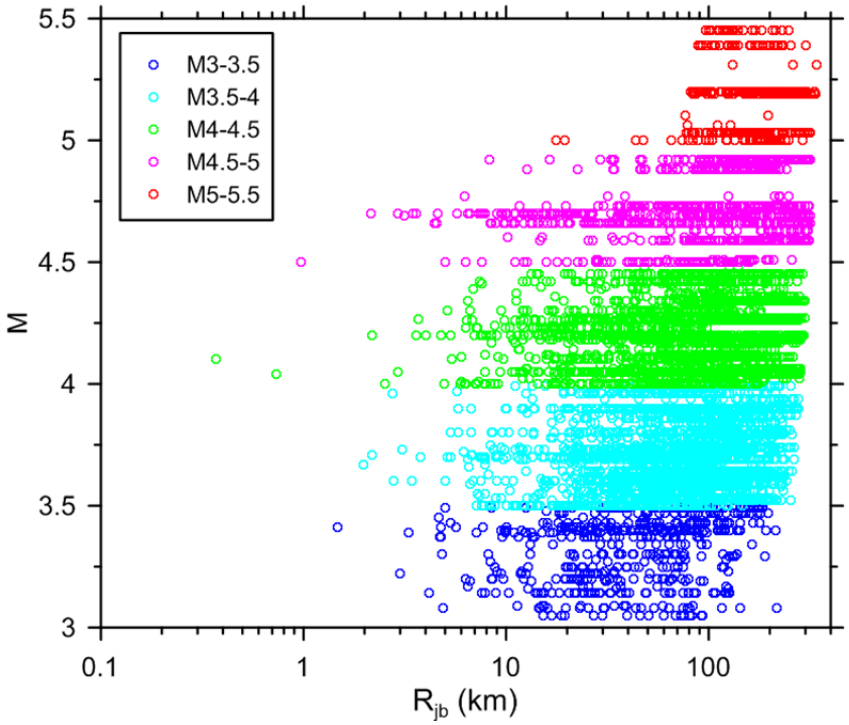

Figure 4.1 **Binned groups of California data in NGA-West 2 flatfile used for constraint of apparent anelastic attenuation term. The data for the M 5-5.5 bin was not used due to poor sampling for R_{JB} < 80 km.**

Examples of the distance dependence for several ground-motion IMs for the **M**4–4.5 bin are given in Figure 4.2. Note that the data at high frequencies (e.g., PGA) exhibit substantial curvature (indicating negative c_3) whereas the data for medium to long periods (e.g., PSA at 1.0 sec) exhibit negligible curvature. The resulting values of c_1' and c_3 are plotted for the various **M** bins in Figure 4.3. As expected, the c_1' terms are all negative, indicating attenuation with distance, with the absolute value decreasing (less decay) as magnitude increases. Conversely, the

c_3 terms are relatively independent of **M**, which is expected if they represent processes other than geometric spreading, such as apparent anelastic attenuation. The selected coefficients for c_3 are also shown in Figure 4.3. The applicability of these coefficients, which are based on California data, for other regions is examined in Section 4.4. Figure 4.4 compares the selected coefficients with those used in BA08. The c_3 terms are roughly similar between the two models, but the BSSA c_3 values are based on many more data.

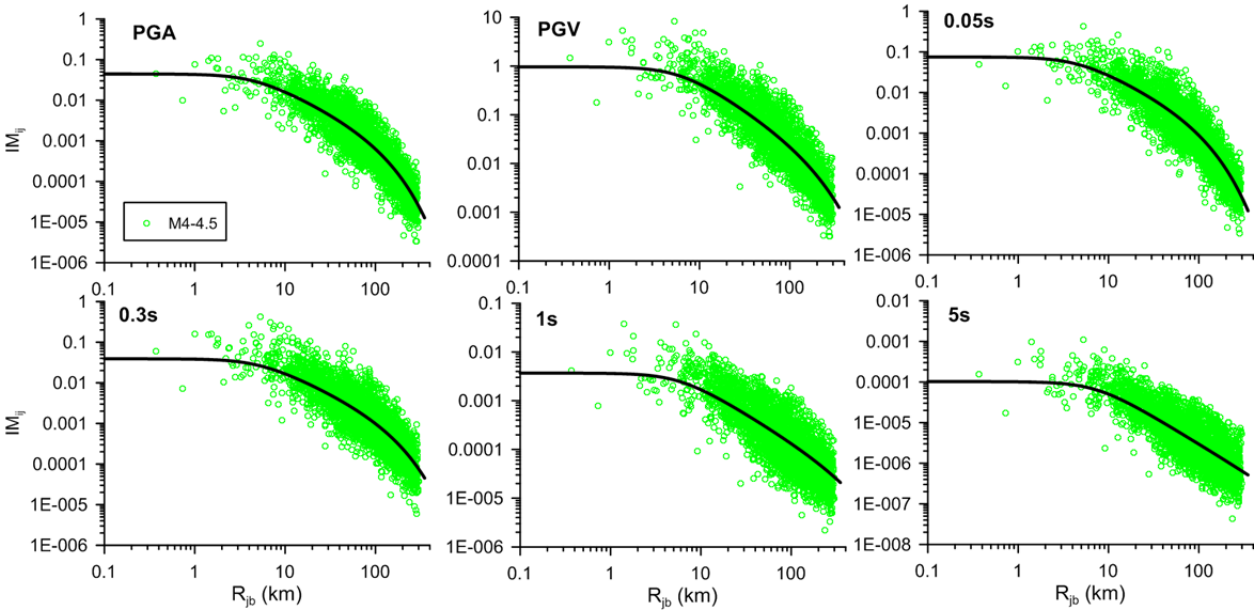

Figure 4.2 **California data and fit curve [Equation (4.1)] for M4–4.5 events. Data corrected to V_{S30} = 760 m/sec. Results show strong effects of apparent anelastic attenuation at high frequencies and negligible effects for $T \geq 1$ sec.**

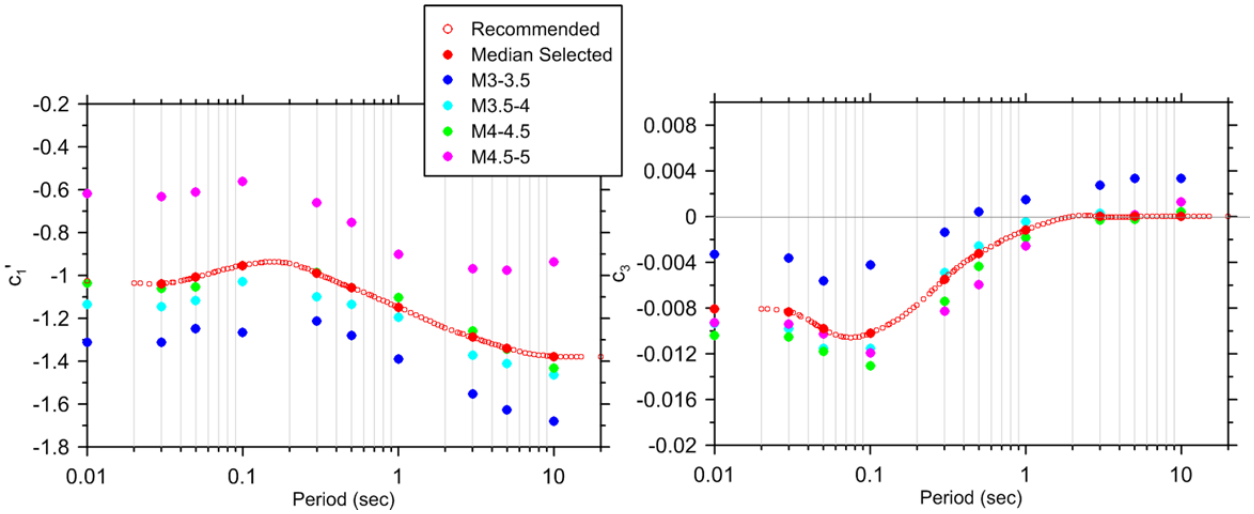

Figure 4.3 **Trends of apparent geometric spreading (c_1') and apparent anelastic attenuation (c_3) terms with period and magnitude. Results show significant M-dependence for c_1' but not for c_3.**

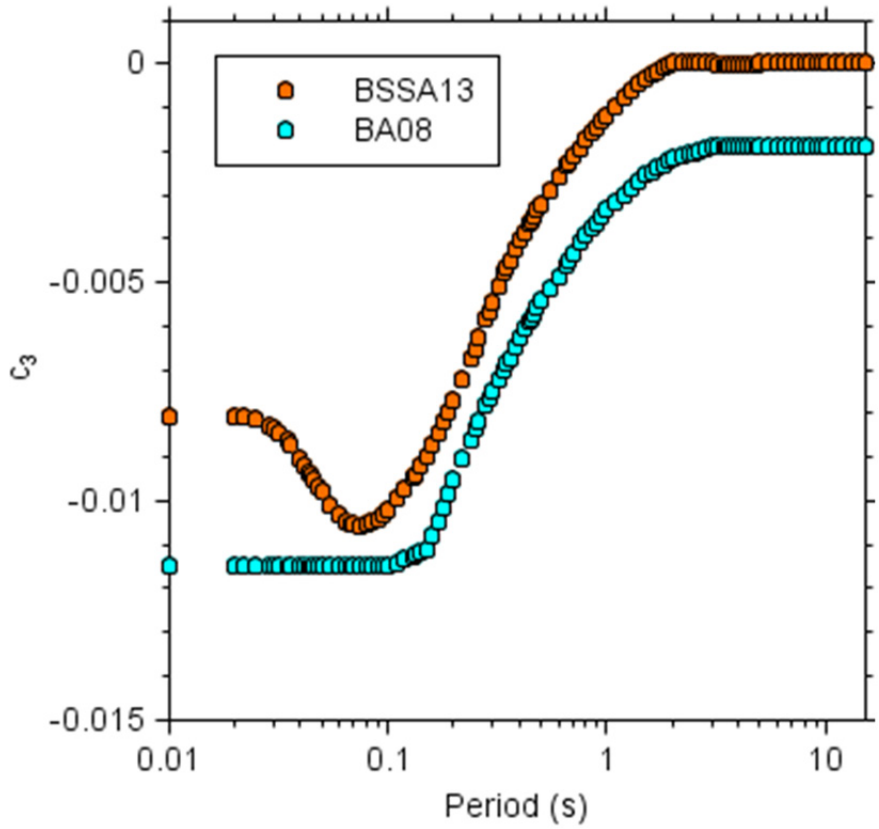

Figure 4.4 **Apparent anelastic attenuation terms (c_3) used in present model (BSSA13) and in BA08.**

4.2.2 Site Response

The model equations are as given in Section 3.2 with the $\ln(F_{lin})$ term representing V_{S30}-scaling and the $\ln(F_{nl})$ term representing nonlinear site response. We first constrain the nonlinear portion of the site response to enable robust determination of the linear part of the model. The nonlinear site response model is described briefly here, with further details given in Stewart and Seyhan [2013] (SS13). In this section, we briefly present the process by which the site factors were developed.

Model development occurs in two stages, the first to develop the nonlinear model and the second to develop the V_{S30}-scaling model. (Note: both of these two "stages" are substeps within the Phase 1 GMPE model building framework.)

Stage 1 Analysis of Site Response

The Stage 1 analyses develop estimates of parameter f_2 (see Equation 3.10) on the basis of available simulations and from the interpretation of NGA-West 2 data. The considered simulations are of one-dimensional ground response for many site profiles and input motions [Kamai et al. 2013; hereafter KEA13]. Our synthesis of the results from KEA13, and the manner by which f_2 values were extracted, is described in Section 4.3 of SS13 and is not repeated here.

The NGA-West 2 data analysis begins with the computation of rock residuals for each recording in the selected data set:

$$R_{ij} = \ln Y_{ij} - \left[\left(\mu_r \right)_{ij} + \eta_i \right] \tag{4.2}$$

where R_{ij} is the rock residual, Y_{ij} is the j^{th} observed (recorded) value of the ground-motion IM, μ_r is the mean (in natural log units) of a GMPE for rock conditions, and η_i is the event term for earthquake *i*. The rock site condition used in the computations is V_{S30} = 760 m/sec. Regarding the GMPE used to compute μ_r, our analyses were performed iteratively with respect to the development of the Phase 2 GMPE. Essentially, we began with an early (November 2012) version of the Phase 2 GMPE, from which site terms were regressed. Those site terms were then used in a subsequent Phase 2 GMPE derivation, and so on. The final set of site terms are consistent with the base-case GMPE described in Section 4.3 and include adjustments for regional apparent anelastic attenuation in high-Q and low-Q regions described in Section 4.4. In these analyses, we consider a much broader set of distances per the data selection criteria shown in Figure 2.1.

To investigate nonlinearity, we compile values of R_{ij} within bins of V_{S30} (< 200, 200–310, 310–520, 520–760, > 760 m/sec), which are plotted against PGA_r (median peak acceleration on rock) in Figure 4.5. We use least-squares regression to fit to the data an expression of the form given in Equation (3.10) with f_3 fixed at 0.1*g* (justification for this is given in Chapter 4 of SS13) to provide estimates of f_1 and f_2. The results illustrate similar trends between the simulations and the data.

Figure 4.6 shows values of the nonlinear parameter f_2 from data analysis and simulations. Also shown are slopes evaluated by Afacan et al. [2013] (using a fitting procedure similar to that described above), based on centrifuge modeling of soft clays. The simulation-based slopes are slightly steeper than the data-based slopes at short periods ($T < 0.5$ sec) but flatter (and even positive) for longer periods ($T > 1.0$ sec). The slopes derived from centrifuge modeling (at 100–120 m/sec) are similar to those at the lower limit of V_{S30} (V_{S30} = 150–200 m/sec) from simulations and data analysis for $T \leq 1.0$ sec. This suggests that a minimum floor on nonlinearity may be present for very soft sites, although such a feature is not presently included in our model, which we consider applicable for $V_{S30} = 150$ m/sec.

The nonlinear term f_2 is parameterized relative to V_{S30} following the functional form of Chiou and Youngs [2008] as given in Equation (3.11). Parameter f_4 controls the overall level of nonlinearity for soft soils. Parameter f_5 controls the shape of the V_{S30} dependency of the slope f_2. These parameters are plotted against period in Figure 4.7, along with the corresponding values used in CY08 (for comparison).

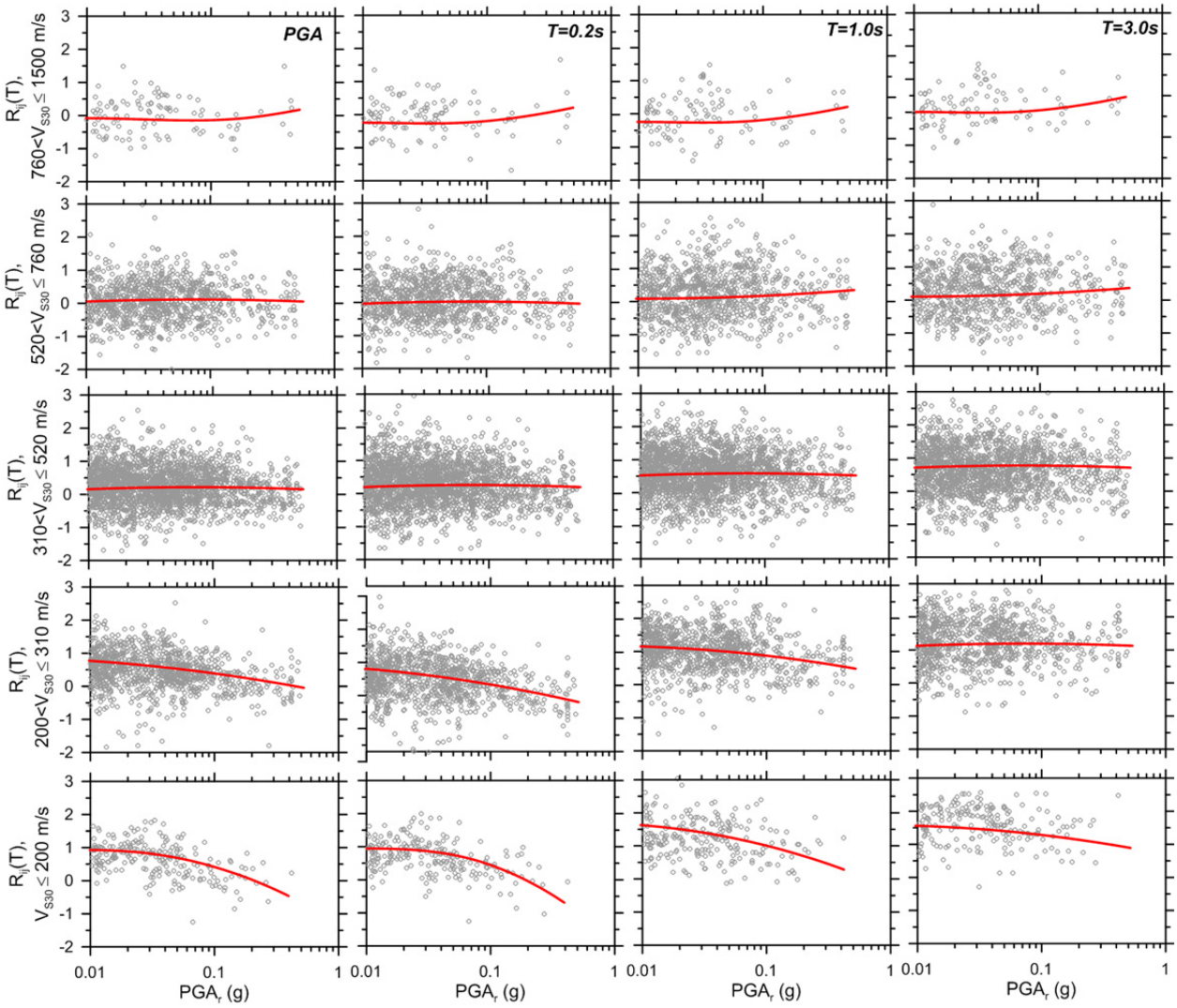

Figure 4.5 **Variation of site amplification factors with PGA_r within V_{S30} bins using full data set. Discrete symbols are intra-event residuals [R_{ij}, Equation (4.2)], line is nonlinear fit from Equation (3.10).**

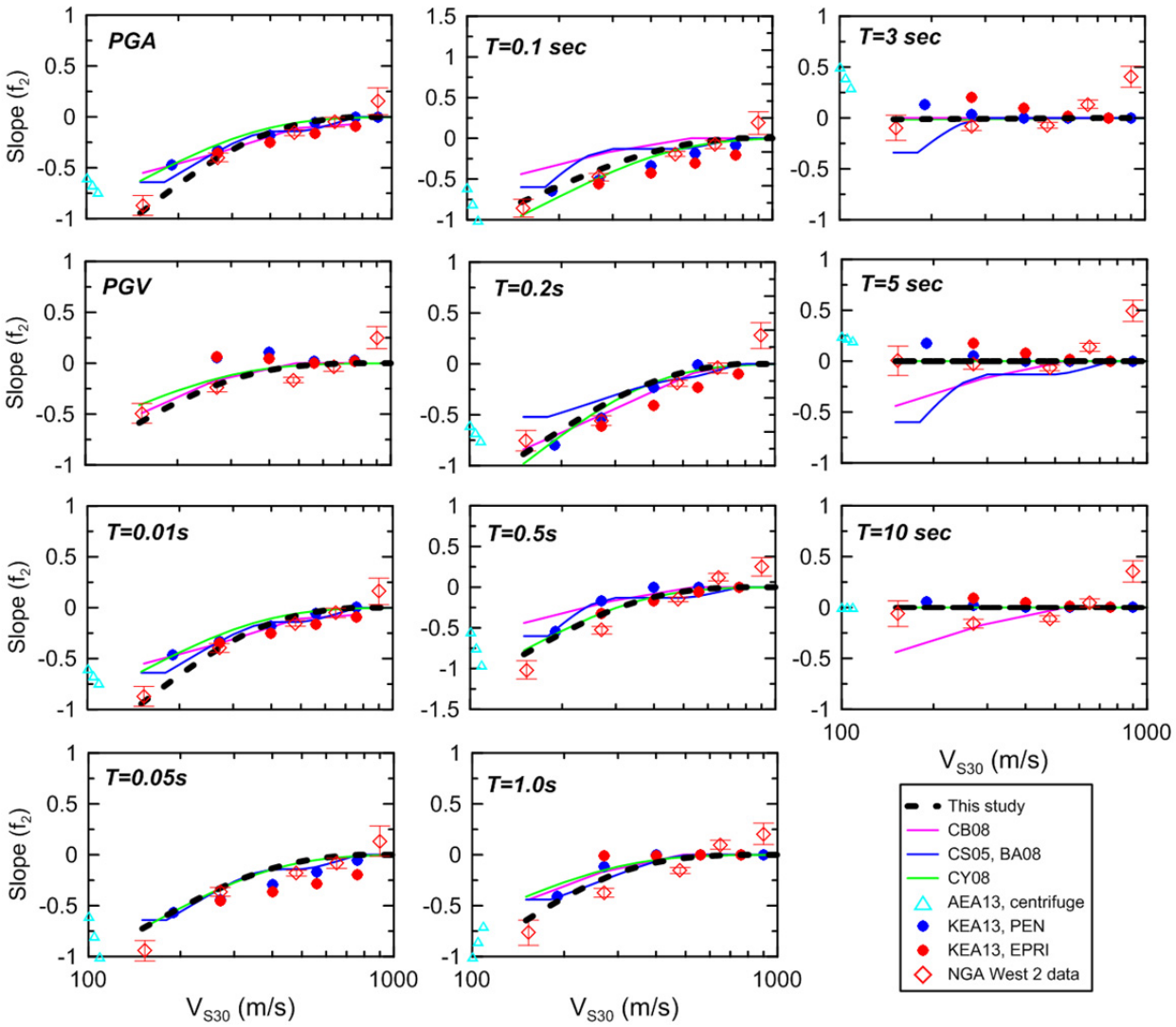

Figure 4.6 **Variation of slope f_2 with V_{S30} from NGA-West 2 data, centrifuge test data of AEA13, KEA13 simulation results (using modulus reduction curves labeled PEN for Peninsular range and EPRI), and site models in CB08 and CY08 GMPEs. The proposed model for this study is also given.**

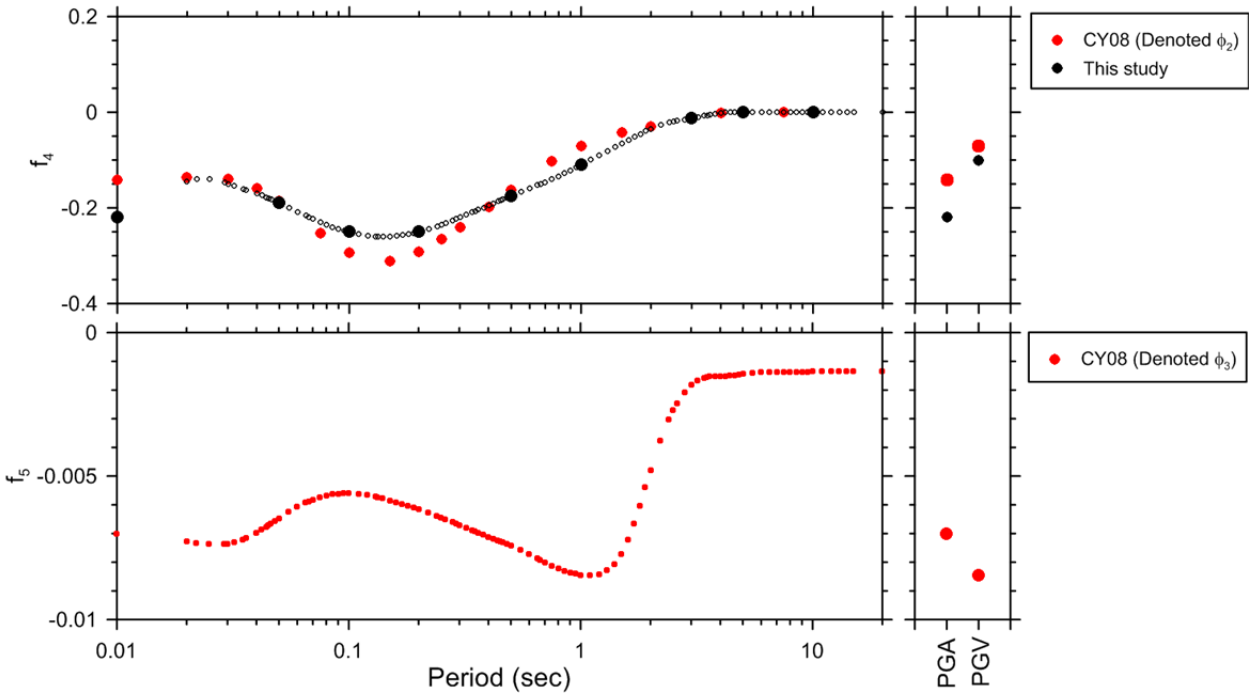

Figure 4.7 **Parameters f_4 and f_5 for nonlinear site amplification model as proposed by Chiou and Youngs [2008] (CY08) and revised for present study. Parameter f_4 and f_5 as used here were denoted ϕ_2 and ϕ_3 by CY08. We adopted CY08 values of f_5.**

Stage 2 Analysis of Site Response

We begin with residuals R_{ij} [Equation (4.2)], which are adjusted by removing nonlinear effects as predicted by the F_{nl} model [Equation (3.10)]:

$$R_k^{lin} = R_{i,j} - \ln(F_{nl}) \tag{4.3}$$

The modified residual, R_k^{lin}, is intended to apply for linear (small strain) conditions. Subscript k in R_k^{lin} is an index spanning across all available data points; we drop the event and within-event subscripts (i and j, respectively) because of the removal of event terms in the computation of R_{ij}, which allows all data points to be weighted equally. The residuals for the full (combined) data set and individual regions are then regressed in a least-squares sense against V_{S30} [using Equation (3.9)] to establish the c parameter for $V_{S30} < V_c$. Results for several periods and regions are plotted in Figure 4.8. Slopes are generally negative, which is expected, as this indicates stronger ground motion for softer soils. Slopes also tend to increase with period over the range considered, which is also consistent with past experience (e.g., BJF97 and the 2008 NGA models).

Note that the results from California in Figure 4.8 indicate a break in the V_{S30} scaling for fast velocities and longer periods (as seen in the results for $T = 1.0$ sec). It is this break in slope

that motivated the use of the corner velocity V_c in the linear portion of the site amplification function [Equation (3.9)].

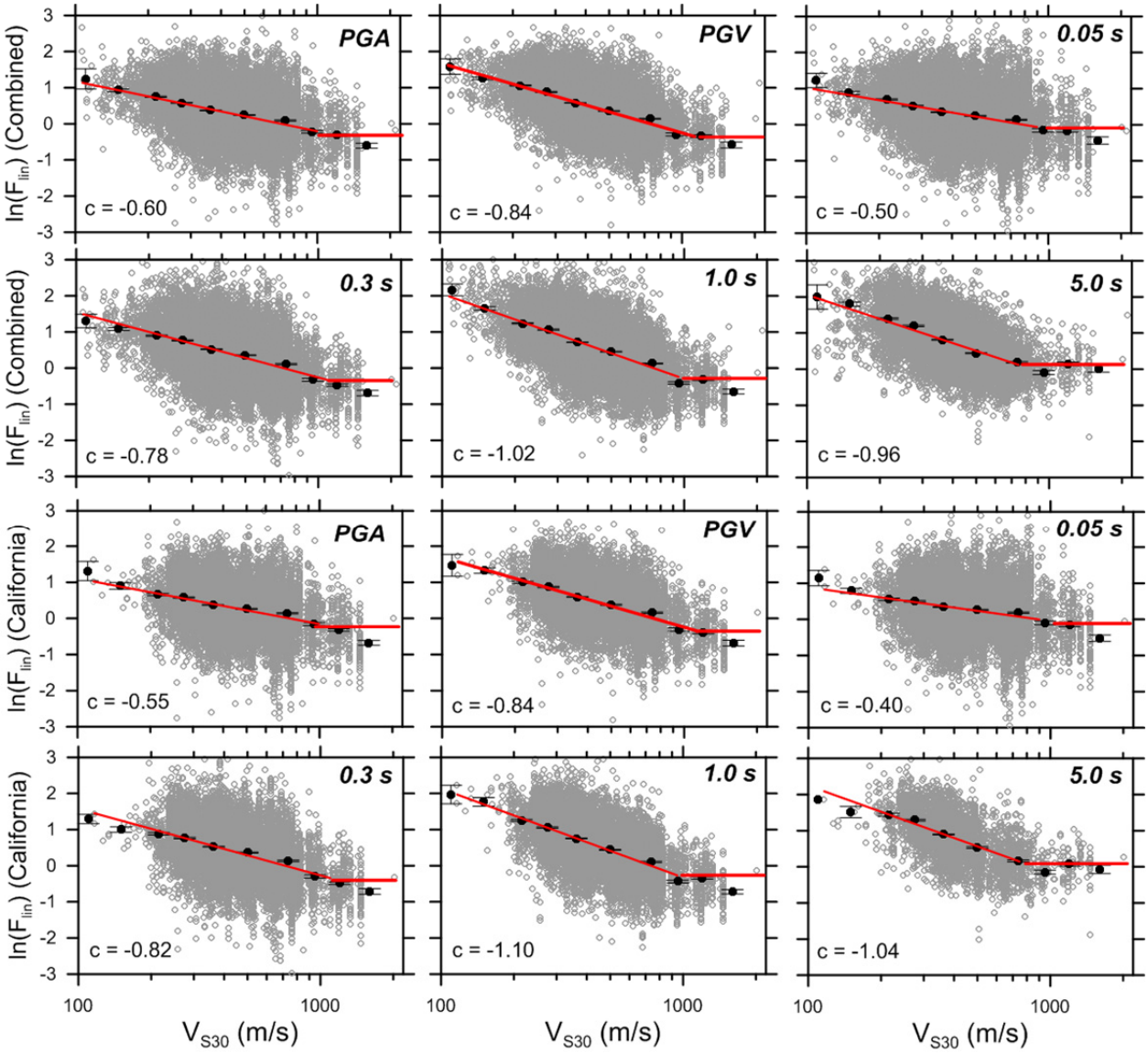

Figure 4.8a **Variation of linearized site amplification [Equation (4.3)] with V_{S30} for combined data set and subset from California. Red line indicates model prediction, black dots are binned means and their 95% confidence intervals.**

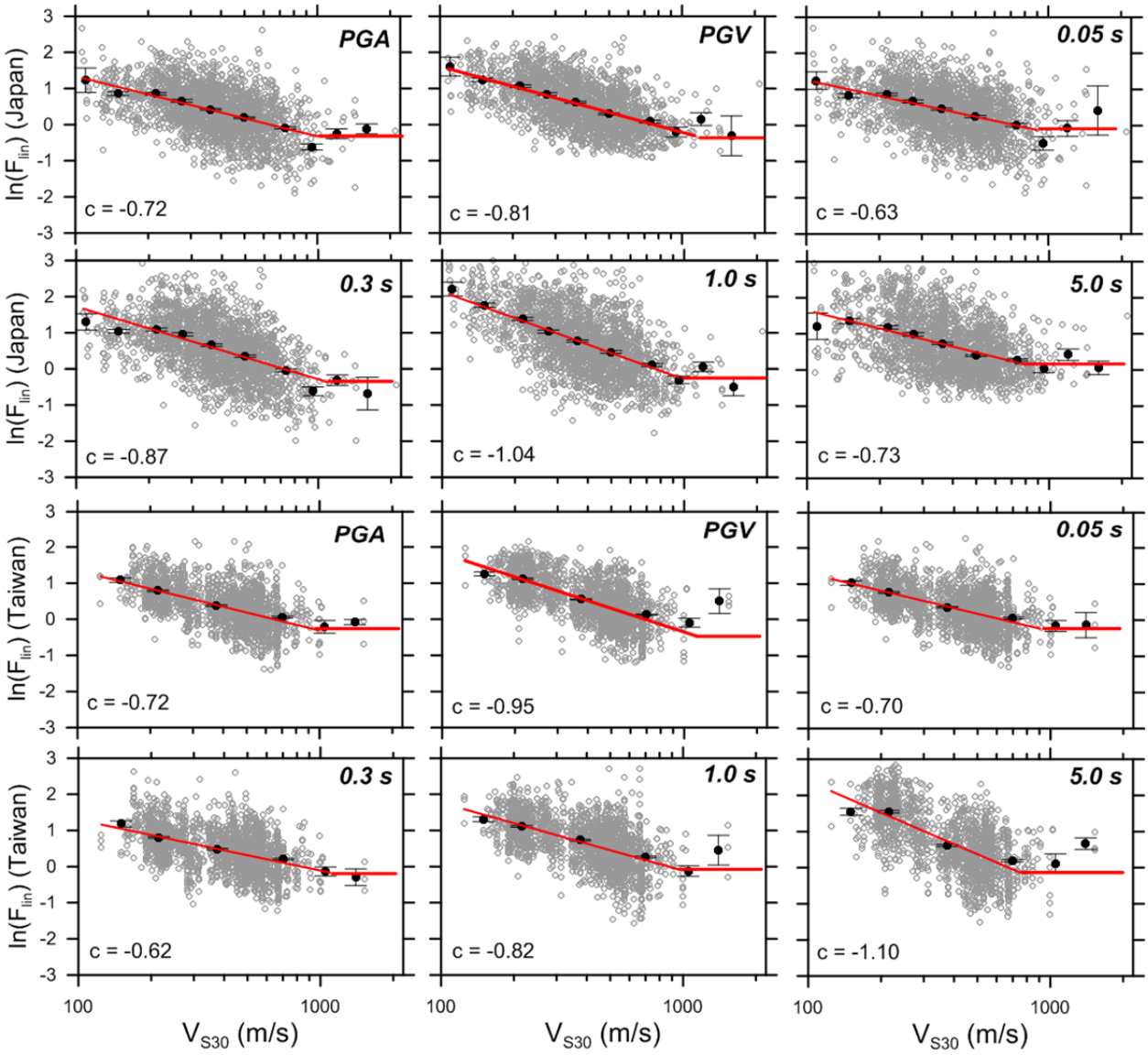

Figure 4.8b Variation of linearized site amplification [Equation (4.3)] with V_{S30} for subset of data from Japan and Taiwan.

We plot in Figure 4.9 the slope parameter c for V_{S30}-scaling as a function of spectral period for the combined data set and various regions (California, Japan, Taiwan, and other). Additional regions are considered in SS13. Since the regression for c is least squares, all data points are weighted equally. Accordingly, the 'combined' result is influenced strongly by regions with large amounts of data relative to those with fewer data (weights are listed in Figure 4.9). We find relatively consistent values of c for all regions, especially at short periods. As shown in Section 4.2 of SS13, strong regional variations in c could be found if the data were interpreted differently. In particular, if a data cut-off distance of 80 km is applied (i.e., to avoid the use of recordings having potentially significant effects of anelastic attenuation), c values vary strongly between regions. Similar sensitivites of the V_{S30} slope parameter have been observed previously by Chiou and Youngs [2012].

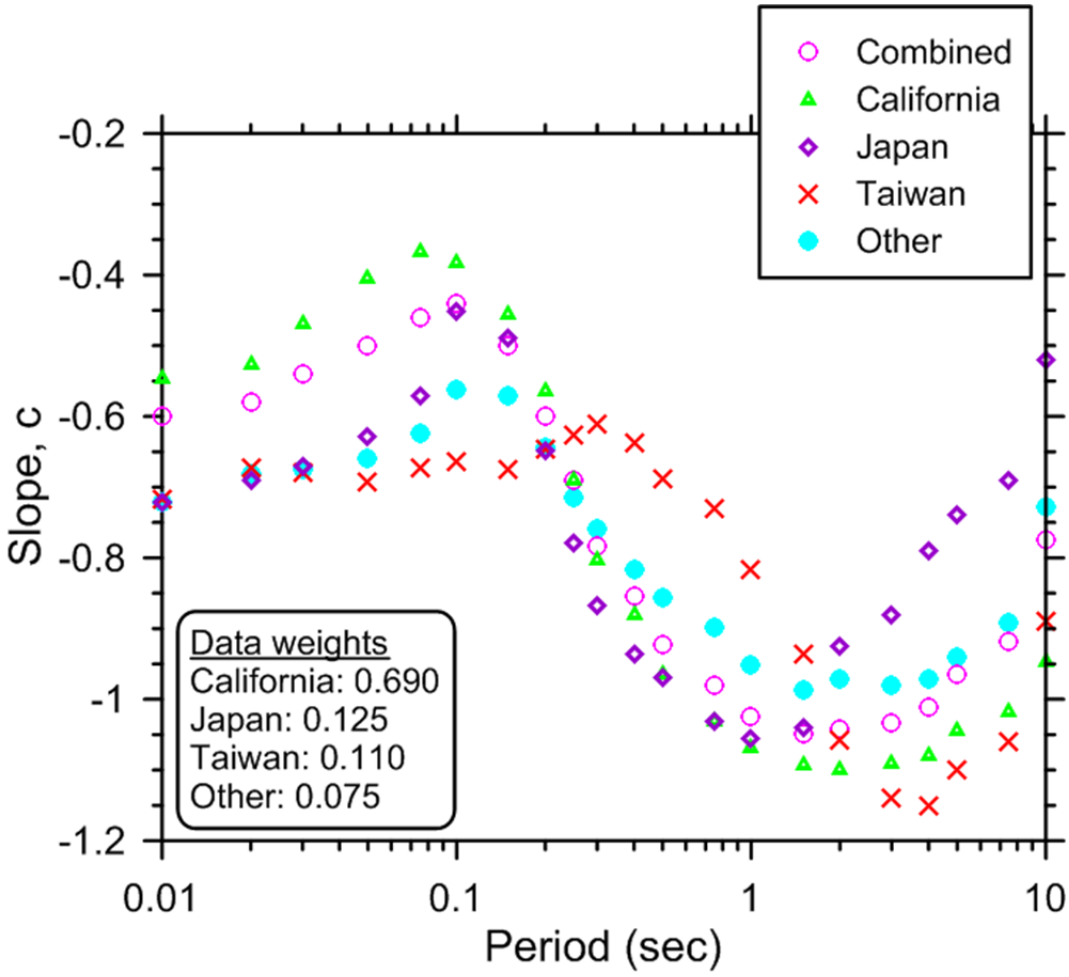

Figure 4.9 **Variation of slope (*c*) within spectral periods for combined data set and various regions. Data weights refer to the relative contributions to the 'combined' slope.**

At this stage, we are not recommending a regional c term for V_{S30}-scaling. However, we recognize that: (*i*) the variability of c terms is relatively high, especially at longer periods; and (*ii*) the lack of a dependence of c on region is difficult to reconcile with the findings of previous site-response studies pointing to the strong amplification of sites in Japan at short periods (e.g., Atkinson and Casey [2003]; Ghofrani et al. [2013]; Stewart et al. 2013; and Anderson et al. [2013]). Thus, we may return to this issue of regionalization of the site-response term at a later stage.

4.3 PHASE 2: TWO-STAGE REGRESSIONS

4.3.1 Two Stage Methodology

The selected ground motion IMs of PGA, PGV, and PSA from the NGA-West 2 flatfile were regressed against predictor variables using Equation (3.1) to determine $F_{P,B}$ and F_E, after first adjusting all observations to the reference velocity of 760 m/sec, using the site amplification model given in Section 3.2. This allows us to perform the regression analyses for the case where $F_S = 0$. The analyses were performed using the two-stage regression discussed by Joyner and Boore [1993, 1994]. In Stage 1, we evaluate the $F_{P,B}$ component of the model, the average motions at the reference distance R_{ref} (which are used in Stage 2), and the within-event aleatory variability, ϕ. In Stage 2, we evaluate the F_E component of the model and the between-event variability, τ. All regressions were done period-by-period without smoothing, although some of the constrained coefficients were smoothed.

The coefficients for PGA_r used in the nonlinear site amplification function were determined by an iterative series of regressions; this is a refinement relative to the BA08 methodology. We started with assumed coefficients to determine PGA_r, then after Stage 1 regression we adjusted them to match the coefficients obtained in the regression for PGA. Typically around 3 to 6 iterations were required before the PGA_r coefficients had little change between iterations. The iteration allows us to ensure that the base-case GMPE for PGA is the same as that used in determining the nonlinear site amplification adjustments (in BA08 the regression equation for PGA did not exactly match that used to determine PGA_r).

All computations were performed using Fortran programs developed by the first author, in some cases incorporating legacy code from programs and subroutines written by W. B. Joyner.

4.3.2 Stage 1: Distance Dependence

The distance dependence is determined in the Stage 1 regression, where the dependent ground-motion IMs are PGA, PGV or PSA at a selected period, in each case adjusted to the reference velocity of 760 m/s by subtracting F_S as defined in Equation (3.8) from the $\ln Y$ observed ground-motion IM. The adjusted ground-motion IMs for our selected subset of the NGA dataset (described in Section 2.1) are regressed against distance using Equation (4.4), which is the same as Equation (3.3) but with event-term variables $\left(\overline{\ln Y}\right)_j$ added to represent the average observations for earthquake *j* adjusted to $R_{JB} = R_{ref}$:

$$F_{P,B}\left(R_{JB}, \mathbf{M}\right) = \left(\overline{\ln Y}\right)_j + \left[c_1 + c_2\left(\mathbf{M} - \mathbf{M}_{ref}\right)\right]\ln\left(R / R_{ref}\right) + c_3\left(R - R_{ref}\right) \tag{4.4}$$

In Equation (4.4), $\left(\overline{\ln Y}\right)_j$ is shorthand for the sum

$$\left(\overline{\ln Y}\right)_1 \delta_1 + \left(\overline{\ln Y}\right)_2 \delta_2 + \cdots + \left(\overline{\ln Y}\right)_{NE} \delta_{NE} \tag{4.5}$$

where δ_j is a dummy variable that equals 1 for event j and zero otherwise, and NE is the number of earthquakes.

In this regression, the apparent anelastic attenuation term c_3 is pre-set using the values obtained from the Phase 1 study, as described in Section 4.2.1. We consider this to be a reasonable initial approach that is tested later by examining residual trends in Section 4.4 for the data set as a whole and subsets of data organized by region.

With c_3 constrained, we performed the regression indicated in Equation (4.4) to estimate c_1, c_2, and h, as well as $\left(\overline{\ln Y}\right)_j$ for each earthquake. All data passing the exclusion criteria discussed in Section 2.1 were used, to a maximum distance of R_{JB} = 80 km. The c_1 coefficient is the apparent geometric spreading rate (slope) for an event of $\mathbf{M} = \mathbf{M}_{\text{ref}}$, while c_2 modifies the slope for **M** greater or smaller than $\mathbf{M}_{\text{ref}}$ (i.e., magnitude-dependent geometric spreading). A preliminary estimate of within-event aleatory uncertainty ϕ is given by the standard deviation of the residuals from the Stage 1 regression.

In the regressions, we assigned values for: (*i*) the reference distance, R_{ref}, at which near-source predictions are pegged, and (*ii*) the reference magnitude, $\mathbf{M}_{ref}$, to which the magnitude dependence of the geometric spreading is referenced. The assigned values for these reference values are arbitrary, and are largely a matter of convenience. For $\mathbf{M}_{ref}$, we chose a value of 4.5, since this is the approximate magnitude of much of the data used to determine the fixed c_3 coefficients. The consequence of this choice is that the magnitude dependence of the slope will be referenced to that observed for small events. We use R_{ref} = 1 km, which is convenient because the curves describing the distance dependence pivot around $R = R_{ref}$. The geometric spreading for larger magnitudes is flatter than for smaller magnitudes, which can lead to overlap of IM versus R_{JB} curves at distances less than the pivot distance. Thus, the selection of $R_{ref} = 1\,\text{km}$ prevents unrealistic "crossing" of the IM versus R_{JB} curves at close distances. (Note: any value of $R_{ref} < h$ (minimized over all periods) would prevent undesirable overlapping of prediction curves near the source.)

We encountered a difficulty in the regression having to do with coupling between the Stage 1 and 2 regressions, which is a consequence of the magnitude-dependent apparent geometric spreading. In our initial regressions, in which we fixed c_3 but used data to $R_{JB} = 400$ km (as in BA08), we found the Stage 2 magnitude scaling to be very different from that obtained by BA08. Following the advice of K. Campbell [2012, *personal communication*], we redid the regressions using data for $R_{JB} \leq 80$ km (still including fixed values of c_3). This stabilized the results and provided better-behaved magnitude scaling. Hence, the rationale for using just the data at $R_{JB} < 80$ km in the Phase 2 regression is that it provides for relatively robust magnitude scaling. However, we recognize that the GMPE must perform reasonably well at greater distances to be useful for general seismic hazard applications. Thus we address the applicability of the attenuation for larger distances from residuals analysis.

4.3.3 Stage 2: Magnitude and Fault-Type Dependence

The $\left(\overline{\ln Y}\right)_j$ terms from the Stage 1 regression (subsequently referred to as $\overline{\ln Y}$) were used in a weighted Stage 2 regression to evaluate the magnitude scaling of ground-motion IMs. As described in Section 2.1, only events with more than four observations with $R_{JB} \leq 80$ km were used in the regression.

The functional form selected for magnitude scaling matches that used in BA08, but we made three significant changes to the BA08 procedure, which we discuss in greater detail below:

1. Based on examination of plots of $\overline{\ln Y}$ versus **M**, we determined that the hinge magnitude $\mathbf{M}_h$ should increase with *T*, whereas it had been fixed at 6.75 in BA08.
2. In BA08 the magnitude regression initially used a single quadratic. If the peak of the quadratic occurred at $\mathbf{M} \leq 8.5$, the regression was performed a second time using two polynomials hinged at $\mathbf{M}_h$ (quadratic for $M \leq \mathbf{M}_h$, linear for $M > \mathbf{M}_h$). If the slope of the linear function was negative, the regression was performed a third time, with the constraint that the slope of the linear function is zero. Typically the magnitude function was made up of two polynomials for periods less than about 2 sec, and one polynomial for greater periods. When we used this procedure with the NGA-West 2 flatfile, we found that when plotted versus period the switch from two polynomials to one polynomial led to a discontinuity in PSA for large magnitudes, as illustrated in Figure 4.10. We found that the discontinuities could be removed by always using two polynomials.
3. We removed the requirement imposed by BA08 that the slope of the magnitude scaling function [e_6 in Equation (3.5b)] for $\mathbf{M} > \mathbf{M}_h$ must be greater than zero.

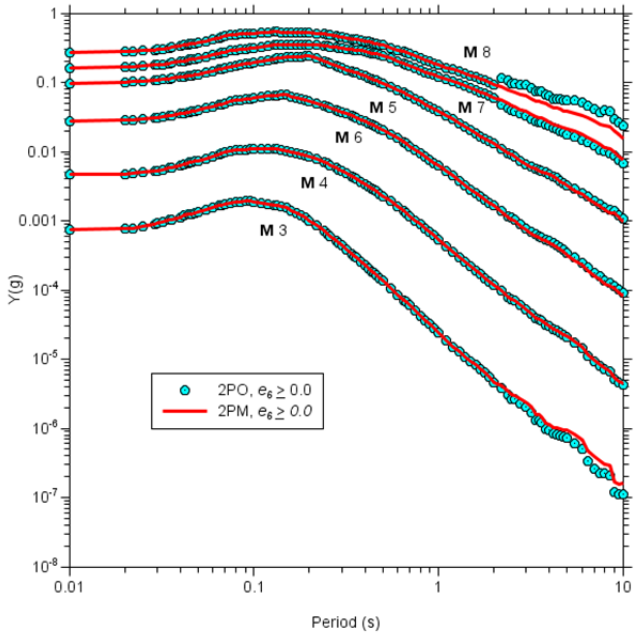

Figure 4.10 **PSA from GMPEs developed during an early stage of our analysis. "2PO" and '2PM" stand for "two polynomials optional" and "two polynomials mandatory".**

Choice of M_h:

Plots of $\overline{\ln Y}$ against $\mathbf{M}$ were evaluated independently by the three senior members of the developer team for various ground-motion IMs, and each member independently picked values of $\mathbf{M}_h$ to be used in Stage 2 regressions. Selections of $\mathbf{M}_h$ become quite large for long periods, and formal regression using the larger values of $\mathbf{M}_h$ often found small or even negative values of e_6 for these long-period IMs. This is contrary to general seismological theory, as illustrated by the prediction of simulations regarding magnitude scaling shown in Figure 4.11 (and supported by the trends in the sparse large magnitude data), and is a consequence of the few data available to constrain the slope of the linear function for $\mathbf{M} > \mathbf{M}_h$ in a formal regression fit to the data. We experimented with regressions using different values of $\mathbf{M}_h$ roughly consistent with plots of $\overline{\ln Y}$ against $\mathbf{M}$ and found that we could ensure robust scaling on both sides of the hinge, while allowing appropriate scaling behavior to be data-driven at all periods, by letting the maximum $\mathbf{M}_h$ be 6.2. This is a compromise between using more complex equations for the magnitude scaling and using something that is easy to implement. The dependence of $\mathbf{M}_h$ on T that we adopted is shown in Figure 4.12; it allows a robust determination of the slope of the linear function and provides reasonable agreement with the behavior seen in plots of $\overline{\ln Y}$ against $\mathbf{M}$.

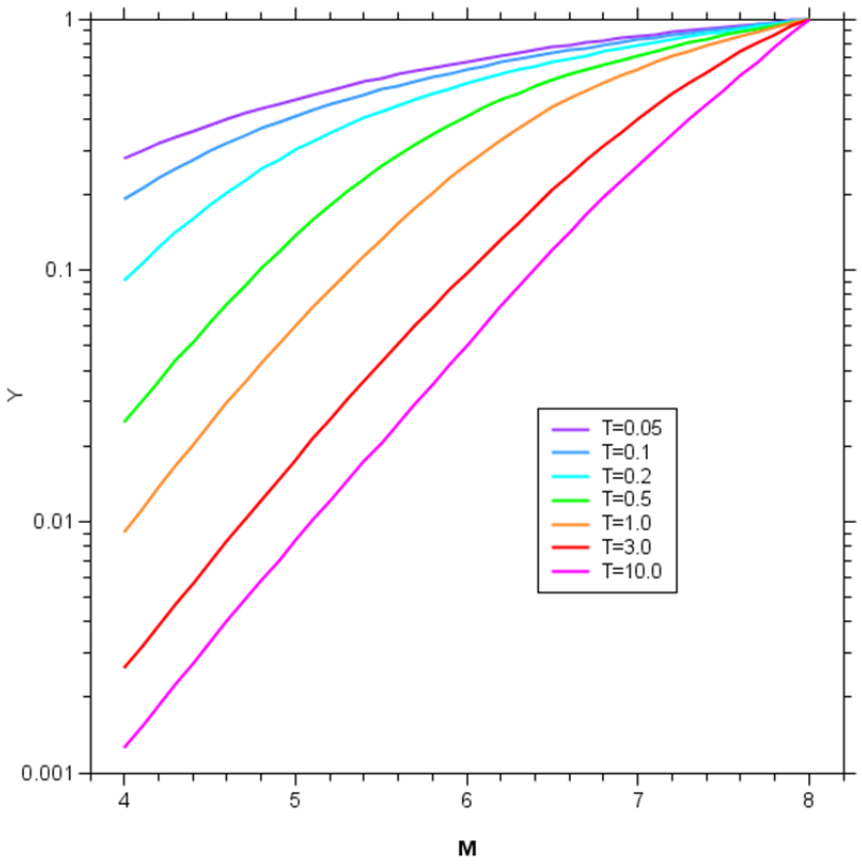

Figure 4.11 **Theoretical magnitude scaling, normalized to the value at M8. The simulations were done using the SMSIM program [Boore 2005], for the Atkinson and Silva [2000] source model, for a closest distance of 0.01 km, modified by Atkinson and Silva's [2000] finite-fault factor (Equation 4 in AS00 and discussion below that equation).**

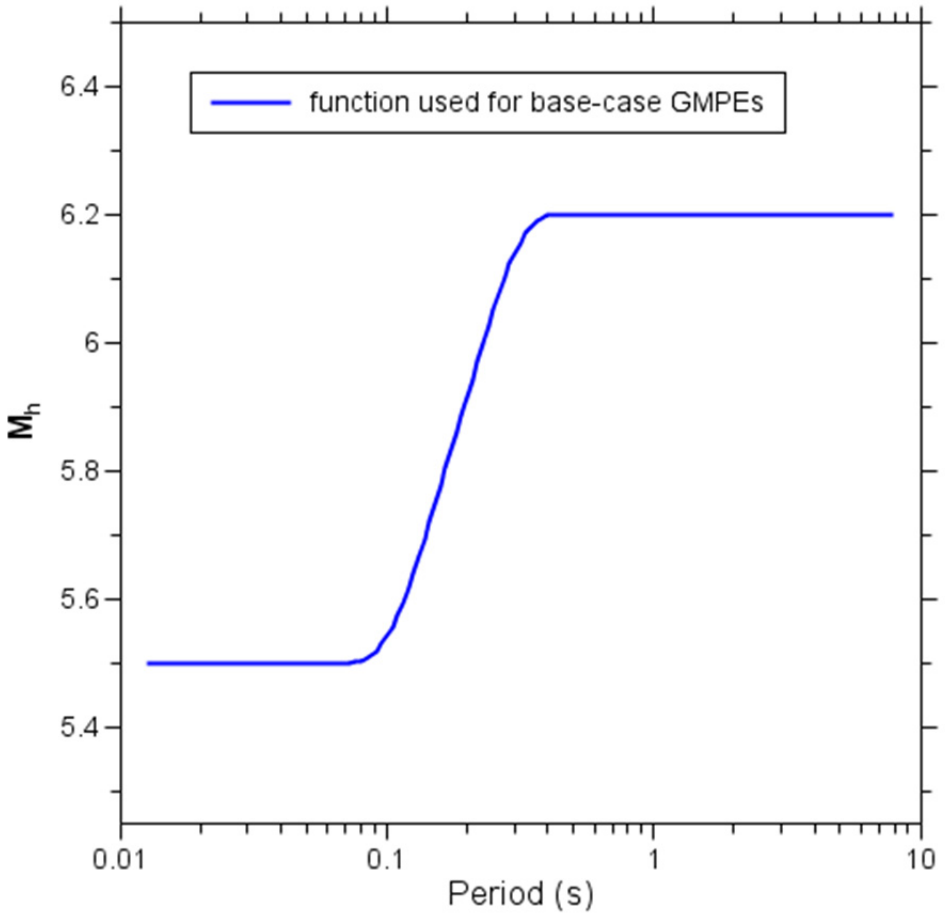

Figure 4.12 **Period variation of hinge magnitude $\mathbf{M}_h$. The original function was tripartite, with hinges at periods of 0.1 and 0.3 sec; we smoothed this slightly to round off the abrupt changes in slope at these periods.**

Magnitude Scaling for $M > M_h$:

We do not constrain the slope of the linear function for $\mathbf{M} > \mathbf{M}_h$ (parameter e_6) to be positive (this is a change from BA08). The NGA-West 2 data strongly support a decrease in $\overline{\ln Y}$ with $\mathbf{M}$ for $\mathbf{M} > \mathbf{M}_h$ at short periods. It is important to realize that even though we allow oversaturation (i.e., $e_6 < 0$) of $\overline{\ln Y}$, the resulting GMPEs do not show oversaturation of PSA for large magnitudes and close distances, as we illustrate below. The explanation of this apparent inconsistency is that the $\overline{\ln Y}$ values are the averages of the observed motions adjusted to a reference distance of 1 km [see Equation 3.5)]. The definition of R is such that it can never be less than the pseudo-depth h, even when $R_{JB} = 0$ km. As h is always greater than 3.9 km, the apparent decrease of motion from the magnitude scaling in Equation (3.5) is more than compensated for by the magnitude-dependent apparent geometrical spreading in Equation (3.3).

Fault-Type Dependence:

In BA08 the Stage 2 regression was performed several times to compute the fault-type coefficients. In the first regression, all $\overline{\ln Y}$ data were regressed against **M**, and then in the second regression this **M**-dependence was fixed and offsets of $\overline{\ln Y}$ for the fault types SS, NS, and RS were determined. We felt that this procedure was too convoluted and could lead to biases, depending on the mix of SS, NS, and RS events. In the current work, we compute the magnitude scaling coefficients and the fault-type coefficients simultaneously. The coefficient for unspecified fault type (e_0) is then computed as a weighted average of the SS, NS, and RS coefficients (e_1, e_2, and e_3). The weights used are 0.58, 0.12, and 0.30 for SS, NS, and RS events, respectively. These weights are the relative fractions of all events that we use for 1.0 sec PSA with **M** $\geq$ 5.0 (the fraction of SS events is larger for smaller events, but we felt that our weights should reflect magnitudes of engineering interest).

4.3.4 Smoothing of Coefficients

The coefficients obtained from the regression analysis (for which each period was analyzed separately) are generally smooth over a wide range of magnitudes and periods, as shown in Figure 4.13a. There is some jaggedness, however, for large and small magnitudes at periods exceeding about 2 sec. This jaggedness is probably due to the decrease in number of recordings available at longer periods (as shown in Figure 2.5).

Because the jaggedness in coefficients leads to undesirable jaggedness in spectra, we removed it by smoothing the regression coefficients. This was done in a series of steps described here. We first smoothed the pseudo-depth variable *h*. As shown in Figure 4.13b, a simple running mean did not produce enough smoothing of the variation over a narrow period range centered at about 2.5 sec. We are not sure what is controlling this variation, but we know of no physical reason for it to occur. For that reason, we smoothed through the oscillation by eye, with the result shown by the red line in Figure 4.13b.

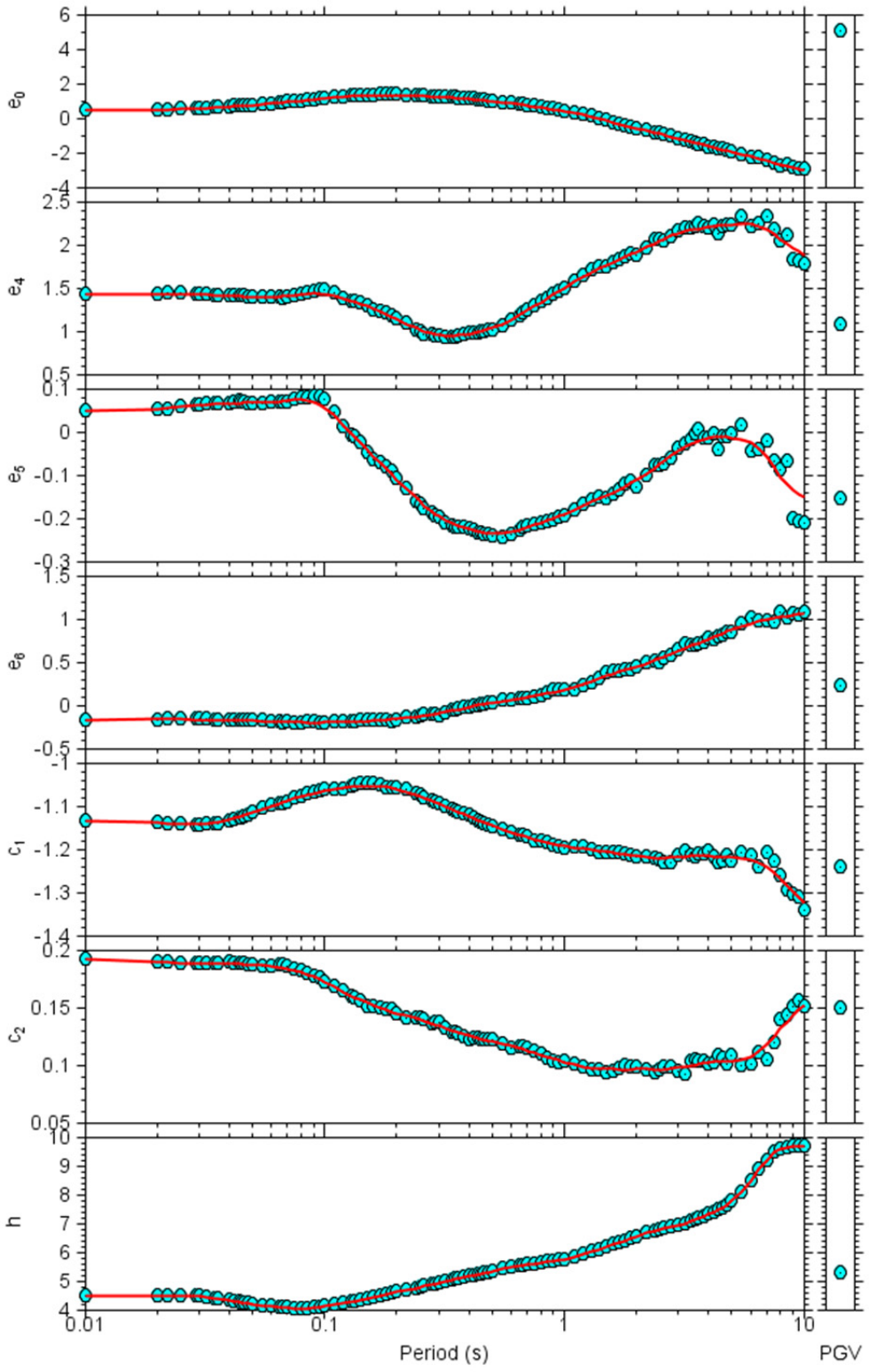

Figure 4.13a **Period variation of model parameters shown in unsmoothed (discrete symbols) and smoothed (red line) forms.**

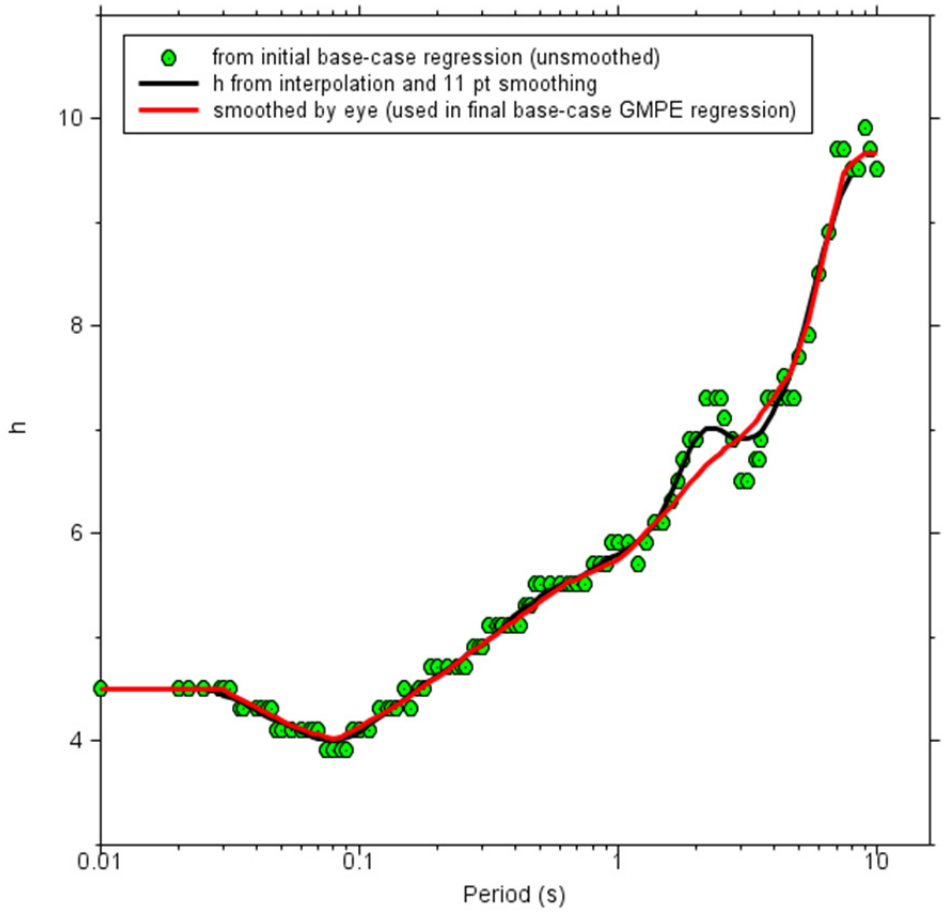

Figure 4.13b Period variation of pseudo-depth *h* with smoothing.

We then re-ran the base-case regression, constraining the values of h at the smoothed values shown in Figure 4.13b (we also constrained $\mathbf{M}_h$, using slightly smoothed values that removed the discontinuity in slope as a function of period, but the effect of using smoothed versus unsmoothed $\mathbf{M}_h$ was imperceptible). The next step was to interpolate the coefficients to periods with constant log spacing of 0.02 log units (the periods in the flatfile do not have constant spacing in log period). These interpolated values were smoothed using a running mean of 3, 5, 7, 9, and 11 points. We determined subjectively that the 11-point running mean provided the best smoothing. These 11-point smoothed values of coefficients were taken for use in the base-case GMPEs (when the periods used in the smoothing function do not align perfectly with the GMPE periods, interpolation was used to sample at the GMPE periods). Figure 4.13a shows the unsmoothed and smoothed coefficients based on the 14 March 2013 flatfile.

4.3.5 Regression Results

Magnitude-Scaling:

Figure 4.14 shows results of Stage 2 regressions of $\overline{\ln Y}$ against $\mathbf{M}$ for various periods. The portion of this plot for $\mathbf{M} > \mathbf{M}_h$ is of particular importance for practical application in the

western U.S. and other active crustal regions. The largest $\mathbf{M}$ events in the data set are two $\mathbf{M}$7.9 earthquakes (Denali, Alaska, and Wenchuan, China) that have relatively low $\overline{\ln Y}$ values. By virtue of having the largest value on the abscissa, they influence slope parameter e_6 to a larger extent than individual events at smaller $\mathbf{M}$. Two effects in particular were examined carefully with respect to the scaling of $\overline{\ln Y}$ against $\mathbf{M}$ for $\mathbf{M} > \mathbf{M}_h$: (1) oversaturation of $\overline{\ln Y}$ at short periods; and (2) sensitivity of e_6 to the Wenchuan event at long periods, due to that earthquake being the sole data source for $T > 7.5$ sec (the Denali data do not meet the low-cut filter criteria in a sufficient number of recordings for the event to be used at such periods).

With regard to the oversaturation issue, Figure 4.14 shows results with and without the constraint that the coefficient e_6 be ≥ 0; this examines the importance of allowing oversaturation of $\overline{\ln Y}$ for $\mathbf{M} > \mathbf{M}_h$. Differences only occur at short periods, and appear to be relatively small. However, as shown in Figure 4.15, the difference in the predicted motions can be substantial for large magnitudes. The maximum difference in Y from the two sets of GMPEs (with and without allowing oversaturation of the magnitude scaling term) is a factor of 1.34 for $\mathbf{M}8.5$. This difference decreases as magnitude decreases. We have opted to allow the data to determine the magnitude scaling, as these are, after all, empirical GMPEs; furthermore, simulation-based studies have provided some support for oversaturation at high frequencies [Schmedes and Archuleta 2008]. The issue of whether the scaling observed in the data is physically-justified, or may be possibly due to some limitations in the database, is a subject that should be pursued in further studies. In the context of the present study, it should be acknowledged that uncertainty in the appropriate magnitude scaling at large magnitudes is a source of epistemic uncertainty in the development and application of empirical GMPEs.

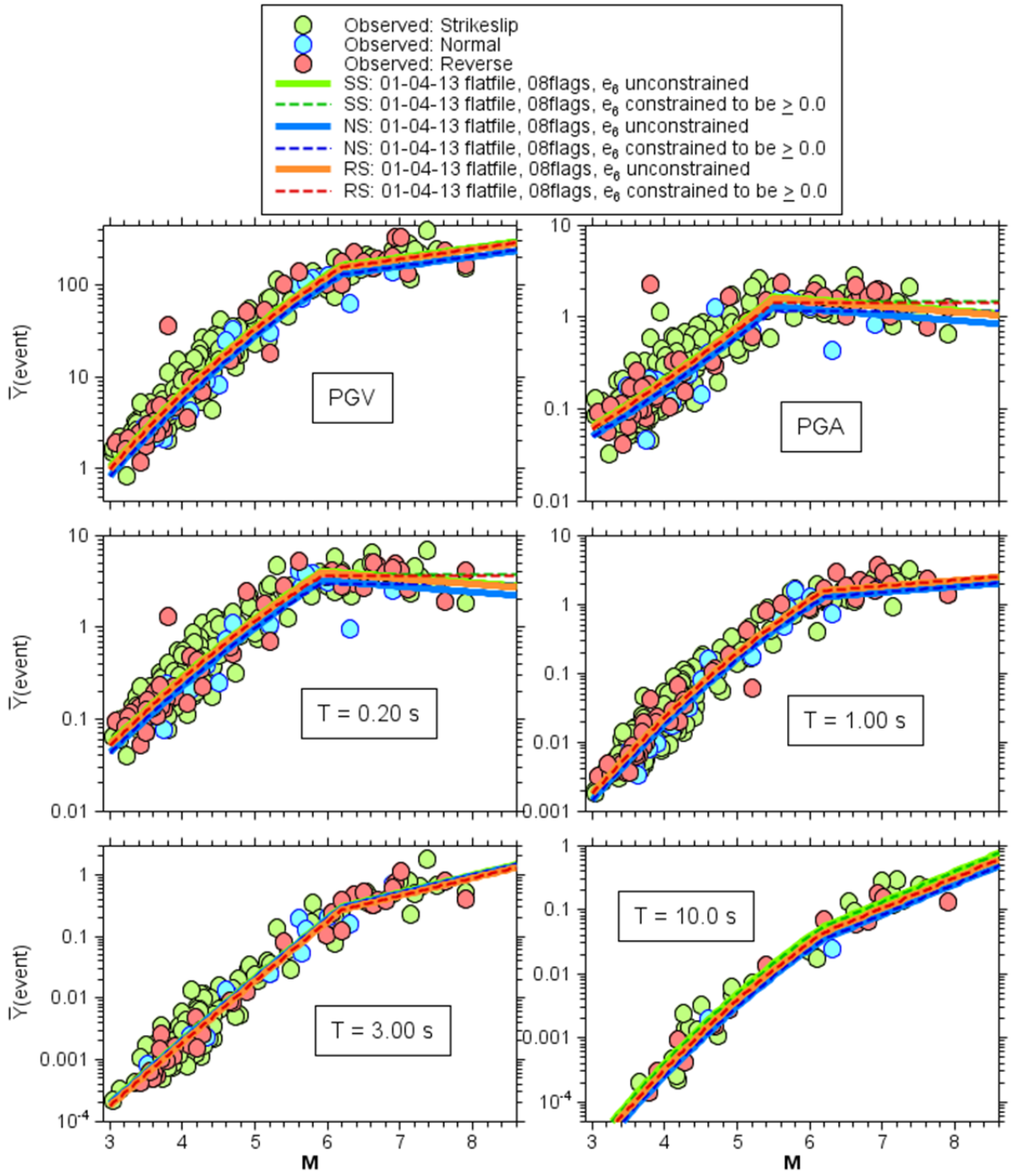

Figure 4.14 $\bar{Y}$ **data points for each event and fit of M-scaling function in Equation (3.5). (This figure is based on an earlier version of the flatfile than the one we used for the final equations; it is used here because the anaysis for constrained** e_6 **was not done for the recent flatfile; the** $\bar{Y}$ **values and curves for unconstrained** e_6 **for the analysis using the most recent flatfile are almost identical to those shown here.)**

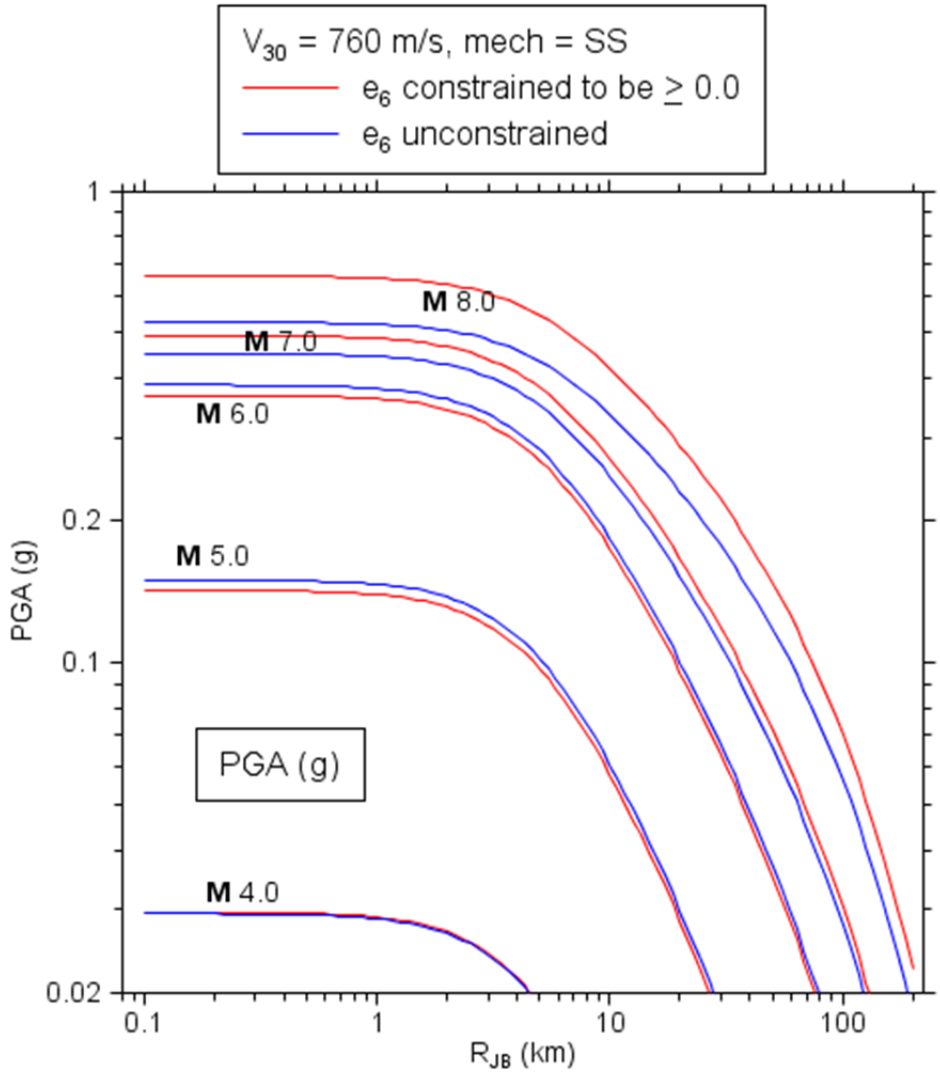

Figure 4.15 Variation of median predicted PGA versus distance for FM function with and without constraint on term e_6. V_{S30} = 760 m/sec.

At longer spectral periods, oversaturation does not occur, but as mentioned previously the results are sensitive to a single earthquake (**M**7.9 Wenchuan, China) for $T > 6$ sec. To examine whether the magnitude scaling at long periods produced by regressions is reasonable, we repeat the regression excluding Wenchuan to examine its impact. Figure 4.16 shows the results of these two regressions for two example periods. The model predictions are plotted for R_{JB} = 70 km and are compared to available data for R_{JB} = 50–100 km as well as simulation results. The results show that the effect of using the Wenchuan data is to reduce e_6. However, the resulting **M** scaling is more consistent with simulations than if Wenchuan is excluded. Accordingly, we chose to retain the Wenchuan mainshock data for our base-case regressions at all periods.

Finally, we note from Figure 4.14 that there is a positive outlier at **M**3.8. We reran the base-case regression without data from this event, but the predictions of PSA from the two sets of GMPE coefficients differed by at most 1% for small magnitudes and short periods. This event (having earthquake number 327) was retained for analysis of the final coefficients.

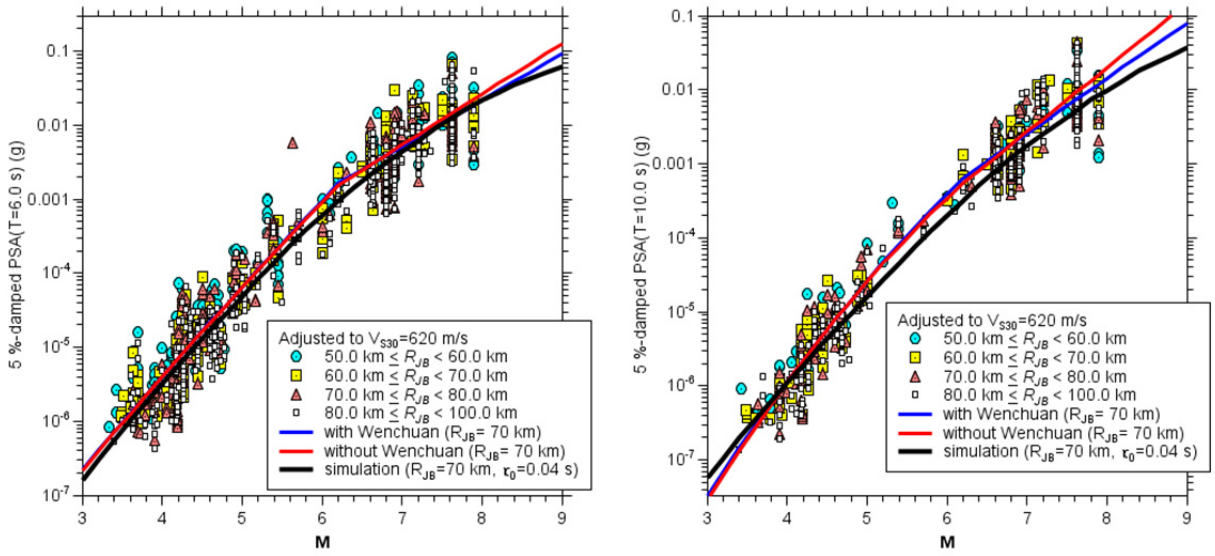

Figure 4.16 **Variation of PSA at T = 6.0 and 1.0 sec with M from Stage 2 regressions with and without inclusion of the Wenchuan event. GMPE medians shown for R_{JB} = 70 km. Site-corrected data for R_{JB} = 50–100 km are shown along with simulation results (simulation procedure and parameter selection protocols are as given in Figure 4.11 caption).**

GMPE Trends:

To illustrate the predictions of our GMPEs, we plot median Y for a range of **M** and R_{JB} in Figure 4.17a and predicted spectra (median Y versus T) in Figure 4.17b. The spectra are drawn using both the unsmoothed and the smoothed coefficients, which illustrates the effectiveness of the smoothing.

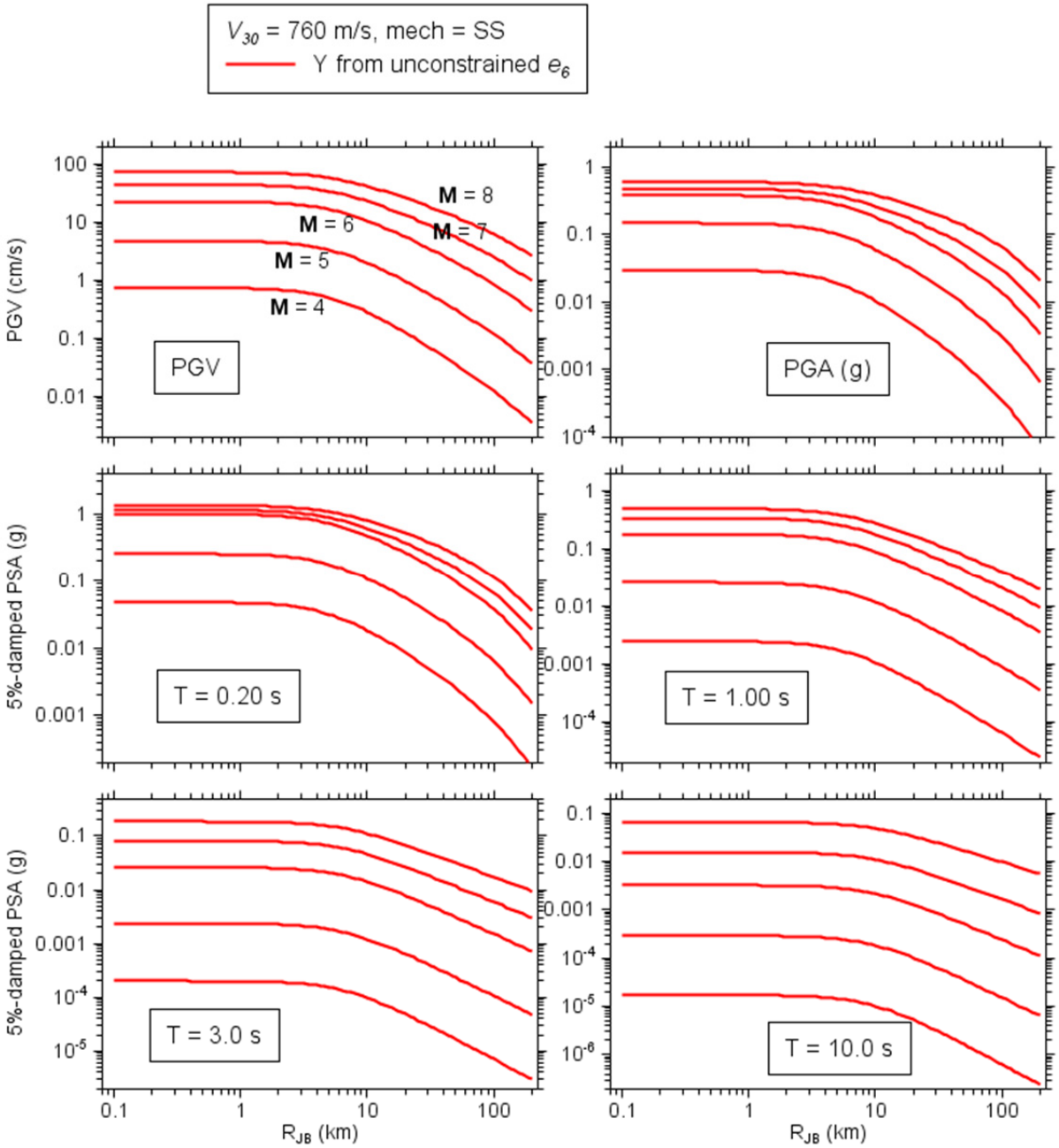

Figure 4.17a Variation of median predicted IMs versus distance for M 4, 5, 6, 7, and 8 strike-slip earthquakes and V_{S30} = 760 m/sec.

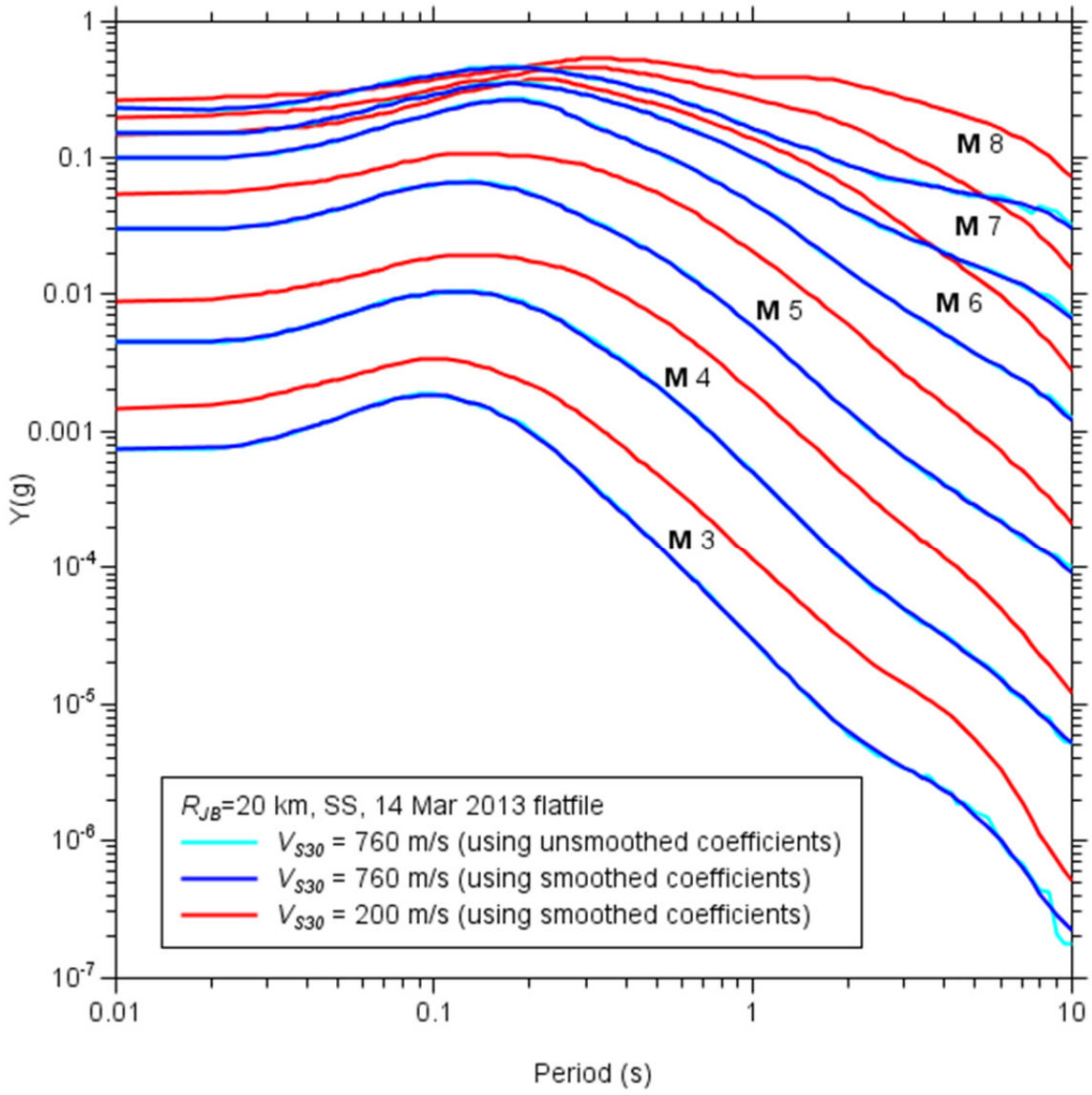

Figure 4.17b Variation of median predicted PSA versus period (*T*) for M 3, 4, 5, 6, 7, and 8 strike-slip earthquakes and V_{S30} = 200 m/sec and V_{S30} = 760 m/sec.

Some well-known features of ground-motion variations with the considered predictor variables are shown in Figures 4.17a and 4.17b. From the PGA plot in Figure 4.17a, we see steep **M**-scaling of the motions for **M** < 6, as shown by the spread of the medians, but very little sensitivity at larger **M**. Conversely, for long-period PSA, we see substantial **M**-scaling over the full range of magnitudes. The distance attenuation trends in Figure 4.17a indicate amplitude-saturation, with amplitudes being nearly constant (flat) for distances R_{JB} < ~ 3–5 km.

For R_{JB} < ~ 10 km, the distance attenuation transitions to a nearly linear slope for periods above about 1 sec while for shorter periods there is significant downward curvature in the lines. This curvature results in apparent anelastic attenuation, which is more important at short periods

than at long periods. For any period the curves steepen as magnitude decreases (a result of the magnitude-dependent geometrical spreading factor).

In Figure 4.17b, many of these features are illustrated by the relative positions of the spectra. This figure is useful in that it shows the magnitude dependence of the predominant period, defined as the period of the peak in the spectrum. For rock-like sites, the predominant period ranges from approximately 0.1 sec for $\mathbf{M}3$ to 0.2 sec for $\mathbf{M} > 6$. Note that for softer site conditions, corresponding to deeper sites, the predominant period shifts towards longer periods of approximately 0.4–0.5 sec due to site response effects.

4.4 PHASE 3: MIXED EFFECTS RESIDUALS ANALYSIS AND MODEL REFINEMENT

In this section, we perform mixed effects residuals analyses having two purposes: (1) to check that the base-case GMPEs developed through the Phase 1 and 2 analyses are not biased with respect to $\mathbf{M}$, R_{JB}, or site-scaling; and (2) to examine trends of residuals against parameters not considered in the Phase 1 and 2 analyses, including regional effects. We also consider a broader set of data. Recall that data were excluded from our Phase 2 analyses based on a number of criteria. For example, no aftershock recordings were used, because there is some concern that the spectral scaling of aftershocks differs from mainshocks (see Boore and Atkinson [1989] and Atkinson [1993]. In this section, we consider the influence of additional factors/data not considered in Phase 2, using residual analysis. The equations were adjusted on the basis of these residuals analyses, as described previously in Chapter 3.

4.4.1 Methodology

The methodology for the analysis of residuals employed here is similar to that described in Scasserra et al. [2009]. We begin by evaluating residuals between the data and the base case GMPE described in Chapter 3 (without the adjustments described in Section 3.1.2). Residuals are calculated as:

$$R_{ij} = \ln Y_{ij} - \mu_{ij}\left(\mathbf{M}, R_{JB}, V_{S30}\right) \tag{4.6}$$

Index i refers to the earthquake event and index j refers to the recording within event i. Hence, R_{ij} is the residual of data from recording j in event i as calculated using the base case GMPE. Term Y_{ij} represents the RotD50 ground-motion IM [Boore 2010] computed from recording j. Term μ_{ij} ($\mathbf{M}$, R_{JB}, V_{S30}) represents the GMPE median in natural log units.

The analysis of residuals with respect to $\mathbf{M}$, distance, and site parameters requires between-event variations to be separated from within-event variations. This is accomplished by performing a mixed effects regression [Abrahamson and Youngs 1992] of residuals according to the following function:

$$R_{ij} = c_k + \eta_i + \varepsilon_{ij} \tag{4.7}$$

where c_k represents a mean offset (or bias) of the data relative to the GMPE (i.e., $c_k = \bar{R}$), η_i represents the event term for event i (explained below), and ε_{ij} represents the intra-event residual for recording j in event i. Event term η_i represents approximately the mean offset of the data for event i from the predictions provided by the GMPE median (after adjusting for mean offset c_k, which is based on all events). Event terms are used to evaluate GMPE performance relative to source predictor variables, such as $\mathbf{M}$. Event terms have zero mean and standard deviation=τ (natural log units). Within-event error ε is has zero mean and standard deviation = ϕ. Mixed-effects analyses per Equation (4.7) are performed using the NLME operator in program R [Pinheiro et al. 2013].

Data selection criteria for Phase 3 analysis were relaxed from those for Phase 2 as described in Section 3.2. In particular, we consider data to distances much larger than R_{JB} = 80 km, with cutoff distances being based on magnitude and instrument type (Figure 2.1). We also consider Class 2 (CL2) events (aftershocks); as mentioned in Section 2.1, CL2 events are differentiated from CL1 events (mainshocks) using a minimum centroid R_{JB} separation of 10 km per the criteria of Wooddell and Abrahamson [2012]. The data set obtained with these criteria is approximately twice the size of that used for Phase 2 analysis.

Figure 4.18 shows the average data misfit to the base case GMPE as expressed by parameter c_k (note: this is not the $F_{P,B}$ parameter c_i, where i = 1, 2, or 3). Parameter c_k has some offset from zero and fluctuates with period, being largest at long periods ($T \geq 5$ sec). The non-zero values of c_k result from the difference between the Phase 3 and 2 data sets; c_k values from the data used in Phase 2 are nearly zero.

Subsequent sections examine within-event residuals, between-event residuals (event terms), and standard deviation terms evaluated from these analyses.

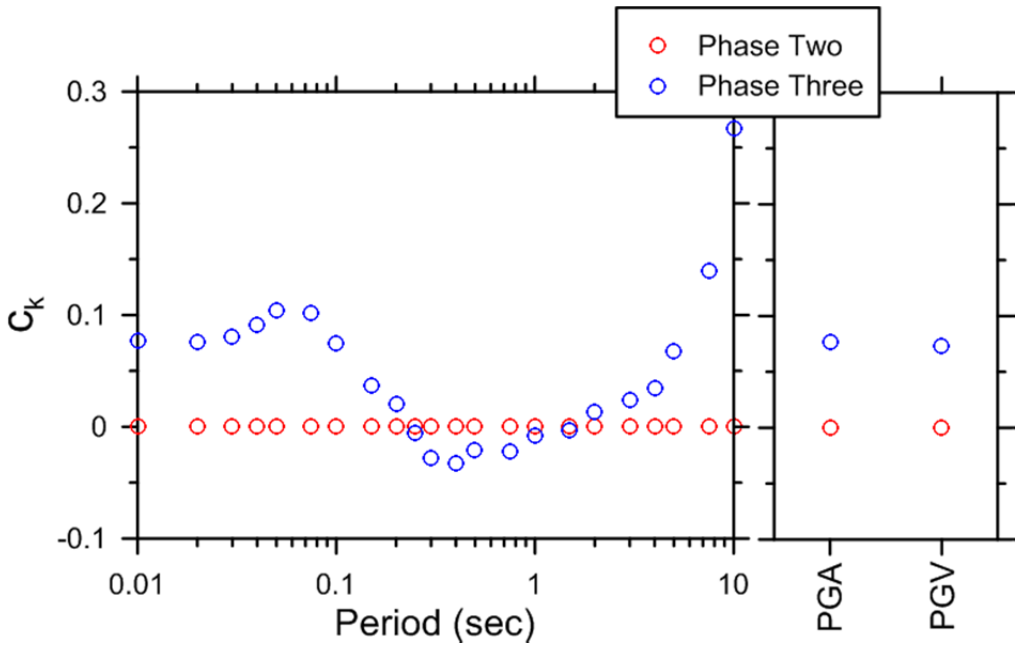

Figure 4.18 **Period-dependence of mean GMPE bias using Phase 3 and Phase 2 data sets.**

4.4.2 Within-Event Residuals Analysis of Path and Site Effects

We use the within-event residuals (ε_{ij}) to examine the performance of the Phase 2 equations relative to the broader Phase 3 data set with respect to path and site effects. The main issue examined through the path analysis is regional variations of apparent anelastic attenuation; since the base-case model uses c_3 terms derived from California data, potential variations for other regions are investigated. The site analyses consider trends of residuals ε_{ij} with V_{S30} (to test the base-case model given in Section 3.2) and z_1 (to examine possible sediment depth effects).

Path Effects:

In Figure 4.19, we plot residuals (ε_{ij}) against R_{JB} using the full data set, with means and standard errors shown within bins equally spaced with respect to $\log R_{JB}$. The results show no perceptible trend, indicating that the base-case path-scaling terms for apparent geometric spreading and apparent anelastic attenuation reasonably represent the data trends. This is an encouraging finding because the base-case regressions were performed using only data at $R_{JB} <$ 80 km with constraint of c_3 from small magnitude data in California (Section 4.2.1). The flatness of the trends for $R_{JB} > 80$ km indicates that the California-derived c_3 values may be a reasonable global average for active crustal regions.

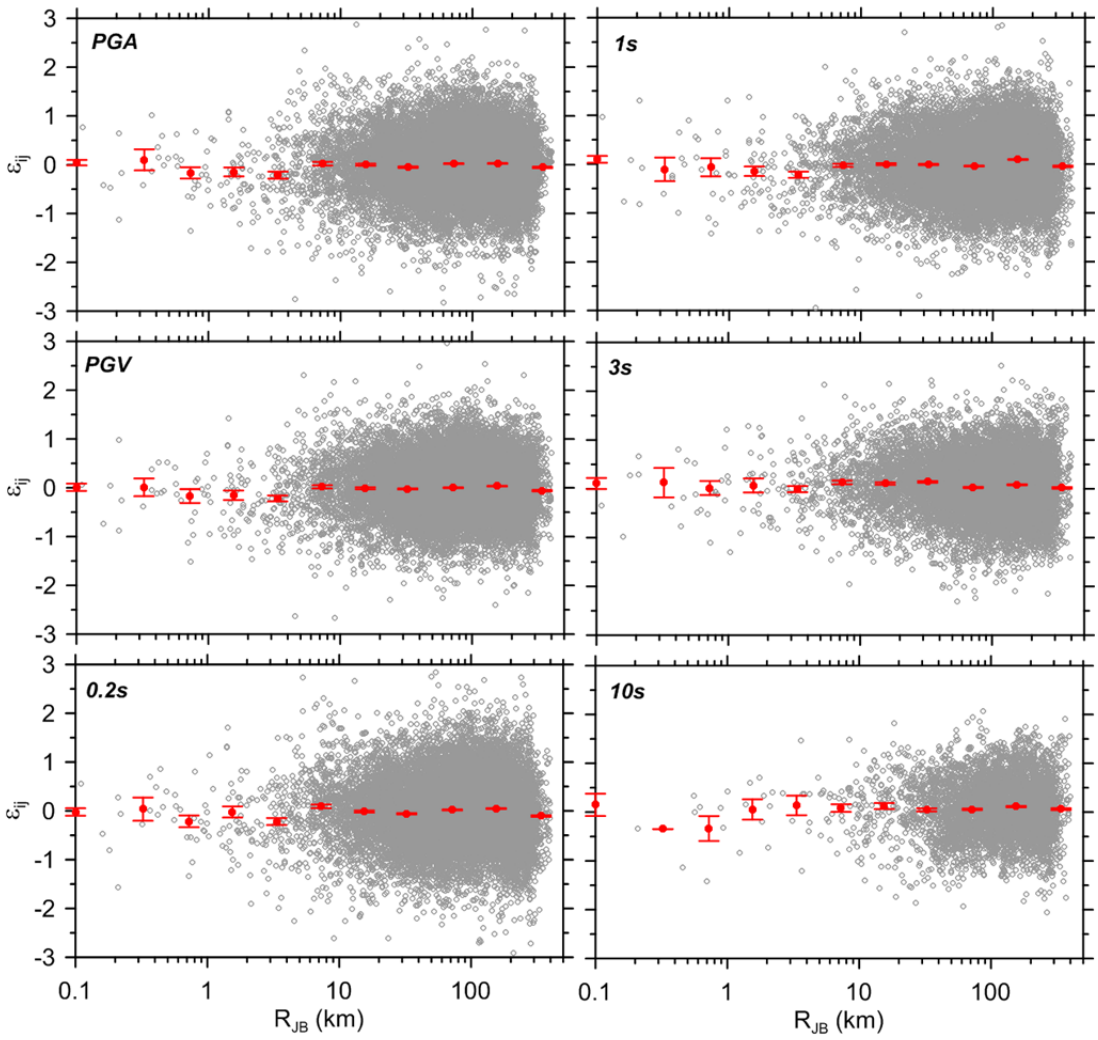

Figure 4.19 **Within event residuals for full Phase 3 data set versus distance, with binned medians (red dots with bars indicating standard errors).**

Figures 4.20 to 4.22 show within-event residuals (ε_{ij}) against R_{JB} using data from various global regions grouped according to their distance-attenuation trends for R_{JB} > ~ 50–100 km. Figure 4.20 shows data from California and Taiwan, for which the flat trends in the global data set are preserved (these same general features are found if the data are plotted for California-only or Taiwan-only). In the figure, this is indicated as an 'average Q' result. Figure 4.21 shows data from Japan and Italy, for which a downward trend is observed, indicating faster distance attenuation (marked as 'low Q'). Similarly fast distance attenuation trends have been observed previously in these regions (e.g., Stewart et al. [2013] and Scasserra et al. [2009]). Figure 4.22 shows data from China and Turkey, for which slower attenuation is observed ('high Q'). The slower attenuation for China is not surprising given the location of the Wenchuan event near the western boundary of a stable continental region as defined by Johnston et al. [1994], with the recordings having been made at sites both in stable continental and active crustal regions [Kottke

2011]. This result for Turkey was not expected, but has been observed by others using larger Turkish data sets [Z. Gulerce 2013, *personal communication*].

For the low and high Q cases, we fit a linear expression through the data according to:

$$\varepsilon = \Delta c_3 \left(R - R_{ref} \right) \tag{4.8}$$

where Δc_3 is additive to the c_3 terms developed in Section 4.2.1 from California [Equation [3.7]). Values of Δc_3 are plotted against period for average, low, and high Q conditions in Figure 4.23. These adjustments are considered to be statistically significant, and Δc_3 was used in the computation of residuals for the remainder of Phase 3 analyses presented below.

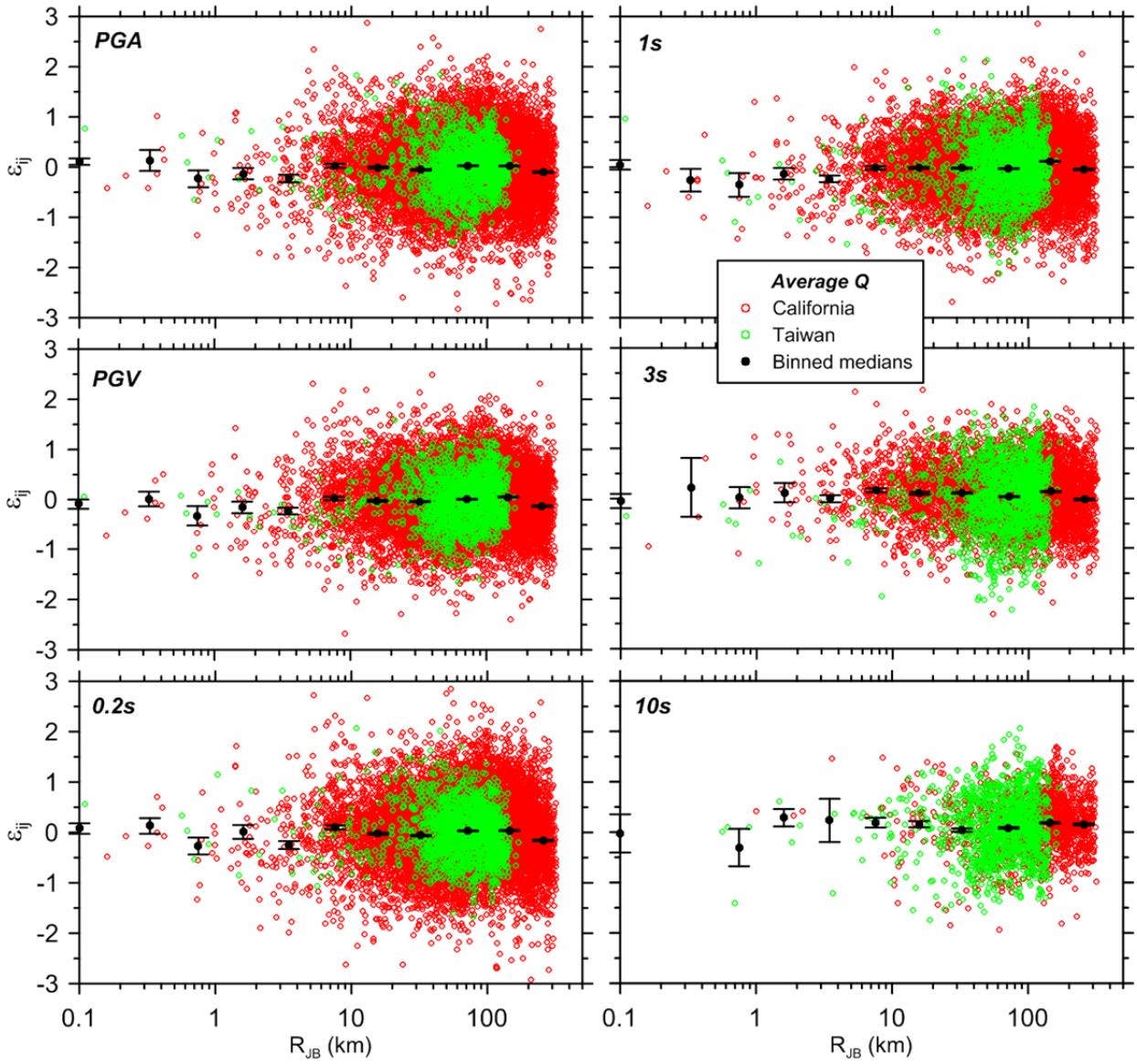

Figure 4.20 **Within event residuals for regions identified as 'average Q' (California and Taiwan) within the flatfile. The residuals in this case demonstrate a flat trend with distance. The larger scatter of California data is due to more small M events.**

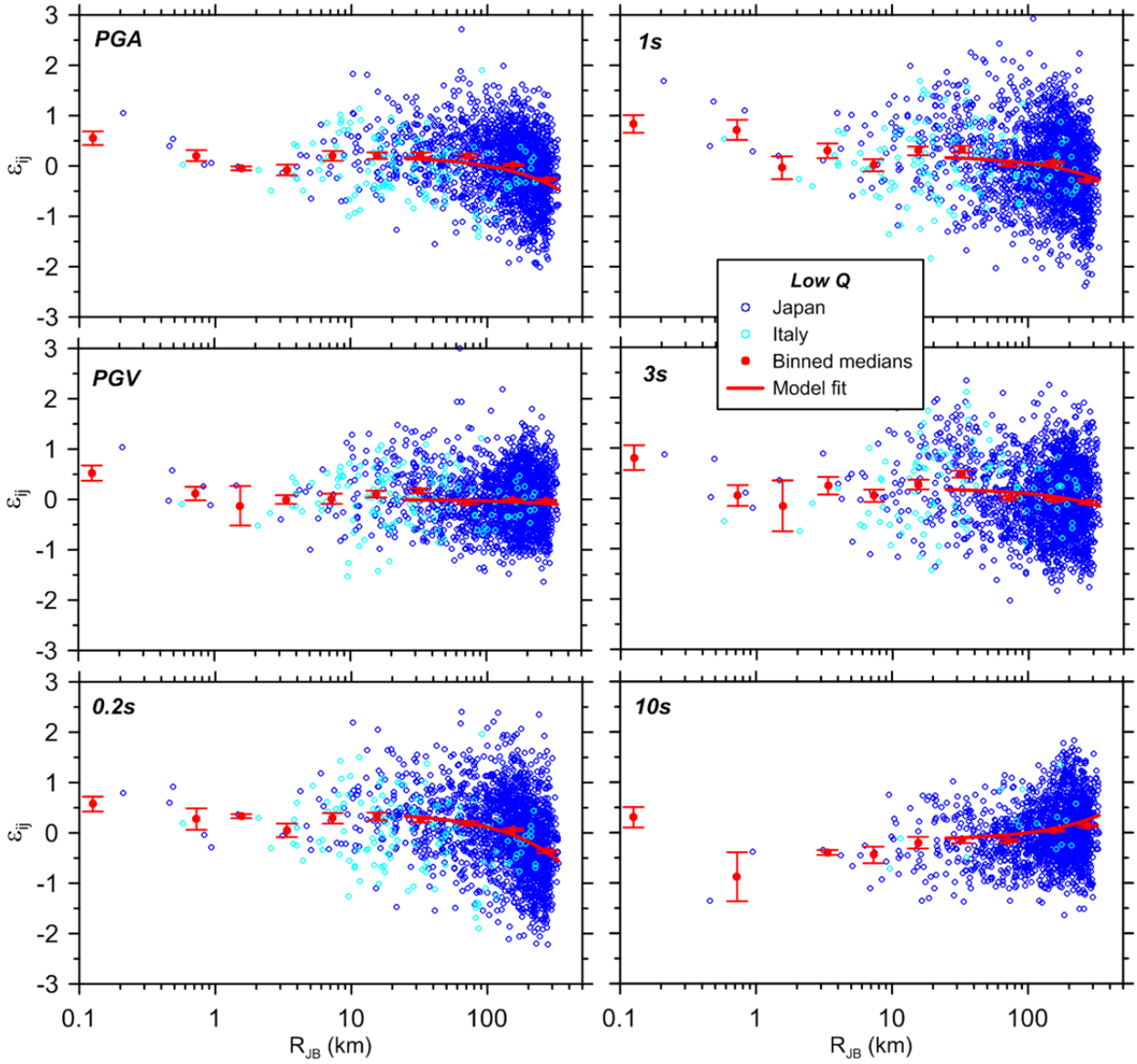

Figure 4.21 **Within event residuals for regions identified as 'low Q' (Italy and Japan) within the flatfile and trend line per Equation (4.8). The residuals demonstrate a decreasing trend with distance.**

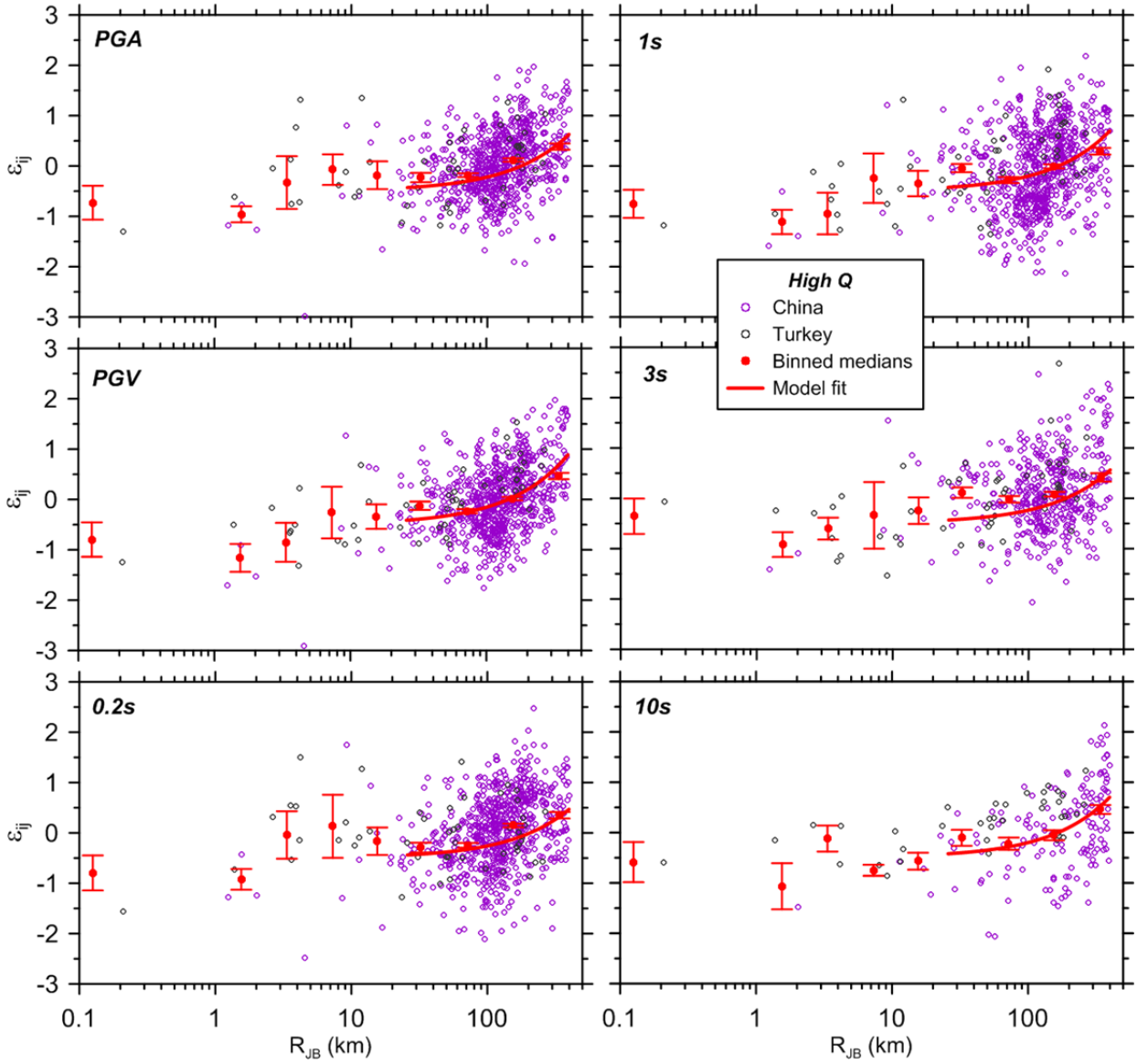

Figure 4.22 **Within event residuals for regions identified as 'high Q' (China and Turkey) within the flatfile and trend line per Equation (4.8). The residuals demonstrate an increasing trend with distance.**

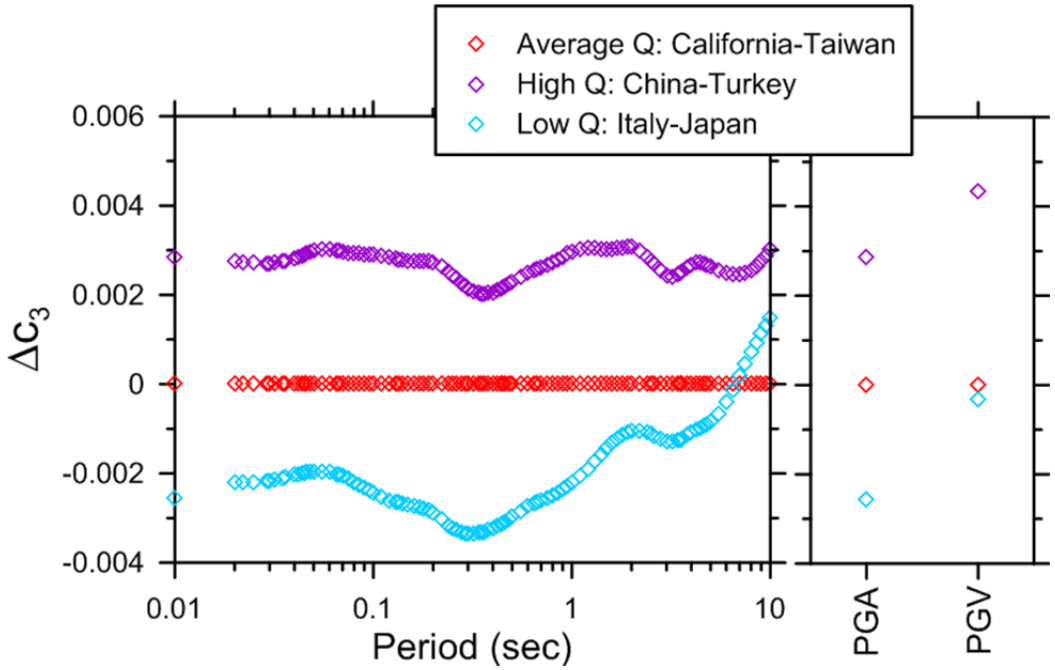

Figure 4.23 **Additive adjustment factors for apparent anelastic attenuation term c_3 for regions exhibiting various distance attenuation rates.**

Check of V_{S30}-Scaling:

In Figure 4.24, we plot residuals (ε_{ij}) against V_{S30} using the full data set. We find no trends, indicating satisfactory performance of the model. When the data is plotted by region, the trends remain flat (not shown).

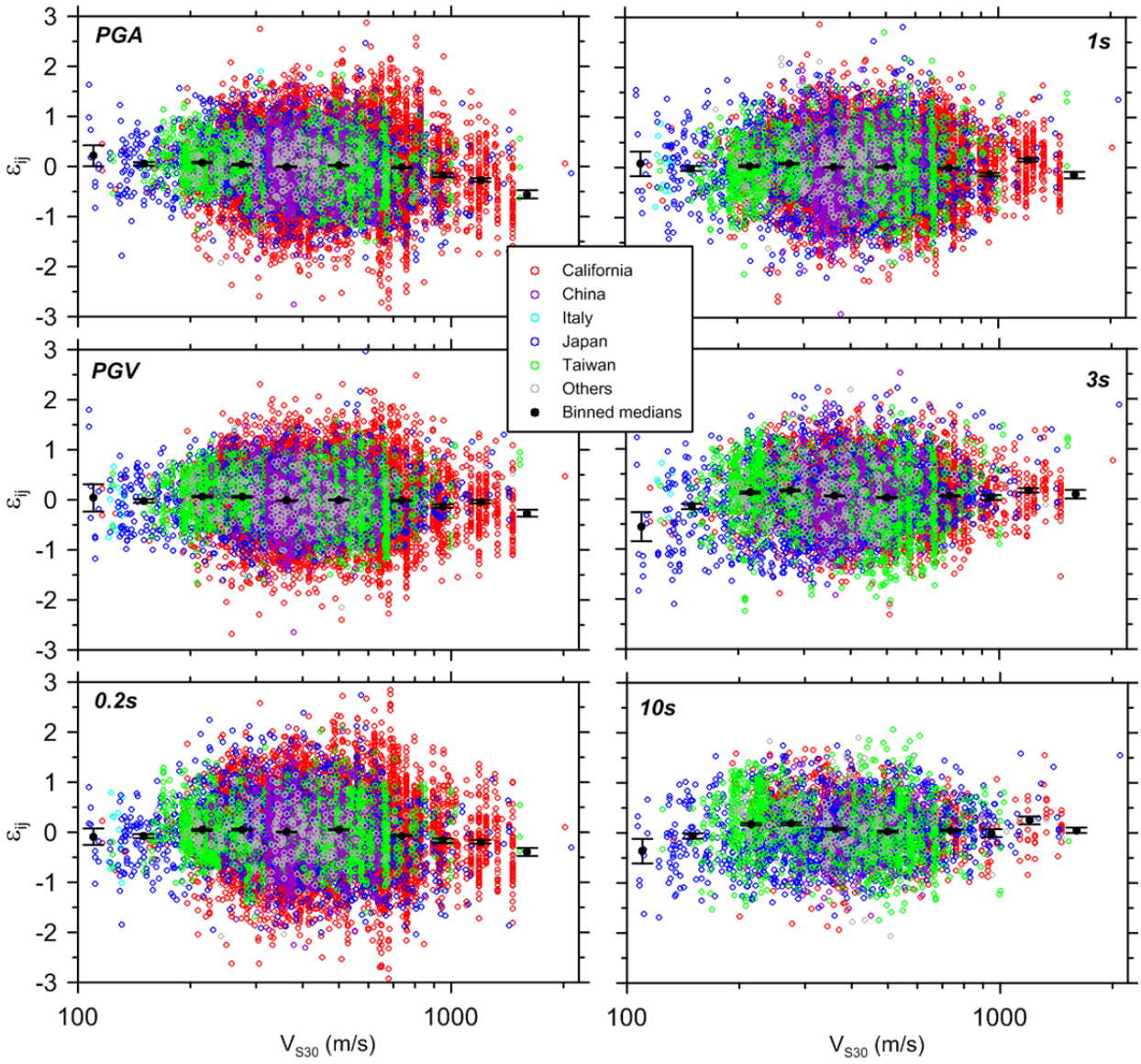

Figure 4.24 Within event residuals against V_{S30}.

Sediment Depth Effects:

The site parameter V_{S30} strictly describes only the characteristics of sediments in the upper 30 m, even though it has been shown to be correlated to deeper structure (e.g., Boore et al. [2011]). There may be additional site amplification effects that are related to the depth of the deposit and that are not captured by the use of V_{S30} alone as a site descriptor. For example, GMPE residuals for ground-motion models that include a V_{S30}-based site term (or similar site

terms related to surface geology) have been shown to correlate to basin depth parameters (e.g., Field [2000]; Lee and Anderson [2000]; Steidl [2000]; Choi et al. [2005]; Abrahamson and Silva [2008]; Campbell and Bozorgnia [2008]; and Chiou and Youngs [2008]). This indicates that depth is describing elements of the site characteristics relevant for ground motion prediction. Since residual trends in prior work are typically strongest at long spectral periods ($T > \sim 1.0$ sec), the depth parameter is descriptive of low-frequency components of the ground motion, which may be related to resonances of sedimentary basin structures. The BA08 model did not include a basin-depth term; here we investigate whether the data support the use of such a term in the present equations.

Basin-depth parameters used to investigate site effects are generally defined as the vertical distance from the ground surface to the first occurrence of a particular shear-wave iso-surface (typically 1.0, 1.5, or 2.5 km/sec). We consider the shallowest metric of z_1 (depth to 1.0 km/sec iso-surface) due to its greater practical utility (i.e., a 1.0 km/sec velocity can be reached through geotechnical drilling in some cases; whereas 2.5 km/sec can rarely be reached) and a lack of clear evidence from prior work indicating that deeper metrics are more descriptive of long-period site effects [Day et al. 2008].

As described in Ancheta et al. [2013], a substantial effort was made in NGA-West 2 to update basin depths in the site database based on new information. Depth parameters have been updated for basin regions in southern California (SC) and the San Francisco Bay Area (SFBA). Depth parameters have also been added for stations in Japan. In total, 54% of the stations in the flatfile have an assigned basin depth. Figure 4.25 shows the distribution of z_1 values against V_{S30} for SC, SFBA, and Japan. Also shown are two correlation relationships developed by B. Chiou [2013, *personal communication*]:

$$\text{California: } \ln\left(\mu_{z1}\right) = \frac{-7.15}{4}\ln\left(\frac{V_{S30}^4 + 570.94^4}{1360^4 + 570.94^4}\right) \tag{4.9a}$$

$$\text{Japan: } \ln\left(\mu_{z1}\right) = \frac{-5.23}{2}\ln\left(\frac{V_{S30}^2 + 412.39^2}{1360^2 + 412.39^2}\right) \tag{4.9b}$$

These relationships can be used to estimate z_1 when only V_{S30} is available. They also provide a convenient mechanism for defining a representative depth for any given V_{S30}. The latter point is important with respect to understanding the implications for basin depth of using the base case GMPE, in which z_1 does not appear. The absence of z_1 in the model does not mean the sites have no depth; rather, when the base-case GMPE is used it is providing estimates of site response for an 'average' depth, an approximate estimate of which is given by Equation (4.9).

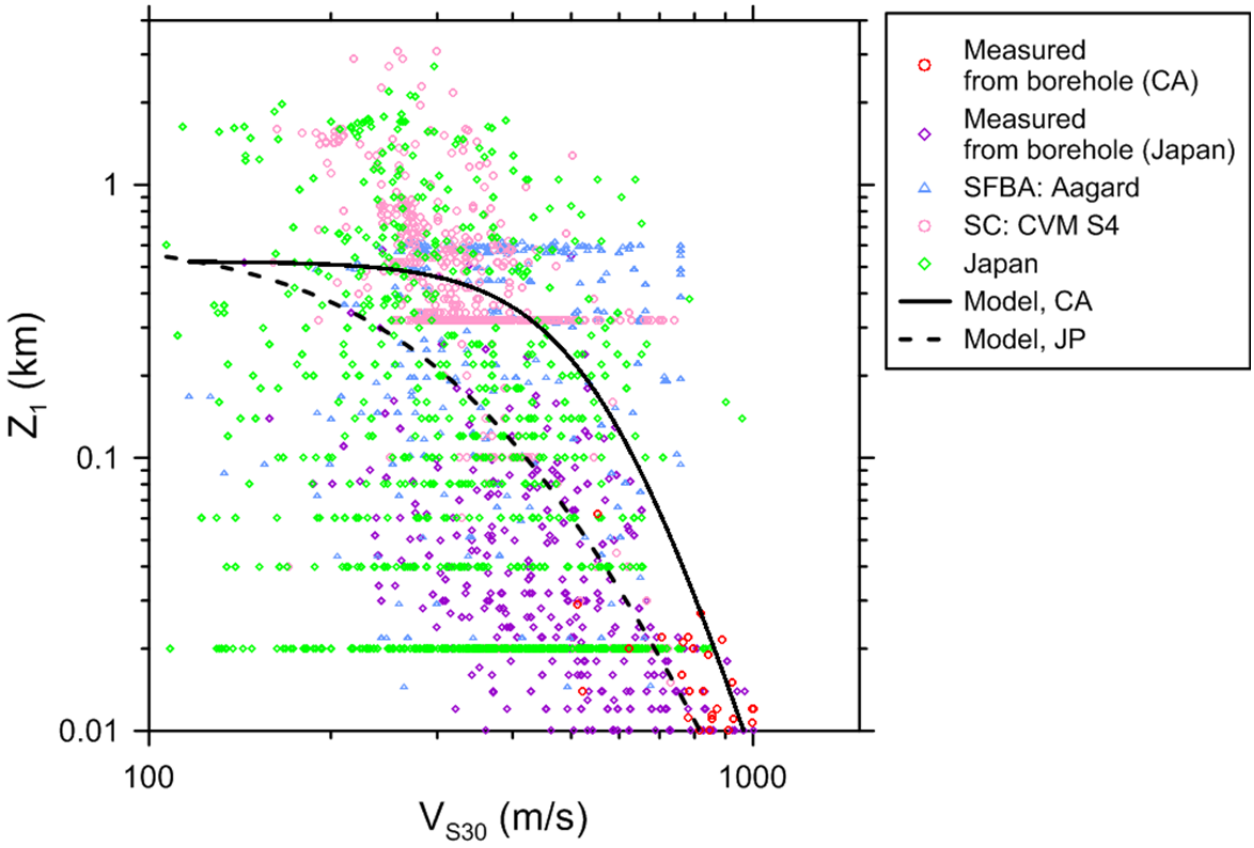

Figure 4.25 **Sediment depth z_1 variation with V_{S30} for basins in southern California (SC), San Francisco Bay Area (SFBA), and Japan. Equations for California and Japan are from B. Chiou [Equation (4.9)].**

Figure 4.26 shows residuals (ε_{ij}) against basin depth z_1. There is little trend for short periods ($T < 1.0$ sec), but at longer periods the trend is strong. Interestingly, the residuals are near zero, with little dependence on z_1, for $z_1 < 0.25$–0.5 km, and again show little change with z_1 for $z_1 > \sim 1.5$ km (but with a nearly constant offset from 0). Since the V_{S30} component of the GMPE already implicitly includes average basin depths [approximately represented by Equation (4.9)], we investigate the possibility of using the differential from the average basin-depth predictor variable:

$$\delta z_1 = z_1 - \mu_{z1}(V_{S30}) \tag{4.10}$$

where $\mu_{z1}(V_{S30})$ is the mean basin depth from the relations in Equation (4.9). In Figure 4.27a, we plot residuals ε_{ij} against δz_1 along with the model fit from Equation (3.13). As before, at short periods there is no effect. For $T \geq 1$ sec, the trends are strong, indicating negative residuals for negative δz_1 and a flat trend beyond approximately $\delta z_1 = 0.5$ km. The δz_1 parameter is more descriptive of data trends and was adopted as the predictor variable [Equation 3.13].

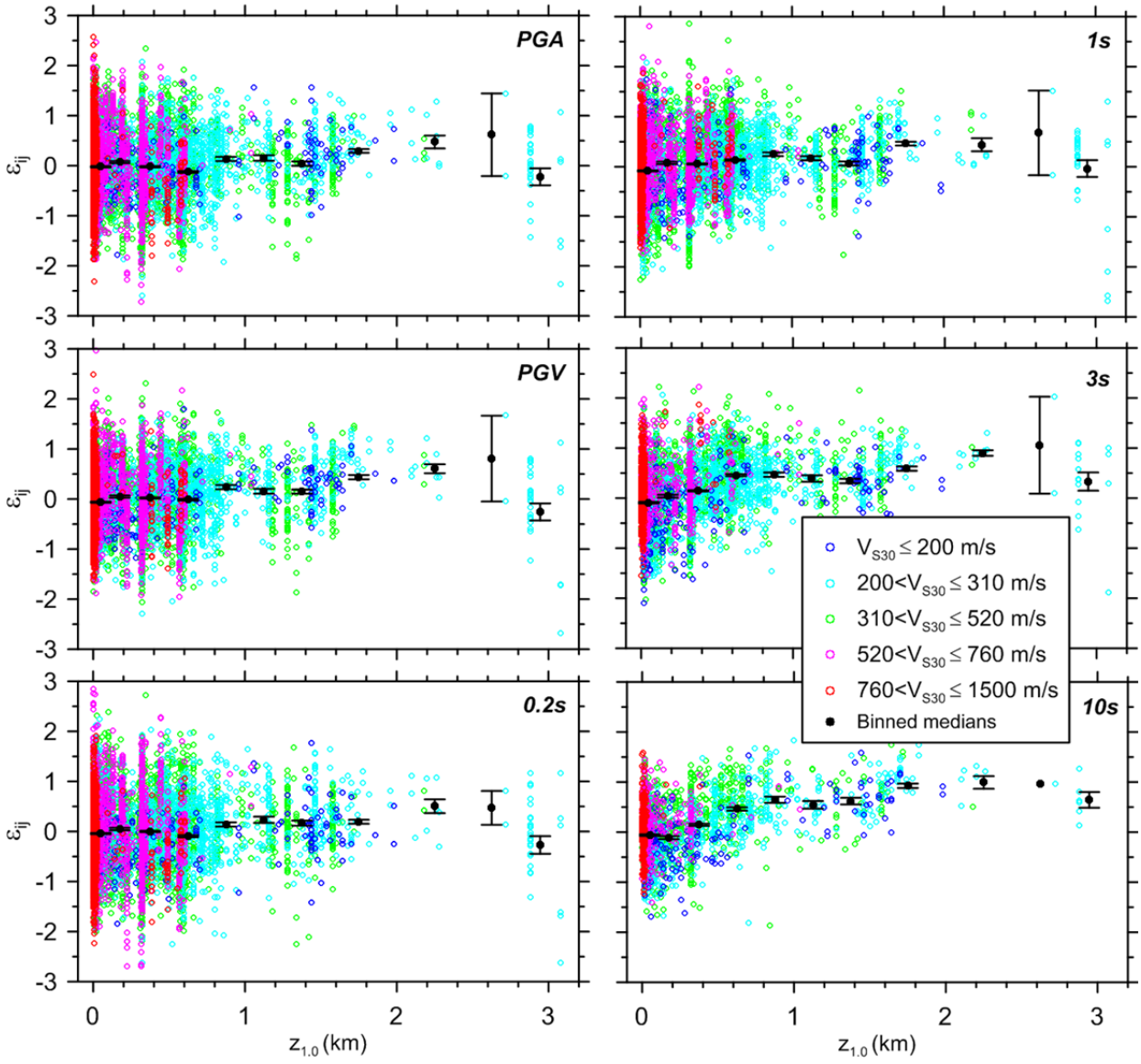

Figure 4.26 Within event residuals against sediment depth parameter z_1.

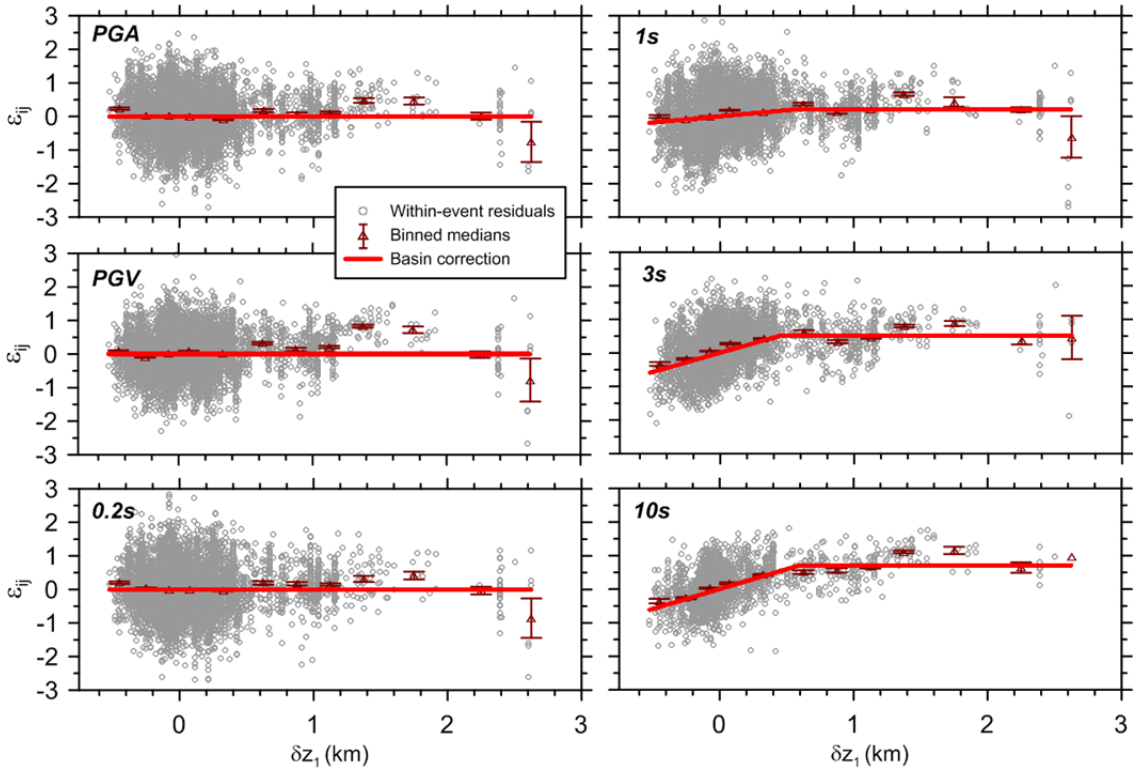

Figure 4.27a **Within event residuals against sediment depth differential δ_{z1} along with proposed basin model**

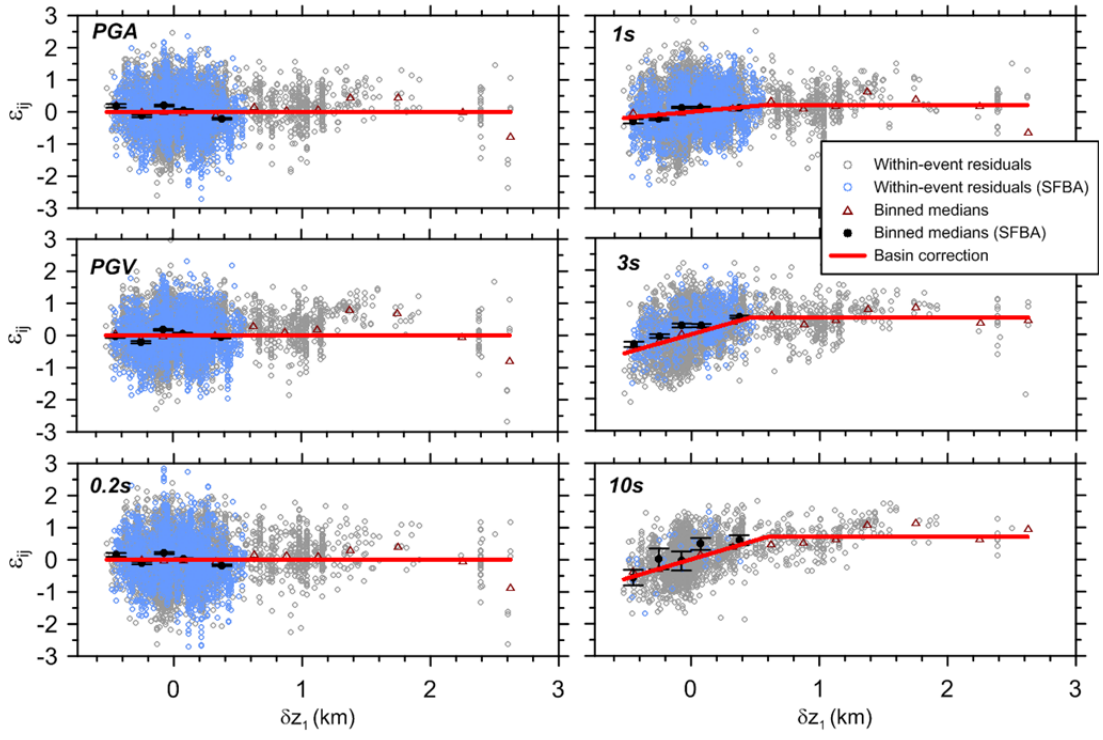

Figure 4.27b **Within event residuals against sediment depth differential δ_{z1}, highlighting SFBA sites. Non-SFBA sites shown with grey circles.**

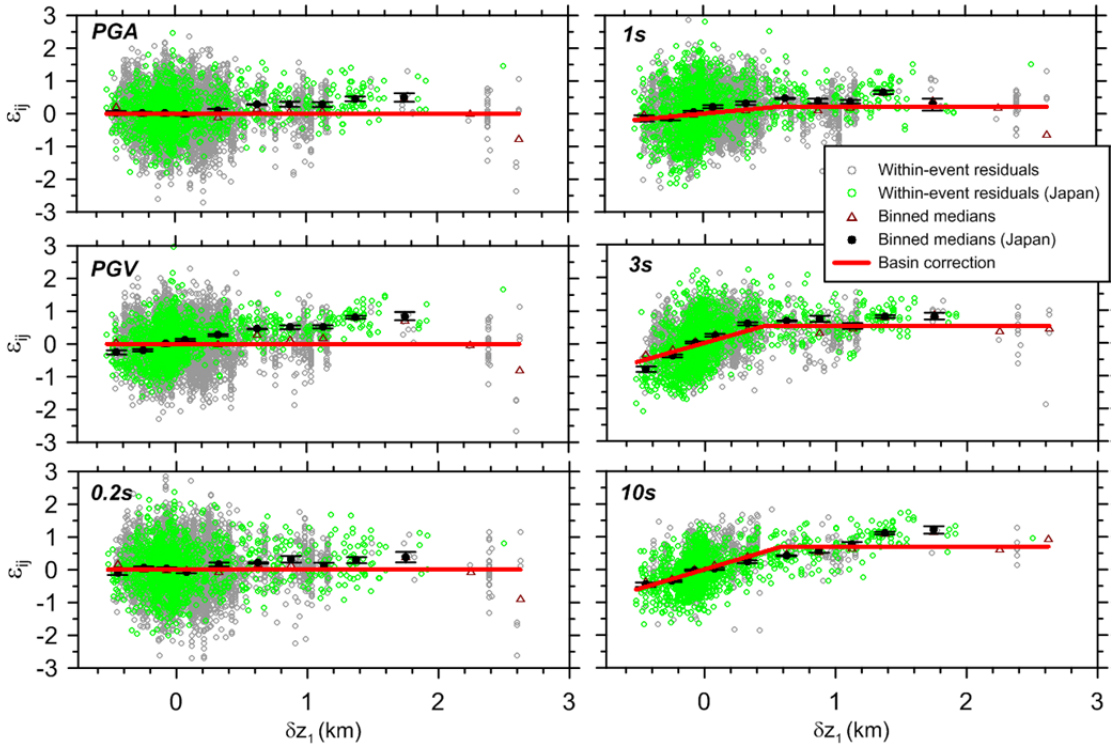

Figure 4.27c **Within event residuals against sediment depth differential δ_{z1}, highlighting Japan sites. Non-Japan sites shown with grey circles.**

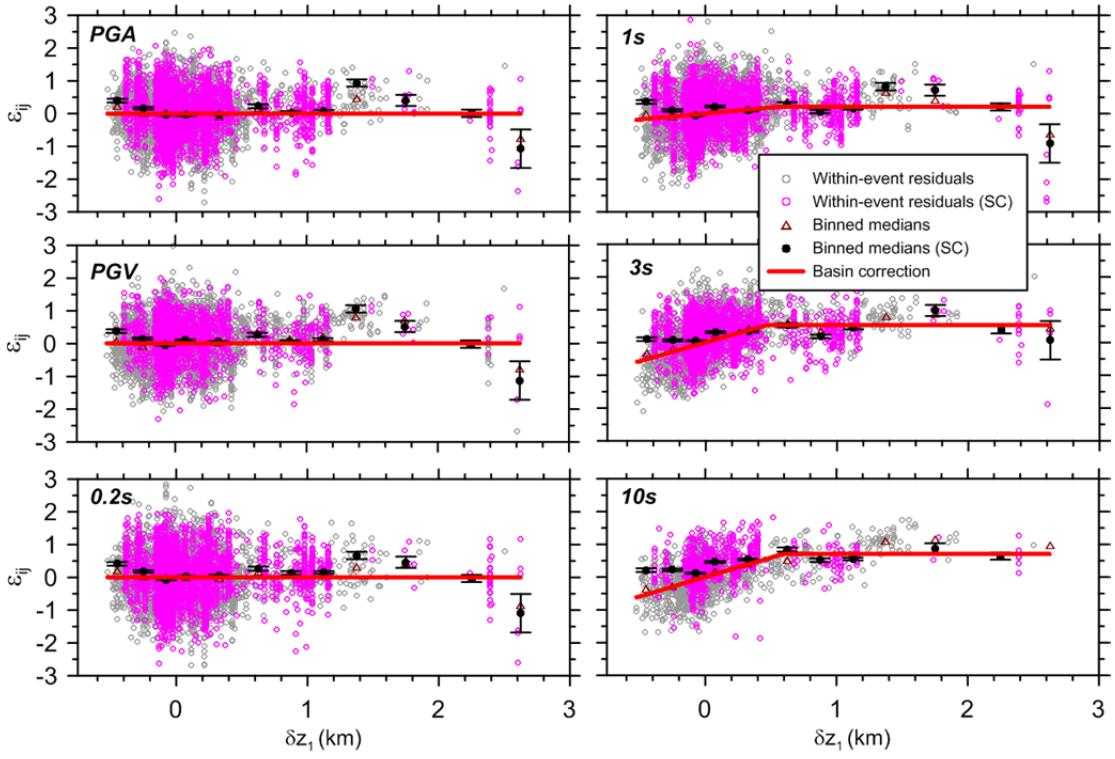

Figure 4.27d **Within event residuals against sediment depth differential δ_{z1}, highlighting SC sites. Non-SC sites shown with grey circles.**

Figures 4.27b-d show the residuals trends with δz_1 for the three regions contributing data (SFBA, Japan, and SC). The trends are strongest for Japan, particularly for negative values of δz_1, and weakest for SC. The levels of maximum mean amplification for positive δz_1 are relatively consistent across regions, being approximately 0.5 to 0.75 (in natural log units) at long periods. Although some regional trends are evident in Figures 4.27, we have chosen to not regionalize the $F_{\delta z1}$ model, aside from the regional nature of the mean V_{S30}-z_1 model [Equation 4.9)].

4.4.3 Analysis of Source Effects Using Between-Event Residuals

In Figure 4.28, we show event terms for both CL1 and CL2 events against magnitude for the five regions contributing most of the data for NGA-West 2. The majority of the events, especially at small **M**, are from California. China contributes a substantial number of events, which are CL2, for **M** ~ 4.5–6. These China CL2 events exhibit unusual trends with respect to **M**-scaling (indicated by the trend for PGA, PGV, and 0.2-sec PSA) or significant negative bias (1.0- and 3.0-sec PSA). We do not understand these unusual features and have elected to not consider further the China CL2 events for subsequent analyses.

Figure 4.29 shows CL1 event terms against **M** along with medians in bins 0.5 **M** in width. From this figure we see that the magnitude-scaling function adequately captures the trends from CL1 events in the broader Phase 3 data set.

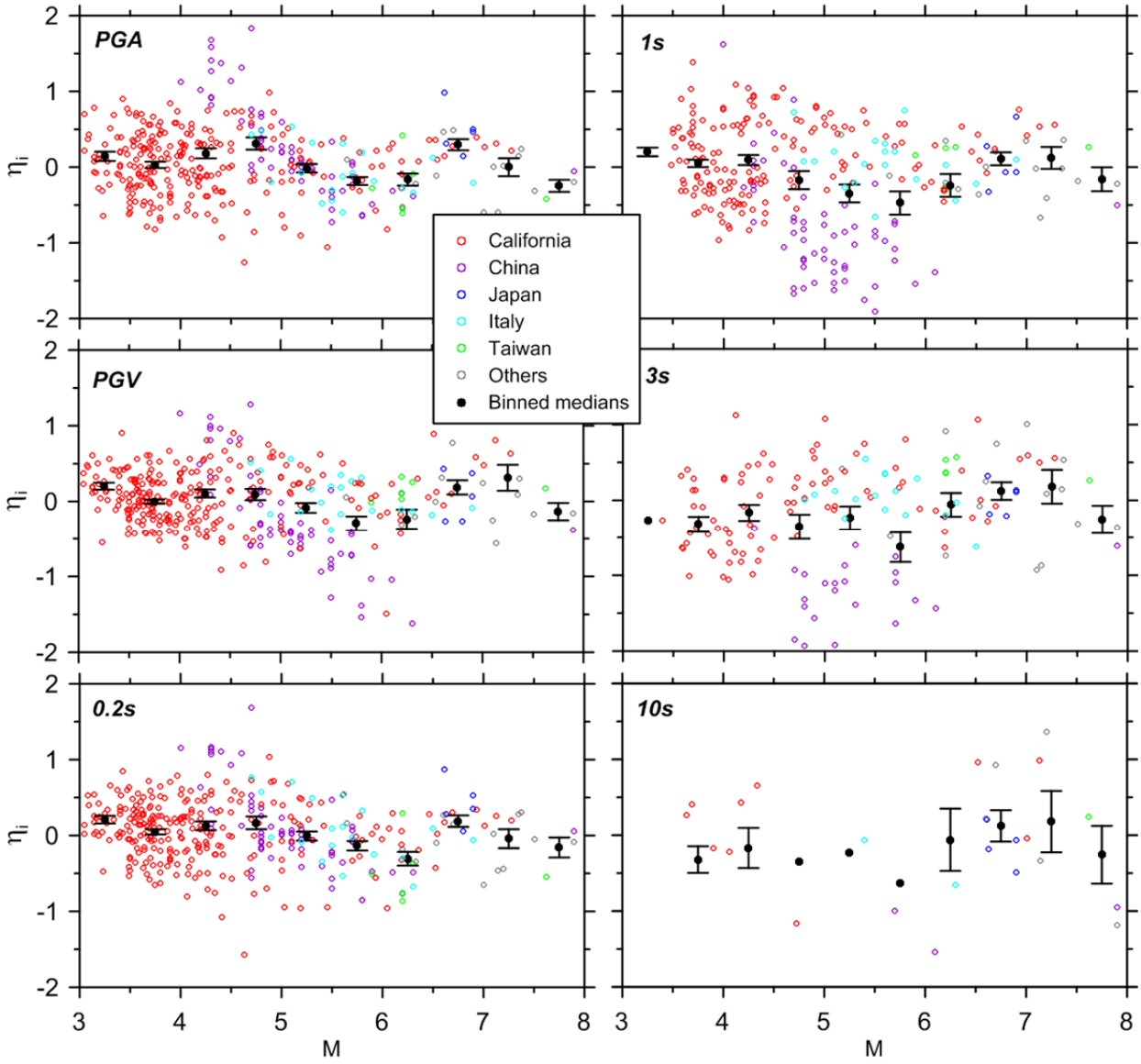

Figure 4.28 **Event terms versus magnitude for CL1 and CL2 events sorted by region.**

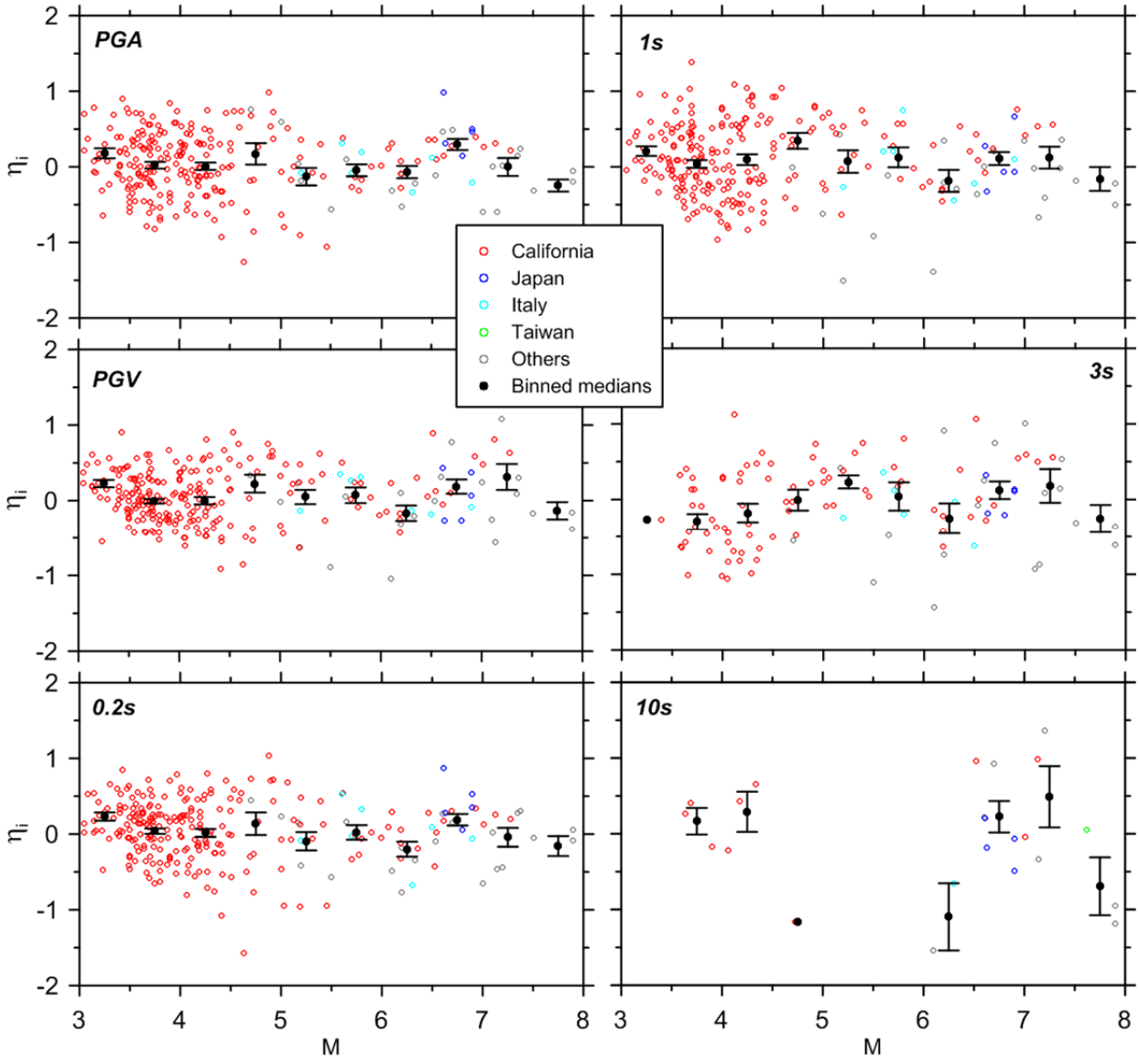

Figure 4.29 Event terms versus magnitude for CL1 events sorted by region.

Potential Bias of CL2 Events:

Recall that all earthquake events in the NGA-West 2 flatfile have been designated as CL1 (foreshocks or mainshocks) or CL2 (interpreted as aftershocks based temporal and spatial attributes; see Wooddell and Abrahamson [2012]). Our examination of the event term results from Phase 3 analysis indicated that for selected regions (e.g., Taiwan), a particular feature of CL1 event terms was often also seen in the subsequent CL2 events associated with the 'parent' CL1 event. In Figure 4.30, we examine such correlations for all CL1 events having CL2 'children' events, sorted by region. The plots show the event term for the CL1 event (η_{C1}) on the x-axis against the mean of the 'children' event terms ($\overline{\eta}_{C2}$) on the y-axis (similar procedures were used to look at mainshock and aftershock site factors by Lee and Anderson [2000].

Although the data do not provide a large correlation coefficient (computed values are generally less than 0.3), there are a striking number of events falling on or near the 45° line. Given the modest relationship between CL1 and CL2 event terms, we elect to examine aftershock effects in the form of the difference $\Delta\eta = \overline{\eta}_{C2} - \eta_{C1}$.

In Figure 4.31, we show $\Delta\eta$ against **M** for various ground-motion IMs. We see no compelling evidence for $\Delta\eta$ being **M**-dependent nor significantly different from zero relative to the data scatter. In Figure 4.32, we show the mean value of $\Delta\eta$ (denoted $\overline{\Delta\eta}$) against period using all data except for the China CL1 event at **M** 6.1, which is a clear outlier and may be unreliable for the same unknown reasons as the China CL2 events discussed above. For comparative purposes, we have also computed the weighted average of CL2 event terms (weights assigned based on the number of data points) for the regions contributing most of the aftershock data (California and Italy). This is denoted in Figure 4.32 as $\left(\overline{\eta}_{CL2}\right)_{CA,IT}$. The values are numerically similar to those for $\overline{\Delta\eta}$, and are computed for more periods. After studying these results, our conclusion is that the data do not justify the use of a CL2 adjustment to the base-case GMPEs.

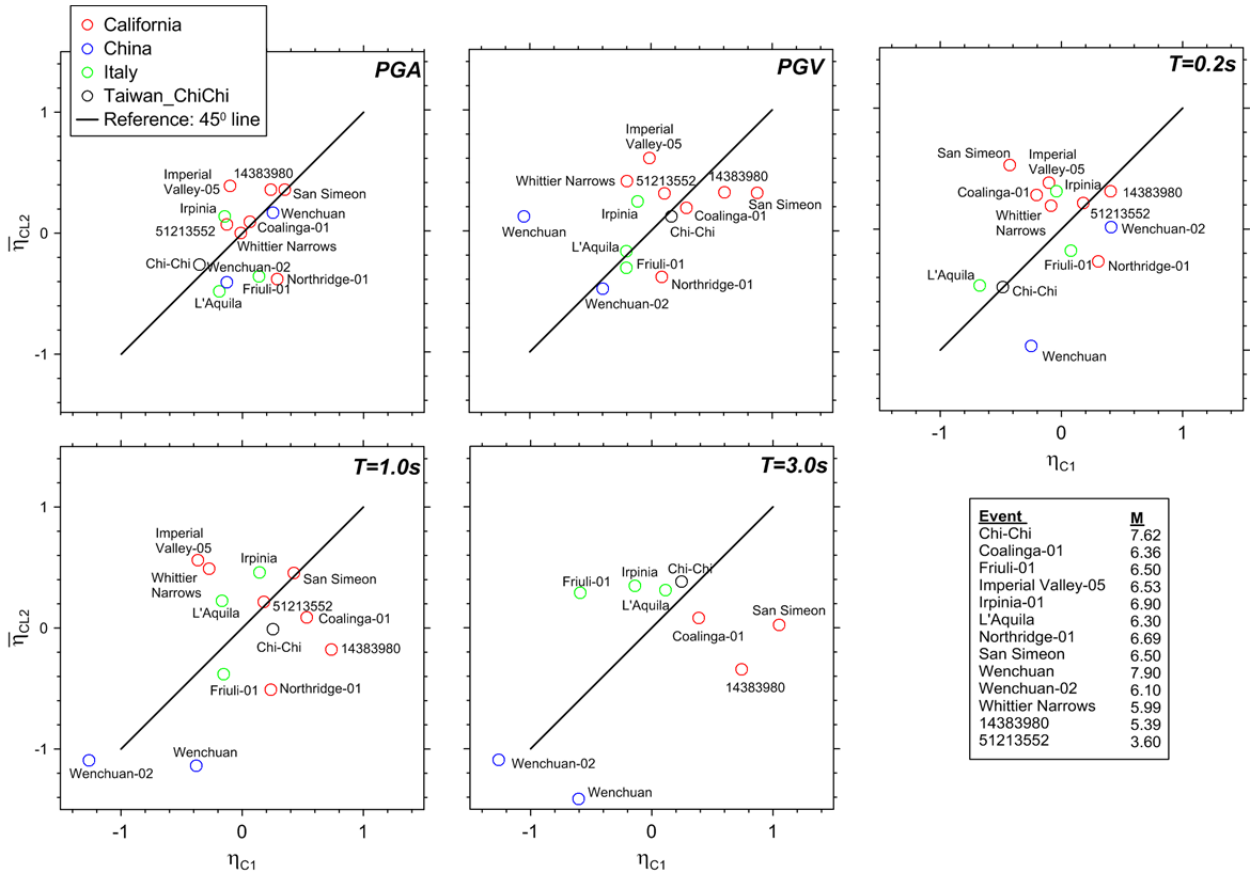

Figure 4.30 **Event terms versus magnitude for CL1 events sorted by region. The numbered events (e.g., 14383980) are California small M events, which were not named in the NGA-West 2 database.**

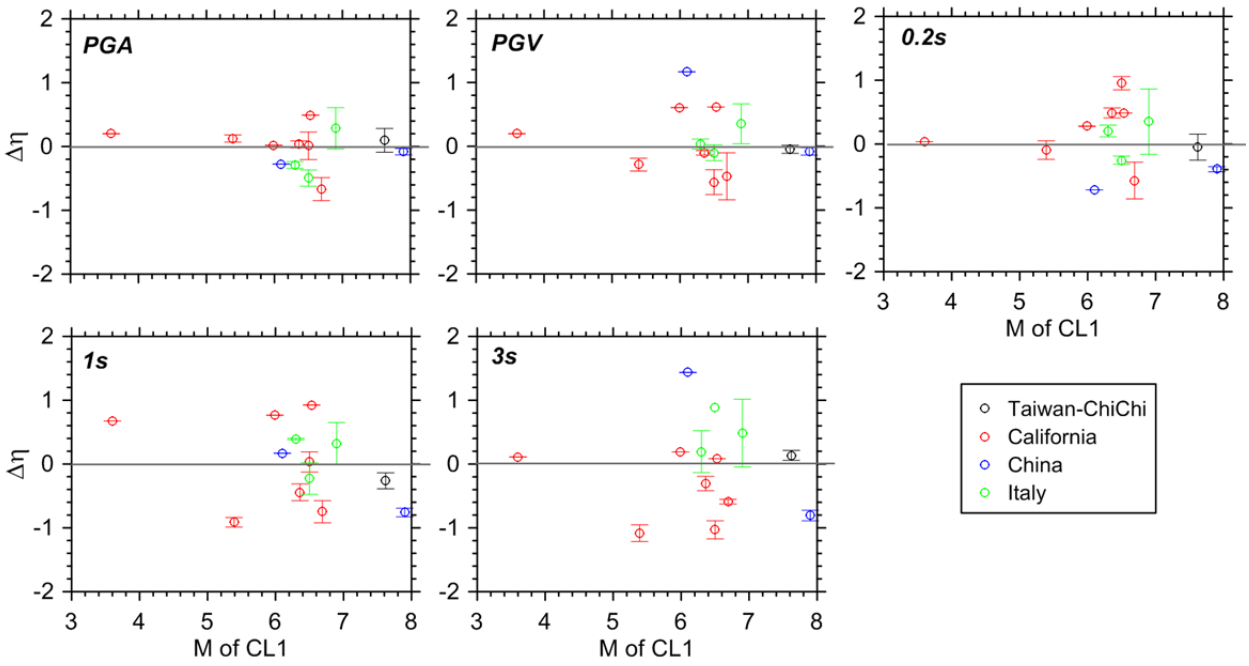

Figure 4.31 **CL2 event term differential $\Delta\eta$ (with standard errors) as function of magnitude for various regions and IMs.**

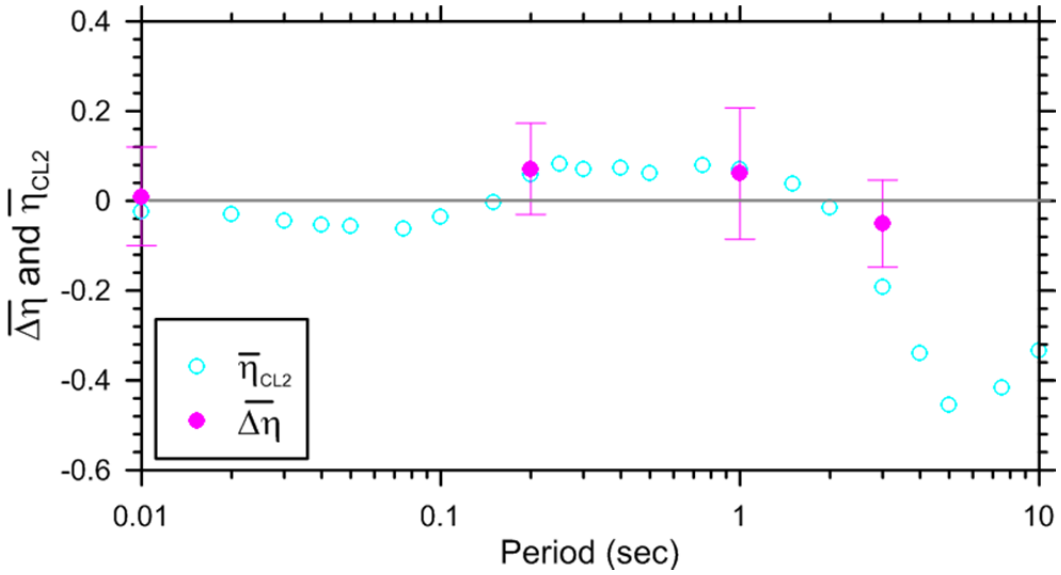

Figure 4.32 **Mean CL2 event term differential (with standard errors) and mean of CL2 event terms.**

Source Depth:

Our path function [Equation (3.3) takes site-source distance as R_{JB}, which is the closest horizontal distance of the site to the surface projection of the fault plane. As such, the depth of rupture is not considered. This could conceivably lead to overprediction of deep events, because the ground motions for such events have a longer travel path to reach recording sites. On the other hand, there are some studies indicating that the stress parameter for earthquake sources tends to increase with depth (e.g., Fletcher et al. [1984]), which could offset the distance effect. In this section, we examine trends of event terms with two depth parameters provided in the NGA-West 2 flatfile: depth to top of rupture (Z_{tor}) and depth to hypocenter (Z_{hypo}).

Figures 4.33 and 4.34 show trends of event terms with Z_{tor} and Z_{hypo} for CL1 and CL2 events sorted by **M** (**M** < 5 and **M** ≥ 5). The **M** < 5 data (Figure 4.33) indicate increasing event terms as depth increases for short periods (PGA and PSA for $T < 0.5$ sec) and a reversal towards a decreasing trend with depth for $T \geq 1.0$ sec PSA. Those trends are present for both considered source depth parameters. However, those trends are not apparent for **M** ≥ 5 data (Figure 4.34). Since the hazard for most engineering applications is governed by relatively large magnitude events, we opted not to include a source depth adjustment to our base-case GMPEs.

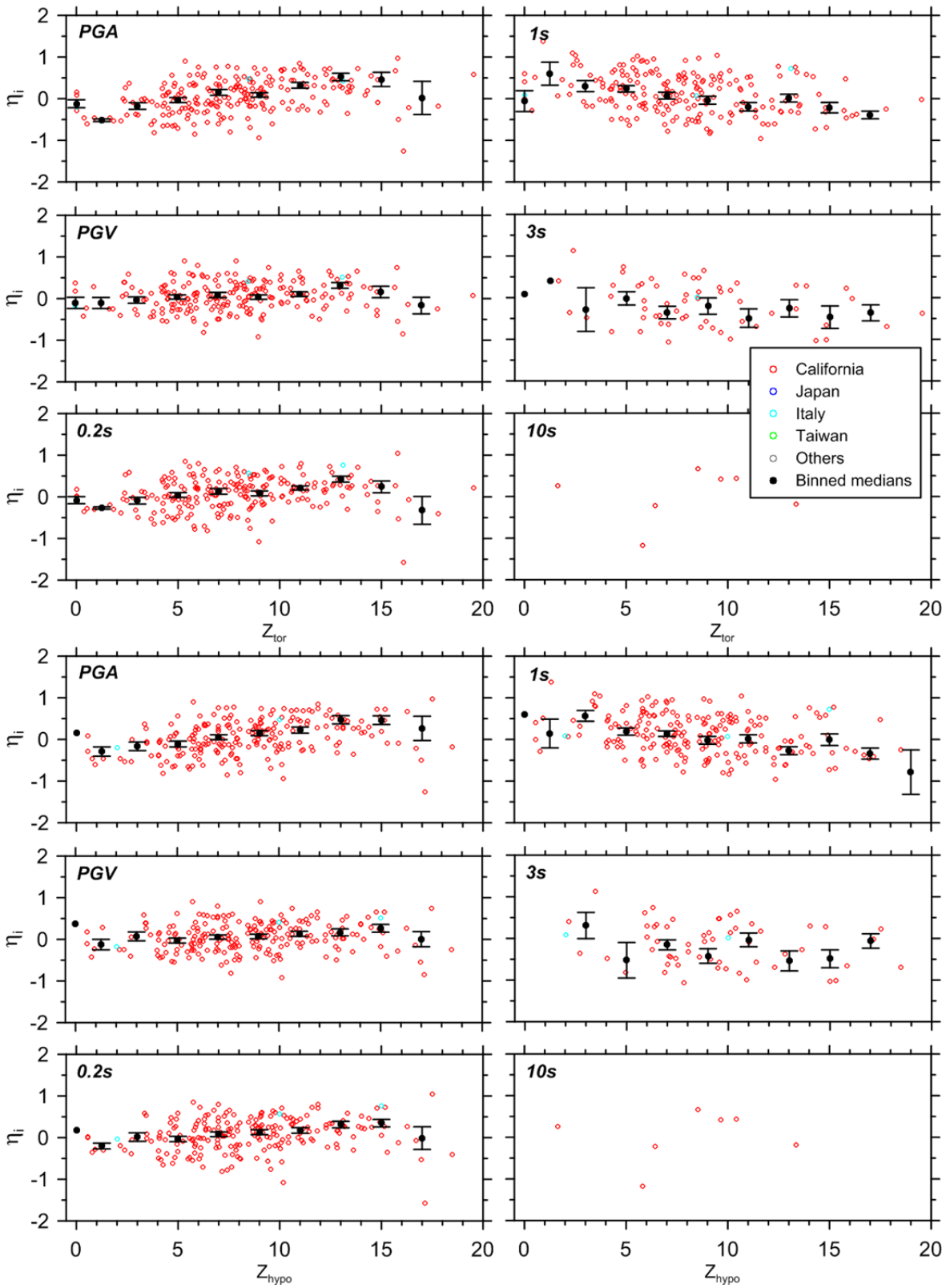

Figure 4.33 **Event terms against depth to top of rupture (Z_{tor}) (top) and hypocentral depth (Z_{hypo}) (bottom) for M < 5 CL1 and CL2 events, for which most events are from California.**

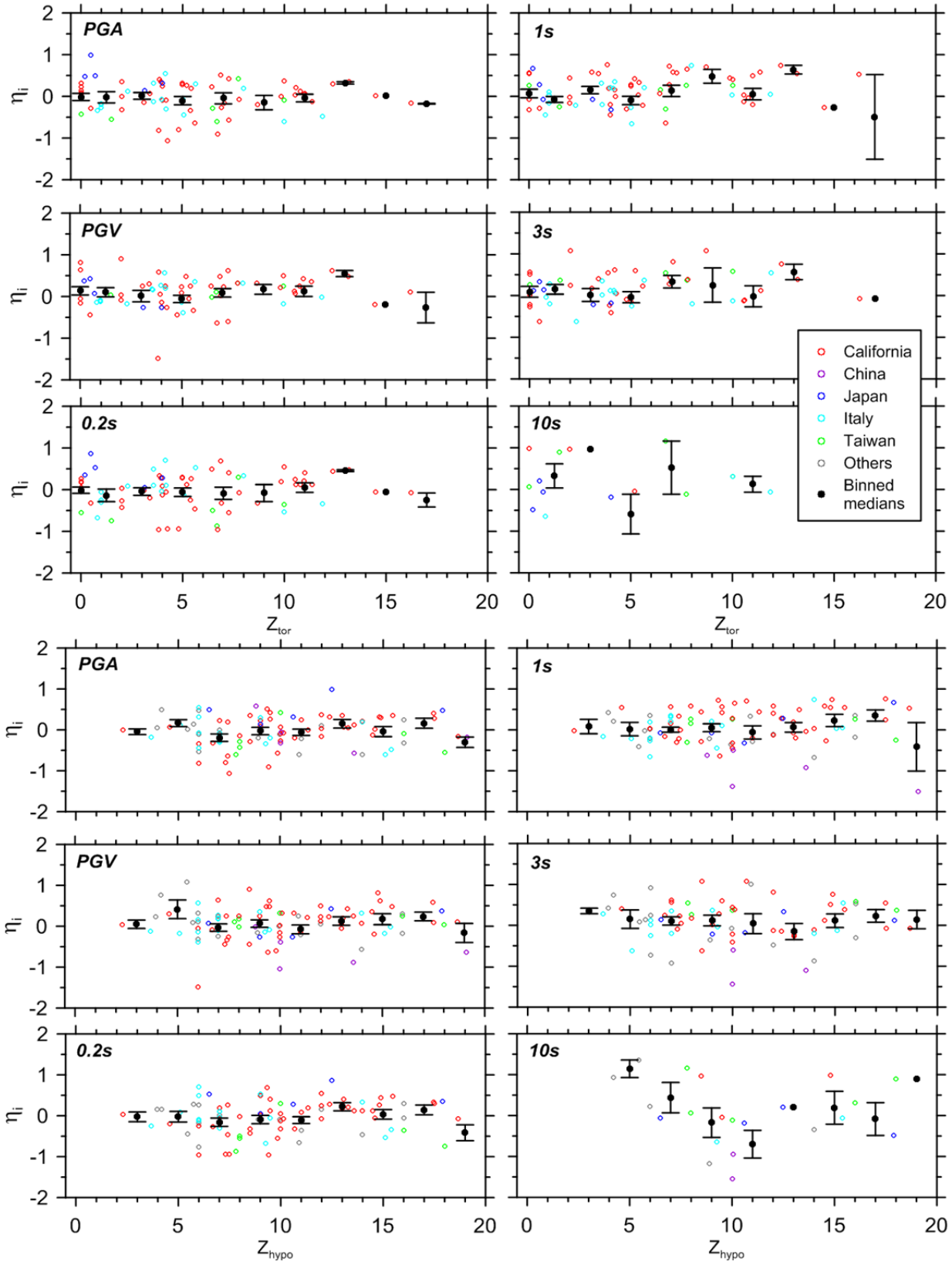

Figure 4.34 **Event term variation with depth to top of rupture (Z_{tor}) (top) and hypocentral depth (Z_{hypo}) (bottom) for M ≥ 5 CL1 and CL2 events.**

Focal Mechanism

Phase 2 regressions include the evaluation of constant terms that depend on dummy variables for four variants of focal mechanism (SS = strike-slip, RS = reverse slip, NS = normal-slip, and U = unknown). Those mechanism descriptors are based on orientations of principal stress axes and not strictly on rake angle, although they are strongly correlated, as shown in Figure 2.4.

The GMPE focal mechanism terms [Equation (3.5)] are independent of magnitude. Figures 4.35 and 4.36 show the trends of event terms with respect to rake angle for two magnitude ranges ($\mathbf{M} < 5$ and $\mathbf{M} \geq 5$). The $\mathbf{M} < 5$ results in Figure 4.35 indicate essentially zero residuals for SS and RS conditions, but positive residuals for NS. The amount of positive bias is comparable to the magnitude of the NS term, suggesting that had that term been zero, the bias would be removed. On the other hand, the $\mathbf{M} \geq 5$ results appear unbiased for SS and NS, but positive bias occurs at long periods for RS, suggesting that the RS term could be increased for $T > 1.0$ sec PSA. This will be considered in future revisions to the GMPE.

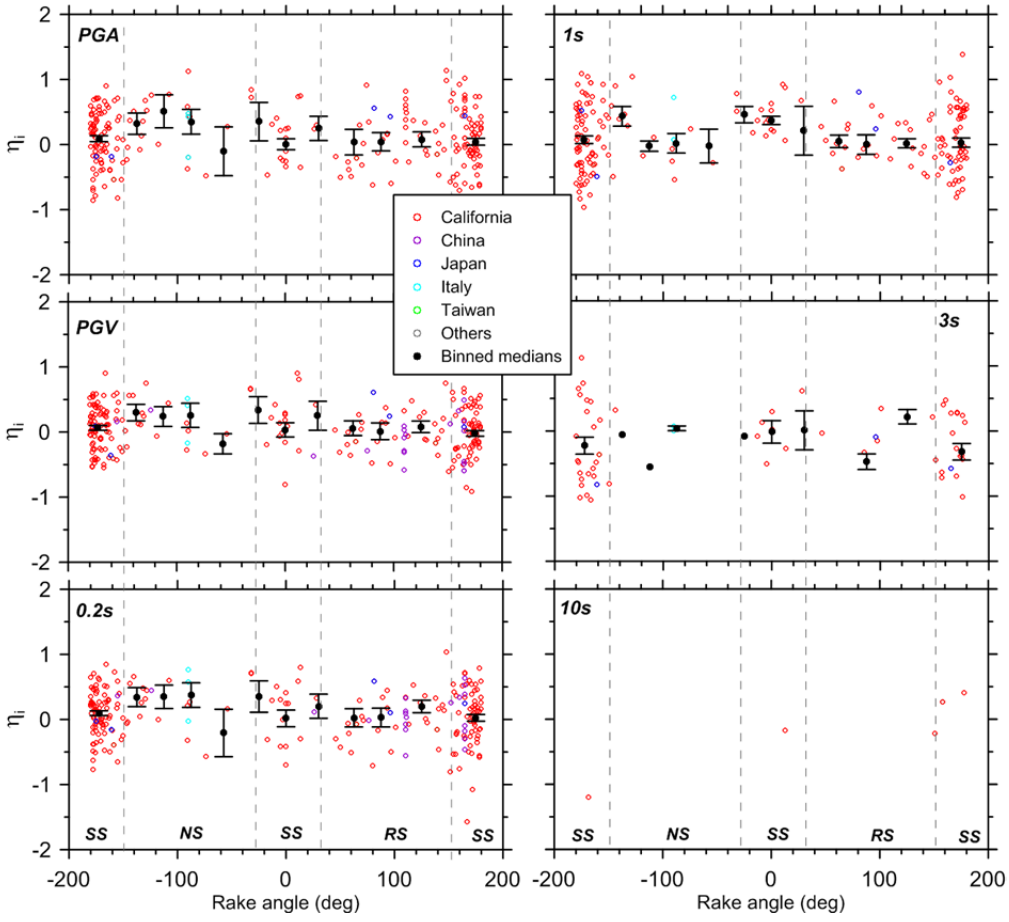

Figure 4.35 Event term variation with rake angle for M < 5 CL1 and CL2 events.

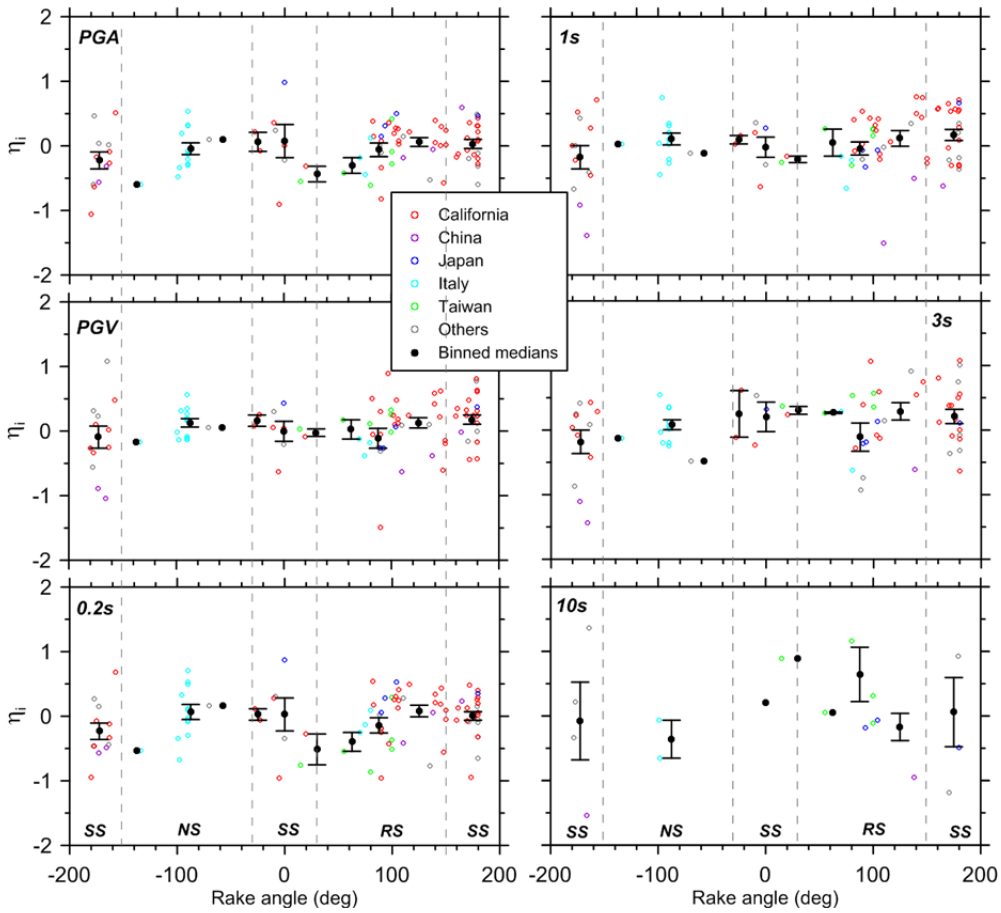

Figure 4.36 Event term variation with rake angle for M ≥ 5 CL1 and CL2 events.

4.4.4 Standard Deviation Terms

Our GMPE is formulated with separation of standard deviation terms into between-event and within-event components, τ and ϕ, respectively [Equation (3.2)]. Figure 4.37 plots τ and ϕ for the base case (Phase 2) GMPE in which the data selection criteria require $R_{JB} < 80$ km and use of only CL1 events. The present standard deviation terms are significantly higher than those in BA08 and have a different period-dependence in which a short-period peak is observed. We believe there is a physical justification for these trends—PGA and very short-period PSA is controlled by longer ground motion periods (in the range of 0.2–1.0 sec)—so dispersions for these periods might be expected to be similar, as observed. At intermediate periods, there is likely energy content in the ground motions affecting the oscillator response, which has high dispersion perhaps from kappa variability. In the remainder of this section, we investigate factors affecting standard deviation and propose appropriate equations for τ and ϕ.

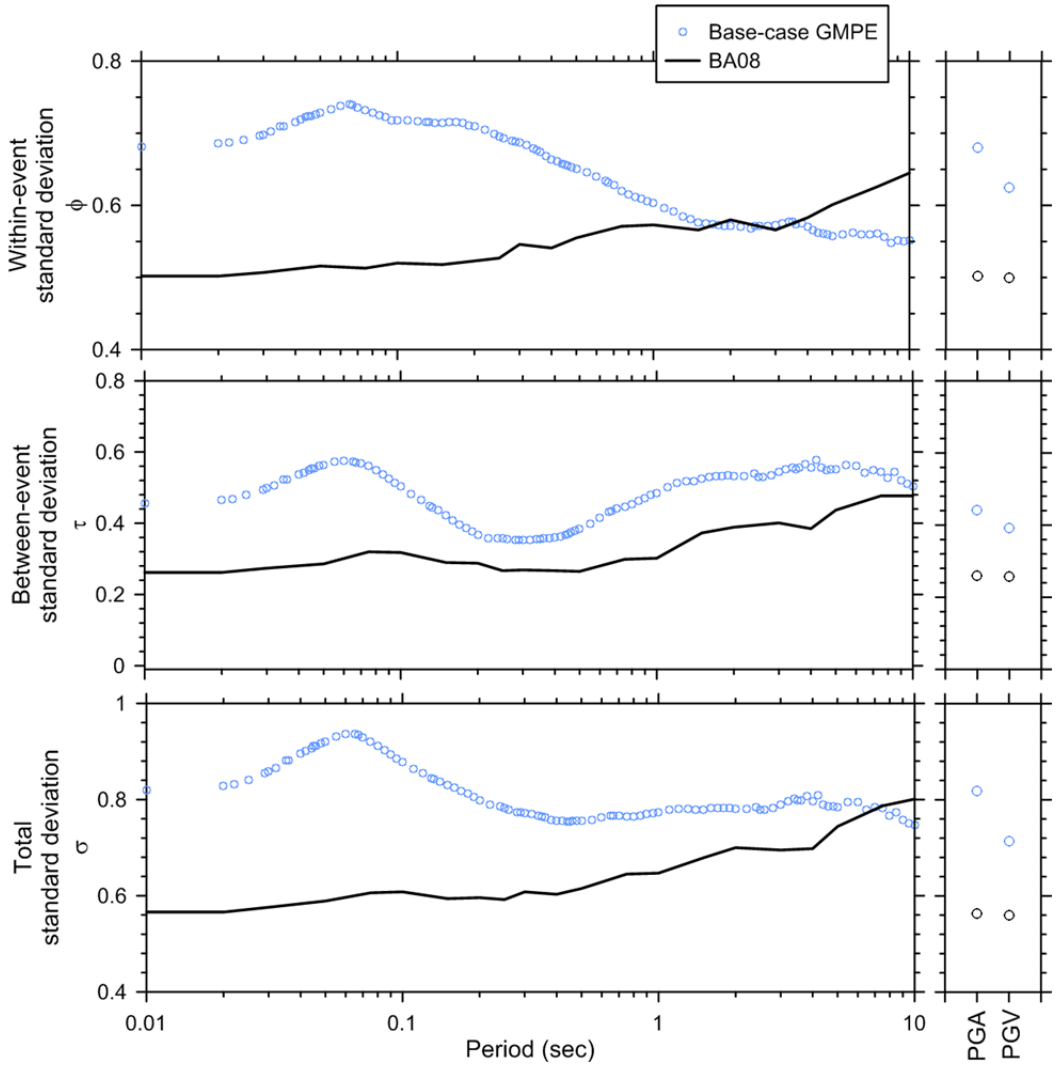

Figure 4.37 Standard deviation terms against period from base-case model from this study and BA08′. Base-case model applies for R_{JB} ≤ 80 km and CL1 events.

Using event terms from the Phase 2 data set, we plot in Figure 4.38 values of τ within 0.5**M** bins for several IMs. We observe that τ decreases with increasing **M**, with most of the change occurring between magnitudes of approximately 4.5 to 5.5. Accordingly, we propose an **M**-dependent between-event standard deviation term as follows:

$$\tau(M) = \begin{cases} \tau_1 & \mathbf{M} \le 4.5 \\ \tau_1 + (\tau_2 - \tau_1)(\mathbf{M} - 4.5) & 4.5 < \mathbf{M} < 5.5 \\ \tau_2 & \mathbf{M} \ge 5.5 \end{cases} \tag{4.11}$$

Values of τ_1 and τ_2 were computed as weighted standard deviations of event terms within the respective magnitude ranges using the Phase 2 data set and GMPE without regionalization (Δc_3=0). In those calculations, weights are proportional to the number of recordings from which

the event terms were established (N_i). Results are shown with the binned values of τ in Figure 4.38 and as a function of period in Figure 4.39a. Next, we investigated several factors not considered in the Phase 2 analyses that might influence τ. In Figure 4.39b, we show τ_1 and τ_2 computed using the same Phase 2 data set, but incorporating regional anelastic attenuation (non-zero Δc_3) and the basin model into the GMPE (labeled as 'Complete GMPE'). The effect of using the modified GMPE is to reduce τ_1, although τ_2 is not much affected. In Figure 4.39c, we add CL2 events to the data set (both CL1 and CL2 are now included), which significantly increases τ_2 but does not affect τ_1. There are a substantial number of CL2 events with **M** > 5.5, which contribute to the τ_2 increase. These are principally from five California mainshocks (including 1994 Northridge and 1983 Coalinga), Chi Chi, Taiwan, Wenchuan, China, and six earthquakes in Italy (including 2009 L'Aquila). For application, we propose the use of the τ_1 and τ_2 values in Figure 4.39b, which apply for CL1 events only; if an analysis requires consideration of aftershocks, we recommend increasing τ_2 by 0.06 at all periods.

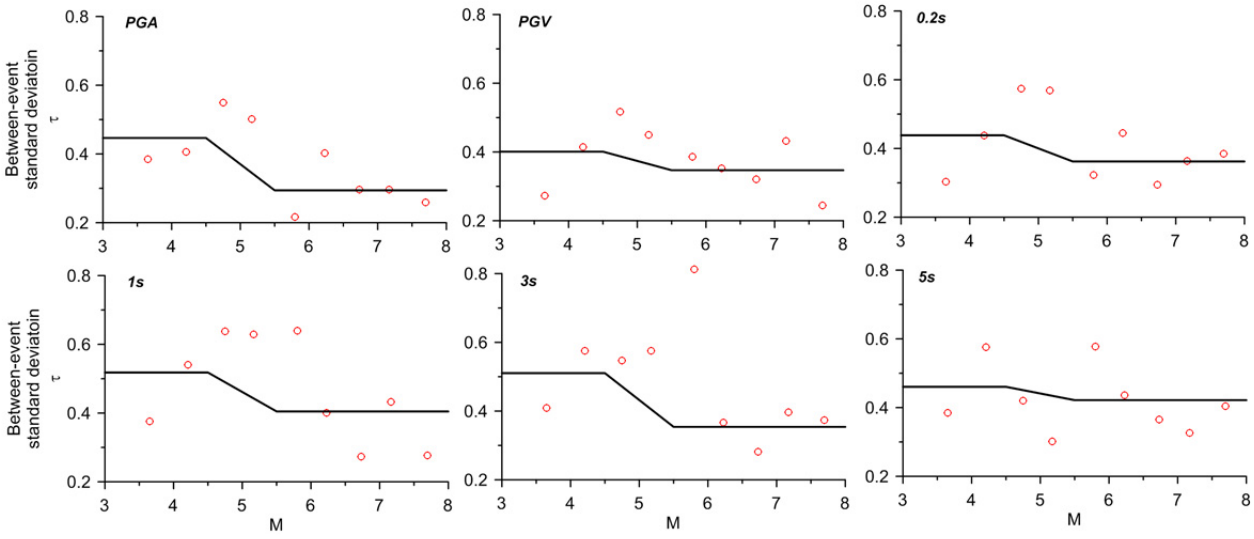

Figure 4.38 **Between-event standard deviation terms against magnitude using Phase 2 data set and base-case GMPE. Horizontal black lines indicate τ values for M < 4.5 and M > 5.5.**

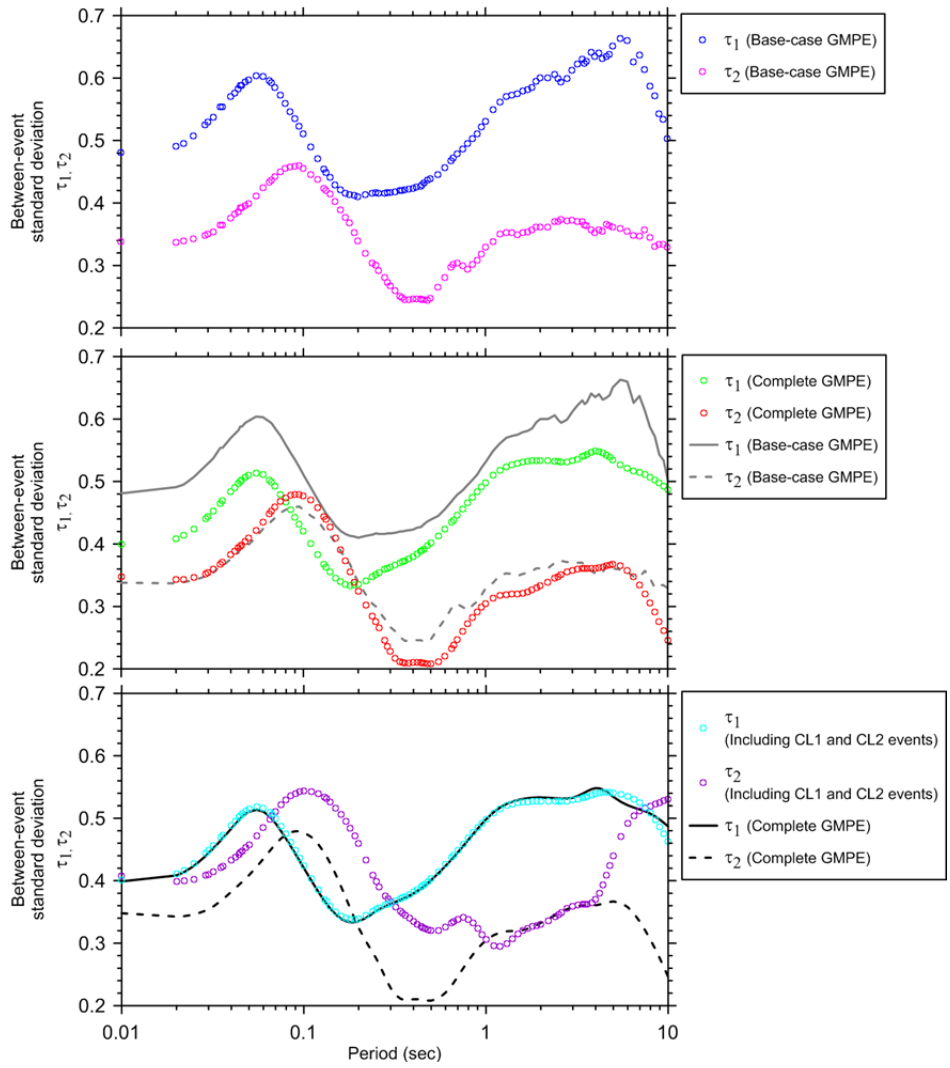

Figure 4.39 **Between-event standard deviation terms against period for (a) base-case GMPE; (b) complete GMPE, which includes regional anelastic attenuation and basin depth terms but not CL2 events; and (c) including both CL1 and CL2 events with the complete GMPE.**

In Figure 4.40, we plot values of within-event standard deviation ϕ within $\mathbf{M}$ bins using the base-case GMPE and Phase 2 data set. Parameter ϕ has a relatively complex relationship with $\mathbf{M}$, decreasing with $\mathbf{M}$ at short periods and increasing with $\mathbf{M}$ at long periods. The decreasing trends with $\mathbf{M}$ for short periods could result from variability in site-related κ (e.g., Douglas and Jousset [2011]). For distances under 80 km, we propose an $\mathbf{M}$-dependent within-event standard deviation term as follows:

$$\phi(\mathbf{M}) = \begin{cases} \phi_1 & \mathbf{M} \le 4.5 \\ \phi_1 + (\phi_2 - \phi_1)(\mathbf{M} - 4.5) & 4.5 < \mathbf{M} < 5.5 \\ \phi_2 & \mathbf{M} \ge 5.5 \end{cases} \tag{4.12}$$

Values of ϕ_1 and ϕ_2 were computed within the respective magnitude ranges using the Phase 2 data set and GMPE without regionalization (Δc_3=0), with the results shown in Figure 4.40 and 4.41a. As with the analysis of τ terms describe above, we considered the effects of including regional anelastic attenuation and the basin depth terms (Figure 4.41b) and including CL2 events (Figure 4.41c). These additional factors have a relatively minor effect on ϕ terms; the small effect of the regionalized anelastic attenuation resulted from restricting the data set to $R_{JB} \leq 80$ km.

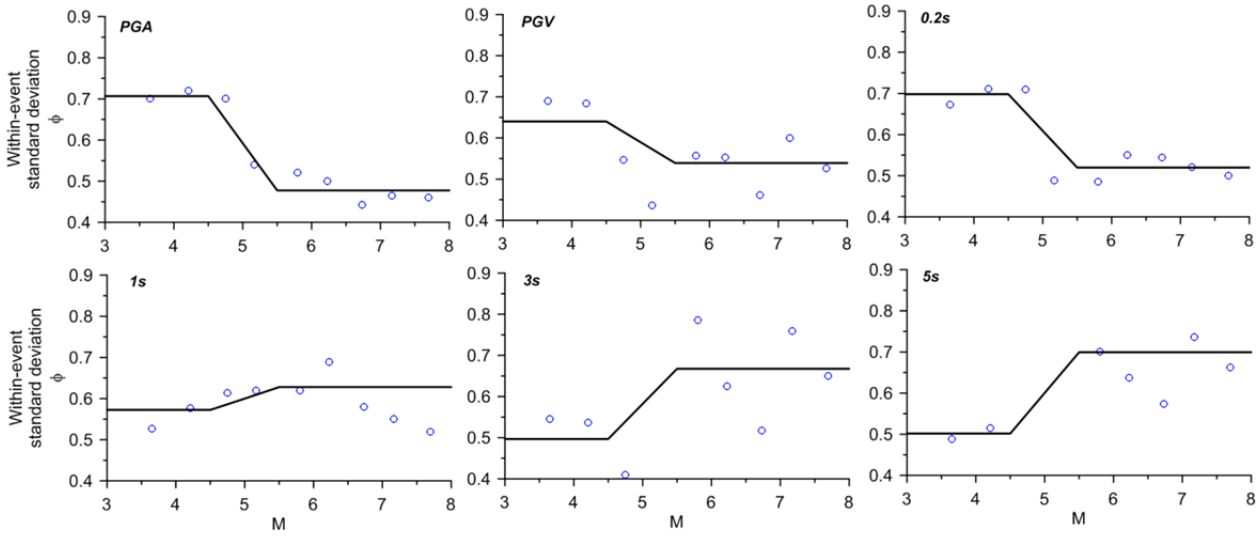

Figure 4.40 **Within-event standard deviation terms against magnitude using Phase 2 data set and base-case GMPE. Horizontal black lines indicate ϕ values for M < 4.5 and M > 5.5.**

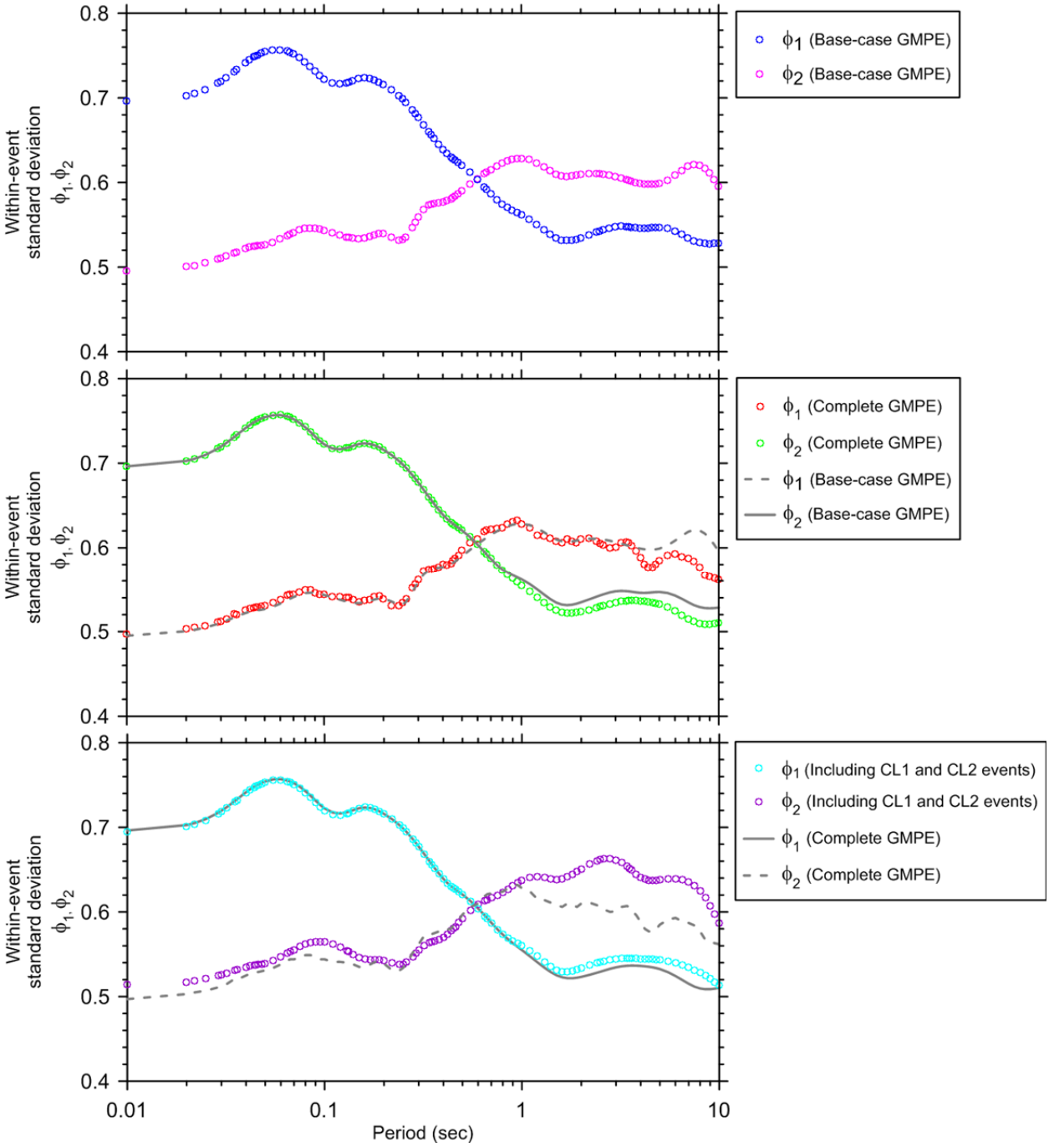

Figure 4.41 **Within-event standard deviation terms against period for (a) base-case GMPE; (b) complete GMPE, which includes regional anelastic attenuation and basin depth terms; and (c) including both CL1 and CL2 events.**

Because many applications of our GMPE will involve source-site distances beyond 80 km, we next consider standard deviations for data beyond 80 km (these analyses use CL1 events only). Because data beyond 80 km is poorly suited to the analysis of event terms, we maintain the event terms and τ evaluated using the Phase 2 data set and 'complete GMPE', as described

above. We compute within-event standard deviations for various distance ranges beyond 80 km, with the results shown in Figure 4.42. We see that ϕ rises as the distance range increases. We attribute this increased standard deviation to variability in regional anelastic attenuation effects that are not fully captured by our model (e.g., there are regions in the data set for which we do not have a regional Δc_3 term). To capture this effect, we adjust the ϕ model from Equation (4.12) to include an additive term that is applicable for $R_{JB} > 80$ km as follows:

$$\phi(\mathbf{M}, R_{JB}) = \begin{cases} \phi(\mathbf{M}) & R_{JB} \le R_1 \\ \phi(\mathbf{M}) + \Delta\phi_R \left(\dfrac{\ln(R_{JB}/R_1)}{\ln(R_2/R_1)} \right) & R_1 < R_{JB} \le R_2 \\ \phi(\mathbf{M}) + \Delta\phi_R & R_{JB} > R_2 \end{cases} \tag{4.13}$$

The term $\Delta\phi_R$ in Equation (4.13) is computed using data for $\mathbf{M} \geq 5.5$ only, because we consider the small-magnitude and large-distance results to have little practical significance for hazard assessment. Terms R_1 and R_2 are selected by visual inspection of many plots similar to those in Figure 4.42; they represent the maximum distance to which the complete GMPE ϕ terms are considered applicable (R_1, generally 80 to 130 km) and the distance beyond which we capped ϕ increases with distance (R_2, generally 200 to 270 km). Parameter $\Delta\phi_R$ ranges from about 0.15 at short periods to about 0.05 at long periods, with PGA at 0.1.

It should be realized that the increased value of ϕ at distances beyond 80 km may be reflecting regional variability in attenuation amongst the data included in the NGA-West 2 database. Thus, we expect that this increase is being strongly influenced by epistemic uncertainty in regional attenuation rates, not random site-to-site variability. If such epistemic uncertainty is being captured in a seismic hazard analysis by the use of alternative GMPEs, it should not be double-counted by including it also within the aleatory uncertainty of each GMPE. Mean seismic hazard analysis results are insensitive to whether uncertainty is treated as being epistemic or aleatory (e.g. McGuire [2004]), but the total amount of uncertainty is important. It is therefore important to recognize the extent to which some components of apparent aleatory variability may be epistemic, and avoid double counting of uncertainty in practical applications.

In Figure 4.43, we plot values of ϕ within V_{S30} bins (four equally-spaced bins per log cycle of V_{S30}). We observe ϕ to decrease with V_{S30} at short periods over the approximate range of 150 to 300 m/sec (there are also large changes in ϕ for the fastest V_{S30} bin relative to those before, which is affected by relatively small data size and is not considered meaningful). Similar features have been observed previously [Choi and Stewart 2005], with the lower ϕ values for soft sites being attributed to nonlinear site response, which amplifies weak motions and de-amplifies strong motions, thus reducing standard deviation relative to motions on the underlying reference site conditions.

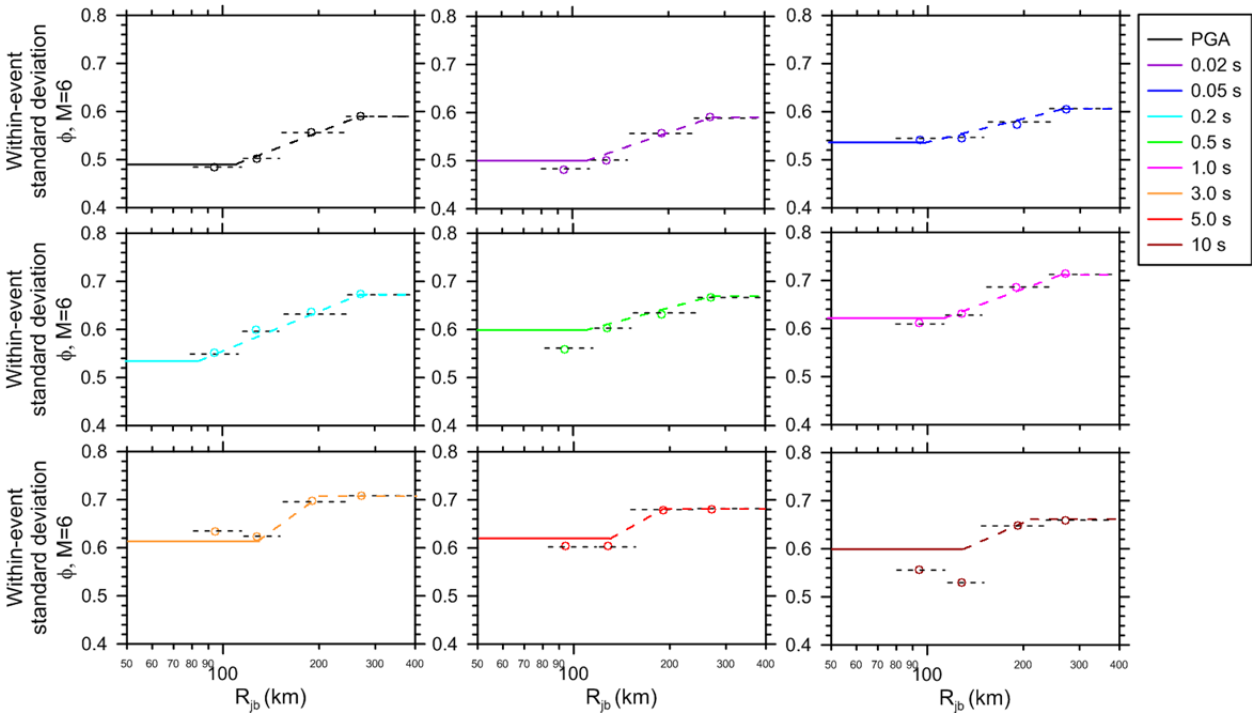

Figure 4.42 **Effects of distance on within-event standard deviation terms for M ≥ 5.5 earthquakes. The discrete symbols indicated computed values of ϕ in non-overlapping distance bins for R_{JB} > 80 km. The horizontal solid lines are values of ϕ_2 shown previously (e.g., from Figures 4.40 and 4.41). The dotted lines are the proposed distance-dependent model from Equation (4.12).**

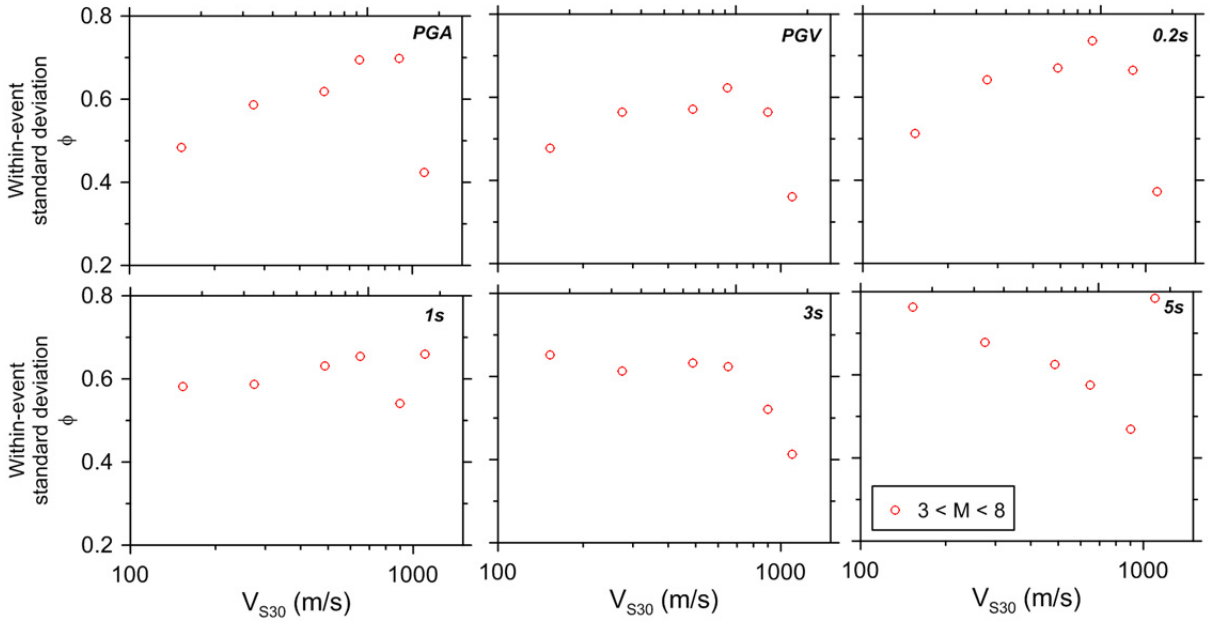

Figure 4.43 **Within-event standard deviation terms against V_{S30} using complete GMPE and using CL1 data for R_{JB} < 300 km and all M.**

In Figure 4.44, we evaluate the V_{S30}-dependent shift of ϕ within $\mathbf{M}$ and R_{JB} bins for subsets of data with $V_{S30} > 300$ m/sec and $V_{S30} < 225$ m/sec. For comparison, the ϕ values from the $\mathbf{M}$ - and R_{JB}-dependent model [Equations (4.12) and (4.13)] are also shown. We observe that in the close-distance data sets ($R_{JB} \le R_1$), the ϕ terms for $V_{S30} > 300$ m/sec match those from the models, so no adjustment is needed for this condition (some offsets are observed for larger distances, which are not considered for our standard deviation models). On the other hand, for $V_{S30} < 225$ m/sec, ϕ terms are reduced relative to the model by amounts generally ranging from 0.05 to 0.1. We capture this effect as follows:

$$\phi(\mathbf{M}, R_{JB}, V_{S30}) = \begin{cases} \phi(\mathbf{M}, R_{JB}) & V_{S30} \ge V_2 \\ \phi(\mathbf{M}, R_{JB}) - \Delta\phi_V \left(\dfrac{\ln(V_2/V_{S30})}{\ln(V_2/V_1)} \right) & V_1 \le V_{S30} \le V_2 \\ \phi(\mathbf{M}, R_{JB}) - \Delta\phi_V & V_{S30} \le V_1 \end{cases} \tag{4.14}$$

The term $\Delta\phi_V$ in Equation (4.14) represents the ϕ term correction, and is shown in the lower-left panel of Figure 4.44. Limiting velocities V_1 and V_2 are taken as 225 and 300 m/sec, respectively. The term $\phi(\mathbf{M}, R_{JB})$ in Equation (4.14) represents the model from Equation (4.13); as such, the relation in Equation. (4.14), when combined with Equations (4.12) and (4.13), represents the recommended relationship for ϕ in our GMPEs.

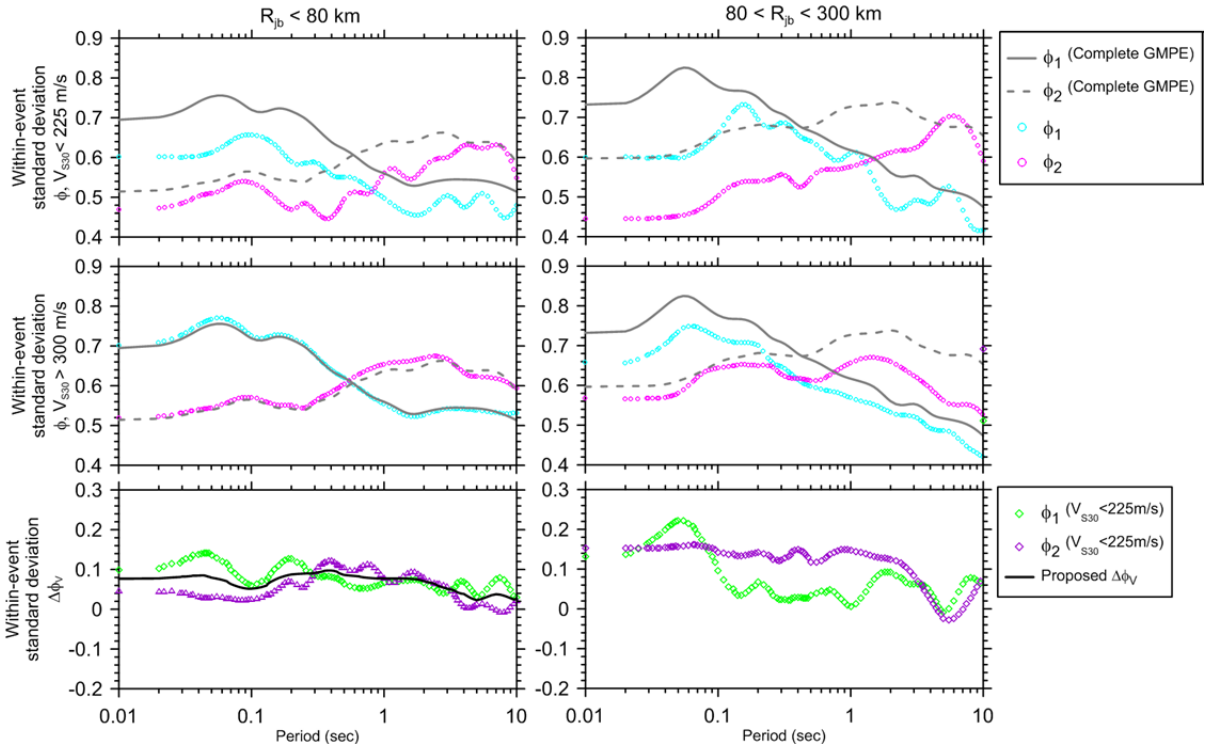

Figure 4.44 Effects of V_{S30} on within-event standard deviation terms. We define correction factor $\Delta\phi_V$ from data with $V_{S30} \le 225$ m/sec and $R_{JB} \le 80$ km.

4.5 COMPARISON TO BA08′ MODEL

Figure 4.45 compares median predictions of BA08′ (as modified in Atkinson and Boore [2011]) to the proposed model. The biggest differences between the predictions from the new GMPEs and those of BA08' are for small magnitudes at distances less than 10 to 20 km, where the motions predicted from the new equations are substantially smaller than those from BA08′. In addition, the predicted motions from the new equations are substantially larger than those from BA08′ at the longest period (T = 10 sec), for which there were few data available to BA08′ (and the available data were dominated by one earthquake—the 1999 Chi-Chi earthquake, as shown in Figure 16 of BA08). The two situations noted (small magnitudes and long periods) correspond to the magnitudes and distances for which there is the most increase of data used in our new work, compared to that available to BA08′, as discussed previously in Section 2.4.

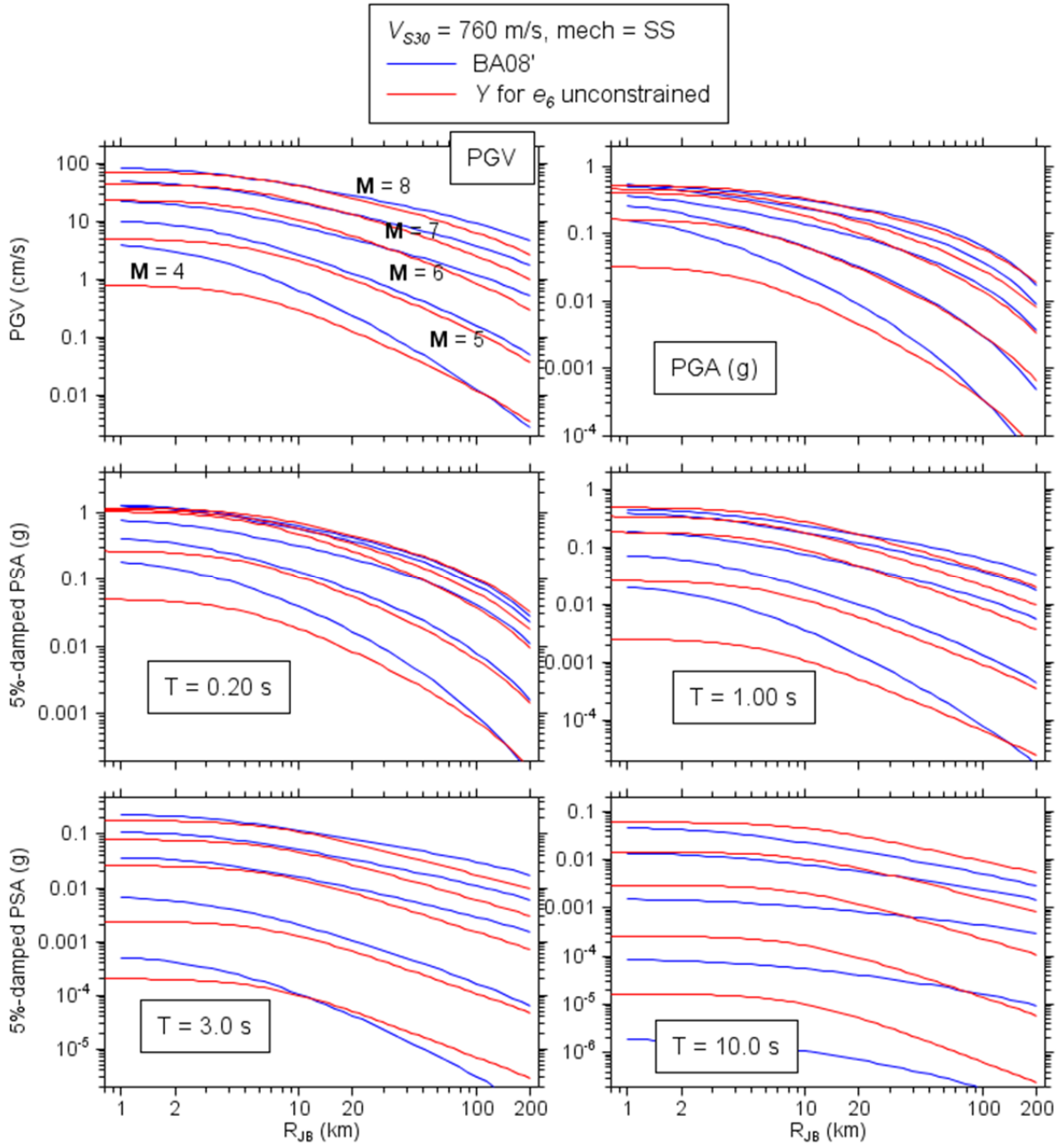

Figure 4.45 **Comparison of median trends of proposed GMPE as compared to BA08′, as a function of distance. The BA08′ values have been adjusted to RotD50 using the ratios RotD50/GMRotI50 in Boore [2010] (maximum adjustment of 1.06 for T = 10 sec).**

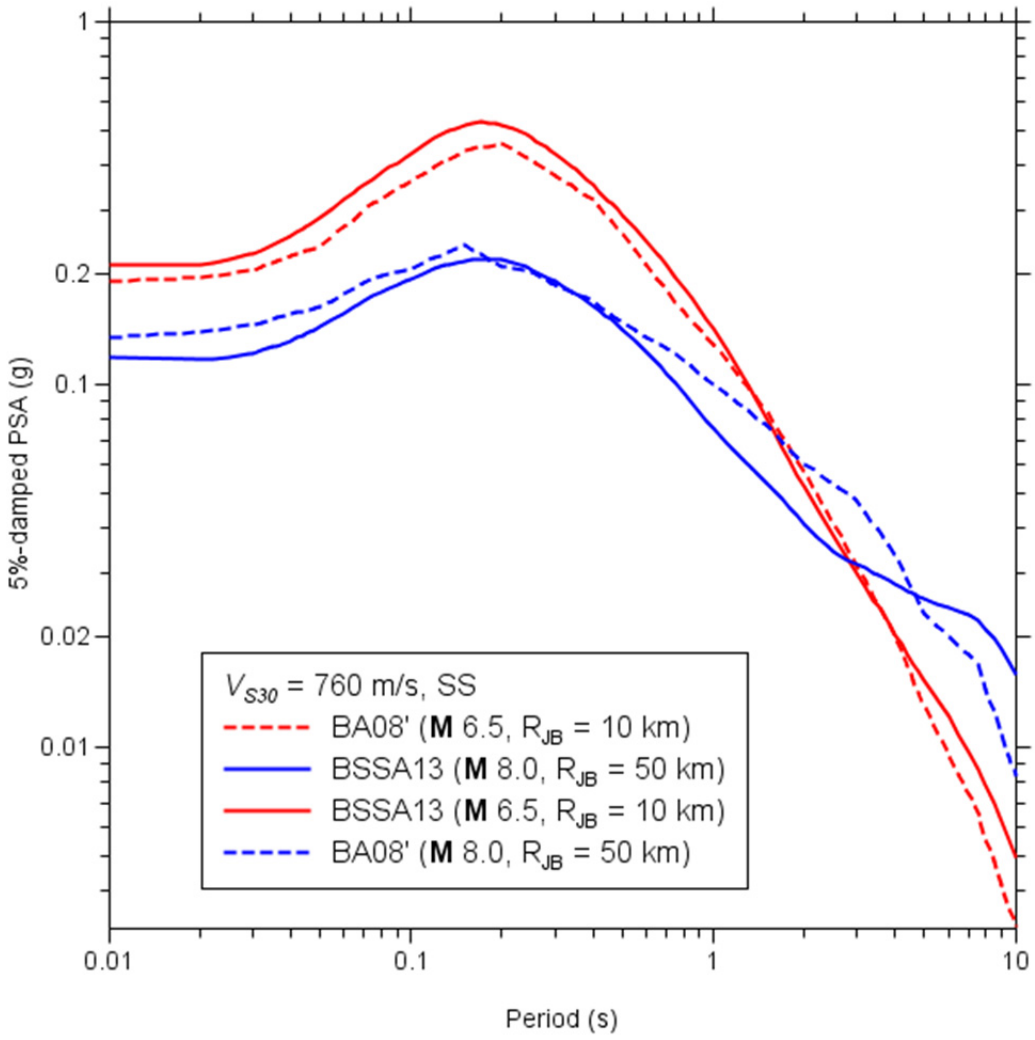

Figure 4.46 **Comparison of median PSA of proposed GMPE as compared to BA08′ for M 6.5 and R_{JB}=10 km event and M 8.0 and R_{JB} = 50 km event. The BA08′ values have been adjusted to RotD50 using the ratios RotD50/GMRotI50 in Boore [2010] (maximum adjustment of 1.06 for T=10 sec).**

Figure 4.46 compares spectra for conditions that are often significant for seismic hazard in the western U.S.—a close-distance **M** 6.5 event and a larger-distance **M** 8.0 event. For the **M** 6.5 event the spectra are slightly increased from BA08′ across nearly the full range of periods. For the **M** 8.0 event, the spectra are not much changed for $T < 0.5$ sec, are reduced by up to 20–30% for periods between 1 and 3 sec, and are increased beyond approximate 4–5 sec. These trends have been examined carefully and are driven by a number of events with $\mathbf{M} > \mathbf{M}_h$ that have been added to the database since 2008.

Figure 4.47 compares standard deviation terms in the present study to those obtained in BA08′. The total standard deviations (σ) from the present study for $\mathbf{M} \geq 5.5$, $R_{JB} \leq 80$ km, and $V_{S30} > 300$ m/sec are generally comparable to those in BA08′, being somewhat higher near $T =$

0.1 sec and lower for $T > 5$ sec. The figure also shows the substantial increase in σ for $\mathbf{M} \leq 4.5$ events in the present study, and the relatively dominant effect of within-event variability (ϕ) as compared to between-event variability (τ).

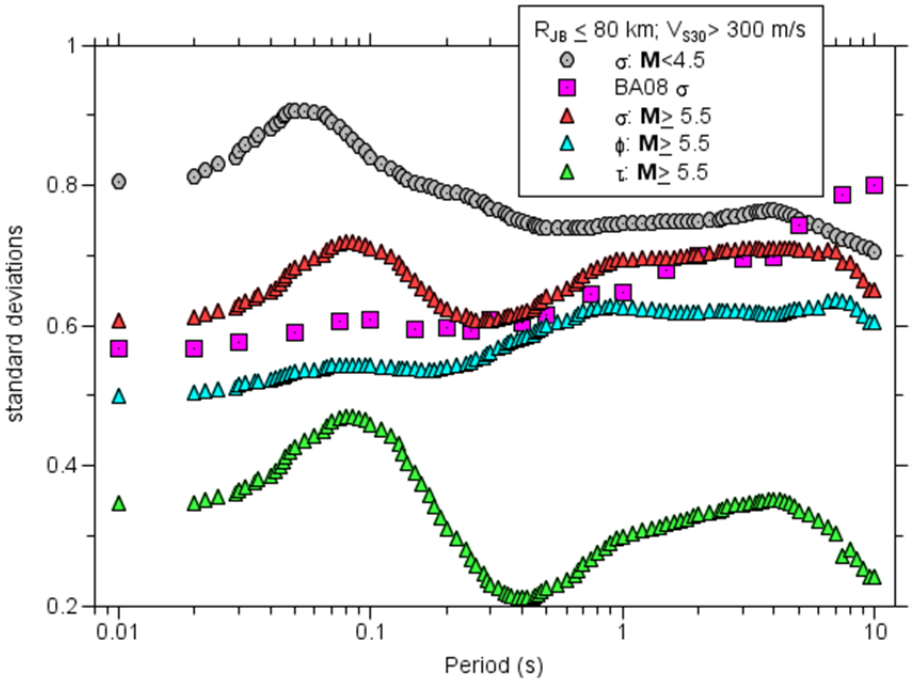

Figure 4.47 Comparison of standard deviation terms in proposed GMPE as compared to BA08′.

5 Guidelines for Usage

5.1 LIMITS ON PREDICTOR VARIABLES

We recommend the following limits for the predictor variables used in our GMPE:

- Strike-slip and reverse-slip earthquakes, **M** = 3 to 8.5
- Normal-slip earthquakes, **M** = 3 to 7
- Distance, R_{JB} = 0 to 300 km
- Time-averaged shear wave velocities of V_{S30} = 150 to 1500 m/sec
- Basin depth, z_1 = 0 to 3.0 km
- CL1 and CL2 event types (mainshocks and aftershocks)

These limits are subjective estimates based on the distributions of the recordings used to develop the equations.

5.2 MODEL LIMITATIONS

The GMPEs presented in this report are intended for application in tectonically active crustal regions. The equations are not recommended for other tectonic regimes such as subduction zones or stable continental regions. The data controlling the equations are derived principally from California, Taiwan, Japan, China, the Mediterranean region (Italy, Greece, Turkey), and Alaska. We have demonstrated some regional variations in ground motions, so application of the GMPE to other areas considered to be active crustal regions carries an additional degree of epistemic uncertainty.

The site effects incorporated into the GMPE provide an average representation of the site effects conditional on specified values of V_{S30} and z_1. Specific sites may exhibit significant differences from these average site effects. This is particularly likely when the geologic structure of the site is significantly different than the 'average' of the NGA-West 2 site database. As shown in other work (e.g., Baturay and Stewart [2003]; Bazzurro and Cornell [2004]), the benefits of site-specific analysis are usually greatest when the site exhibits a significant impedance contrast or highly nonlinear soil response.

6 Summary

We have presented a set of ground-motion prediction equations that we believe are the simplest formulation demanded by the NGA-West 2 database used for the regressions. Future versions of the equations might include additional terms if these can be unambiguously supported by data. Data continue to be recorded (our dataset necessarily had to be limited to earthquakes occurring before 2012), and these new data could potentially support the inclusion of more predictor variables. Nevertheless, we think that our equations will be useful, in spite of the simplified analysis: many predictor variables not included in our equations may be unavailable for use in general seismic hazard analysis applications.

There are a few areas where refinements to the equations are likely over time. One such area of inquiry concerns regional variability of site effects. As noted in this report, the regional variability in the site amplification model found by our analysis was not as large as expected, based particularly on the known tendency of Japanese sites to have peak responses at high frequencies. We intend to further investigate the implications of our current findings in relation to other studies [Ghofrani et al. 2013; Stewart et al. 2013]. We also intend to evaluate our equations further with respect to directivity and hanging wall effects.

In conclusion, the new relations developed here are a significant improvement over BA08′, and provide a demonstrably reliable description of recorded ground-motion amplitudes for shallow crustal earthquakes in active tectonic regions over a wide range of magnitudes, distances, and site conditions.

REFERENCES

Abrahamson N.A., Youngs R.R. (1992). A stable algorithm for regression analyses using the random effects model, *Bull. Seismol. Soc. Am.*, 82: 505–510.

Abrahamson N.A., Silva W.J. (2008). Summary of the Abrahamson and Silva NGA ground motion relations, *Earthq. Spectra,* 24: 67–97.

Afacan K.B., Brandenberg S.J., Stewart J.P. (2013). Centrifuge modeling studies of site response in soft clay over wide strain range, ASCE, *J. Geotech. Geoenv. Eng.,* accepted for publication.

Ancheta T.D., Darragh R.R., Stewart J.P., Seyhan E., Silva W.J., Chiou B., Woodell K., Graves R.W., Kottke A., Baltay A. (2013). PEER NGA-West 2 Database, *PEER Report 201303*/, Pacific Earthquake Engineering Research Center, University of California, Berkeley, CA.

Atkinson G. M. (1993). Earthquake source spectra in eastern North America, *Bull. Seismol. Soc. Am.,* 83: 1778–1798.

Atkinson G.M., Casey R. (2003). A comparison of ground motions from the 2001 M 6.8 in-slab earthquakes in Cascadia and Japan, *Bull. Seismol. Soc. Am.,* 93: 1823–1831.

Atkinson, G. M., and Morrison, M. (2009). "Regional variability in ground motion amplitudes along the west coast of North America," *Bull. Seismol. Soc. Am.,* 99: 2393–2409.

Atkinson G.M., Silva W.J. (2000). Stochastic modeling of California ground motions, *Bull. Seismol. Soc. Am.*, 90: 255–274.

Atkinson G.M., Boore D.M. (2011). Modifications to existing ground-motion prediction equations in light of new data, *Bull. Seismol. Soc. Am.*, 101**:** 1121–1135.

Anderson J., Kawase H., Biasi G., Brune, J. (2013). Ground motions in the Fukushima Hamadori, Japan, normal faulting earthquake, *Bull. Seismol. Soc. Am.*, Vol. 113, in press.

Baturay M. B., Stewart J.P. (2003). Uncertainty and bias in ground motion estimates from ground response analyses, *Bull. Seismol. Soc. Am.*, 93: 2025–2042.

Bazzurro P., Cornell C.A. (2004). Nonlinear soil-site effects in probabilistic seismic-hazard analysis, *Bull. Seismol. Soc. Am.*, 94: 2110-2123.

Bommer J.J., Douglas J., Strasser F.O. (2003). Style-of-faulting in ground-motion prediction equations, *Bull. Earthq. Eng.,* 1: 171–203.

Boore D.M., Atkinson G.M. (1989). Spectral scaling of the 1985-1988 Nahanni, Northwest Territories, earthquakes, *Bull. Seismol. Soc. Am.*, 79: 1736–1761.

Boore D.M., Joyner W.B., Fumal T.E. (1997). Equations for estimating horizontal response spectra and peak acceleration from western North American earthquakes: A summary of recent work (with 2005 Erratum), *Seismol. Res. Lett.,* 68**:** 128–153.

Boore D.M. (2005). SMSIM--Fortran programs for simulating ground motions from earthquakes: Version 2.3--A revision of OFR 96-80-A, U.S. Geological Survery, *USGS Survey Open-File Report 00-509*, revised 15 August 2005, 55 pgs.

Boore D.M., Watson-Lamprey J., Abrahamson N.A. (2006). GMRotD and GMRotI: Orientation-independent measures of ground motion, *Bull. Seismol. Soc. Am.* 94(6A): 1502–1511.

Boore D.M., Atkinson G.M. (2007). Boore-Atkinson NGA ground motion relations for the geometric mean horizontal component of peak and spectral ground motion parameters, *PEER 2007/01*, Pacific Earthquake Engineering Research Center, University of California, Berkeley, CA.

Boore D.M., Atkinson G.M. (2008). Ground motion prediction equations for the average horizontal component of PGA, PGV, and 5%-damped PSA at spectral periods between 0.01 and 10.0 s, *Earthq. Spectra,* 24: 99–138.

Boore D.M. (2010). Orientation-independent, non geometric-mean measures of seismic intensity from two horizontal components of motion, *Bull. Seismol. Soc. Am.* 100: 1830–1835.

Boore D.M., Thompson E.M., Cadet H. (2011). Regional correlations of VS30 and velocities averaged over depths less than and greater than 30 m, *Bull. Seismol. Soc. Am.,* 101: 3046–3059.

Campbell K.W., Bozorgnia Y. (2008). NGA ground motion model for the geometric mean horizontal component of PGA, PGV, PGD and 5% damped linear elastic response spectra for periods ranging from 0.01 to 10 s, *Earthq. Spectra*, 24: 139–172.

Chiou B, Youngs R.R. (2008). Chiou and Youngs PEER-NGA empirical ground motion model for the average horizontal component of peak acceleration and pseudo-spectral acceleration for spectral periods of 0.01 to 10 seconds, *Earthq. Spectra,* 24: 173–215.

Chiou B. Youngs R.R. (2012). Updating the Chiou and Youngs NGA model: Regionalization of anelastic attenuation, *Proceedings, 15th World Conference on Earthquake Engineering,* Lisbon, Portugal.

Chiou B., Darragh R. Gregor N., Silva W.J. (2008). NGA project strong-motion database, *Earthq. Spectra*, 24: 23–44.

Chiou B., Youngs R., Abrahamson N.A., Addo K. (2010). Ground motion attenuation model for small to moderate shallow crustal earthquakes in California and its implications on regionalization of ground motion prediction models, *Earthq. Spectra*, 26: 907–926.

Choi Y., Stewart J. P. (2005). Nonlinear site amplification as function of 30 m shear wave velocity, *Earthq. Spectra*, 21: 1–30.

Choi Y., Stewart J.P., Graves R.W. (2005). Empirical model for basin effects that accounts for basin depth and source location, *Bull. Seismol. Soc. Am.*, 95: 1412–1427.

Day S.M., Graves R.W., Bielak J., Dreger D., Larsen S., Olsen K. B., Pitarka A., Ramirez-Guzman L. (2008). Model for basin effects on long-period response spectra in southern California, *Earthq. Spectra*, 24: 257–277.

Douglas J. (2003). Earthquake ground motion estimation using strong-motion records: A review of equations for the estimation of peak ground acceleration and response spectral ordinates, *Earth-Science Reviews*, 61(1–2): 43–104.

Douglas J. (2011). Ground motion prediction equations 1964-2010, *PEER Report 2011/102*, Pacific Earthquake Engineering Research Center, Berkeley, CA.

Douglas J., Halldórsson B. (2010). On the use of aftershocks when deriving ground-motion prediction equations, *Proceeding, 9th U.S. National and 10th Canadian Conference on Earthquake Engineering*, Paper No 220, 10 pgs., Toronto, Ontario, Canada.

Douglas J., Jousset P. (2011). Modeling the difference in ground-motion magnitude-scaling in small and large earthquakes, *Seismol. Res. Lett.,* 82: 504–508.

Douglas J., Gehl P., Bonilla L.F., Scotti O., Régnier J. Duval A.-M., Bertrand E. (2009). Making the most of available site information for empirical ground-motion prediction, *Bull. Seismol. Soc. Am.* 99: 1502–1520.

Field E.H. (2000). A modified ground motion attenuation relationship for southern California that accounts for detailed site classification and a basin depth effect, *Bull. Seismol. Soc. Am.*, 90: S209–S221.

Fletcher J., Boatwright J., Haar L., Hanks T., McGarr A. (1984). Source parameters for aftershocks of the Oroville, California, earthquake, *Bull. Seismol. Soc. Am.*, 74: 1101–1123.

Ghofrani H., Atkinson G. M., Goda K. (2013). Implications of the 2011 M9.0 Tohoku Japan earthquake for the treatment of site effects in large earthquakes, *Bull. Earthq. Eng*., 11: 171–203.

Johnston A.C., Coppersmith K.J., Kanter L.R., Cornell C.A. (1994). The earthquakes of stable continental regions, *Technical Report TR-102261-VI*, Electric Power Research Institute (EPRI), Palo Alto, CA.

Joyner W.B., Boore D. M. (1993). Methods for regression analysis of strong-motion data, *Bull. Seismol. Soc. Am.*, 83: 469–487.

Joyner W.B., Boore D.M. (1994). Errata: Methods for regression analysis of strong-motion data, *Bull. Seismol. Soc. Am.*, 84: 955–956.

Joyner W.B., Fumal T. E. (1984). Use of measured shear-wave velocity for predicting geologic site effects on strong ground motion, *Proceedings. Eighth World Conference on Earthquake Engineering,* 2: 777–783, San Francisco, CA.

Joyner W.B., Fumal T.E. (1985). Predictive mapping of earthquake ground motion, in *Evaluating Earthquake Hazards in the Los Angeles Region*, J.I. Ziony, Ed., *USGS Professional Paper 1360*, pp. 203–220.

Kamai R., Abrahamson N.A., Silva W.J. (2013). Nonlinear horizontal site response for the NGA-West 2 project, *PEER Report 2013-12*, Pacific Earthquake Engineering Research Center, University of California, Berkeley, CA.

Kottke A. (2011). Selection of Wenchuan stations based on geology, Unpublished internal PEER white paper, November 11, 2011.

Lee Y., Anderson J.G. (2000). Potential for improving ground-motion relations in southern California by incorporating various site parameters, *Bull. Seismol. Soc. Am.*, 90: S170–S186.

McGuire R.K. (2004). *Seismic Hazard and Risk Analysis*, Monograph No. MNO-10, Earthquake Engineering Research Institute, Oakland, CA.

Pinheiro H., Bates D., DebRoy S., Sarkar D., and the R Development Core Team (2013). *NLME: Linear and Nonlinear Mixed Effects Models*, R package version 3.1–108.

Power M. Chiou B. Abrahamson N.A., Bozorgnia Y. Shantz T., Roblee C. (2008). An overview of the NGA project, *Earthq. Spectra*, 24: 3–21.

Scasserra G., Stewart J.P., Bazzurro P., Lanzo G., Mollaioli, F. (2009). A comparison of NGA ground-motion prediction equations to Italian data, *Bull. Seismol. Soc. Am.*, 99: 2961–2978.

Schmedes J., Archuleta R.J. (2008). Near-source ground motion along strike-slip faults: Insights into magnitude saturation of PGV and PGA, *Bull. Seismol. Soc. Am.* 98: 2278–2290.

Steidl J.H. (2000). Site response in southern California for probabilistic seismic hazard analysis, *Bull. Seismol. Soc. Am.* 90: S149–S169.

Stewart J.P., Seyhan E. (2013). Semi-empirical nonlinear site amplification and its application in NEHRP site factors," *PEER Report 2013*, Pacific Earthquake Engineering Research Center, University of California, Berkeley, CA.

Stewart J. P. (2000). Variations between foundation-level and free-field earthquake ground motions, *Earthq. Spectra*, 16: 511–532.

Stewart J.P, Midorikawa S., Graves R.W., Khodaverdi K., Miura H., Bozorgnia Y., Campbell K.W. (2013). Implications of M_w 9.0 Tohoku-oki Japan earthquake for ground motion scaling with source, path, and site parameters, *Earthq. Spectra*, 29: S1–S21.

Wooddell K.E., Abrahamson N. A. (2012). New earthquake classification scheme for mainshocks and aftershocks in the NGA-West 2 ground motion prediction equations (GMPEs), *Proceedings, 15th World Conference on Earthquake Engineering*, Lisbon, Portugal.

APPENDIX: COEFFICIENT TABLES

BSSA13	*Magnitude Scaling*								*Distance Scaling*					
Period(sec)	**e_0**	**e_1**	**e_2**	**e_3**	**e_4**	**e_5**	**e_6**	**M_h**	**c_1**	**c_2**	**c_3**	**M_{ref}**	**R_{ref} (km)**	**h (km)**
-1	5.037	5.078	4.849	5.033	1.073	-0.1536	0.2252	6.2	-1.243	0.1489	-0.00344	4.5	1	5.3
0	0.4473	0.4856	0.2459	0.4539	1.431	0.05053	-0.1662	5.5	-1.134	0.1917	-0.00809	4.5	1	4.5
0.01	0.4534	0.4916	0.2519	0.4599	1.421	0.04932	-0.1659	5.5	-1.134	0.1916	-0.00809	4.5	1	4.5
0.02	0.48598	0.52359	0.29707	0.48875	1.4331	0.053388	-0.16561	5.5	-1.1394	0.18962	-0.00807	4.5	1	4.5
0.022	0.49866	0.53647	0.31347	0.49973	1.4336	0.054888	-0.1652	5.5	-1.1405	0.18924	-0.0081	4.5	1	4.5
0.025	0.52283	0.5613	0.34426	0.51999	1.4328	0.057529	-0.16499	5.5	-1.1419	0.18875	-0.00815	4.5	1	4.5
0.029	0.55949	0.59923	0.39146	0.54995	1.4279	0.060732	-0.16632	5.5	-1.1423	0.18844	-0.00829	4.5	1	4.5
0.03	0.56916	0.6092	0.40391	0.55783	1.4261	0.061444	-0.1669	5.5	-1.1421	0.18842	-0.00834	4.5	1	4.49
0.032	0.58802	0.62875	0.42788	0.5733	1.4227	0.062806	-0.16813	5.5	-1.1412	0.1884	-0.00845	4.5	1	4.45
0.035	0.61636	0.65818	0.46252	0.59704	1.4174	0.064559	-0.17015	5.5	-1.1388	0.18839	-0.00864	4.5	1	4.4
0.036	0.62554	0.66772	0.47338	0.60496	1.4158	0.065028	-0.17083	5.5	-1.1378	0.18837	-0.00872	4.5	1	4.38
0.04	0.66281	0.70604	0.51532	0.63828	1.409	0.066183	-0.17357	5.5	-1.1324	0.18816	-0.00903	4.5	1	4.32
0.042	0.68087	0.72443	0.53445	0.65505	1.4059	0.066438	-0.17485	5.5	-1.1292	0.18797	-0.0092	4.5	1	4.29
0.044	0.69882	0.74277	0.55282	0.67225	1.4033	0.066663	-0.17619	5.5	-1.1259	0.18775	-0.00936	4.5	1	4.27

0.045	0.70822	0.75232	0.56222	0.68139	1.4021	0.066774	-0.17693	5.5	-1.1242	0.18764	-0.00944	4.5	1	4.25
0.046	0.71779	0.76202	0.57166	0.69076	1.4009	0.066891	-0.17769	5.5	-1.1224	0.18752	-0.00952	4.5	1	4.24
0.048	0.73574	0.78015	0.58888	0.70854	1.3991	0.067127	-0.1792	5.5	-1.1192	0.1873	-0.00968	4.5	1	4.22
0.05	0.75436	0.79905	0.60652	0.72726	1.3974	0.067357	-0.18082	5.5	-1.1159	0.18709	-0.00982	4.5	1	4.2
0.055	0.7996	0.8445	0.6477	0.7737	1.3947	0.067797	-0.1848	5.5	-1.1082	0.18655	-0.01012	4.5	1	4.15
0.06	0.84394	0.88884	0.68562	0.82067	1.3954	0.068591	-0.18858	5.5	-1.1009	0.18582	-0.01033	4.5	1	4.11
0.065	0.88655	0.93116	0.71941	0.86724	1.4004	0.070127	-0.19176	5.5	-1.0942	0.18485	-0.01048	4.5	1	4.08
0.067	0.9027	0.94711	0.73171	0.88526	1.4032	0.070895	-0.19291	5.5	-1.0918	0.18442	-0.01052	4.5	1	4.07
0.07	0.92652	0.97057	0.7494	0.91227	1.4082	0.072075	-0.19451	5.5	-1.0884	0.18369	-0.01056	4.5	1	4.06
0.075	0.96447	1.0077	0.77678	0.9563	1.4174	0.073549	-0.19665	5.5	-1.0831	0.18225	-0.01058	4.5	1	4.04
0.08	1.0003	1.0426	0.80161	0.99818	1.4261	0.073735	-0.19816	5.5	-1.0785	0.18052	-0.01056	4.5	1	4.02
0.085	1.034	1.0755	0.82423	1.0379	1.4322	0.07194	-0.19902	5.51	-1.0745	0.17856	-0.01051	4.5	1	4.03
0.09	1.0666	1.1076	0.84591	1.0762	1.435	0.068097	-0.19929	5.52	-1.0709	0.17643	-0.01042	4.5	1	4.07
0.095	1.0981	1.1385	0.86703	1.1127	1.4339	0.062327	-0.199	5.53	-1.0678	0.1742	-0.01032	4.5	1	4.1
0.1	1.1268	1.1669	0.8871	1.1454	1.4293	0.055231	-0.19838	5.54	-1.0652	0.17203	-0.0102	4.5	1	4.13
0.11	1.1785	1.2179	0.92702	1.203	1.411	0.037389	-0.19601	5.57	-1.0607	0.1677	-0.00996	4.5	1	4.19
0.12	1.223	1.2621	0.96616	1.2502	1.3831	0.016373	-0.19265	5.62	-1.0572	0.16352	-0.00972	4.5	1	4.24
0.13	1.2596	1.2986	1.0031	1.2869	1.3497	-0.00516	-0.18898	5.66	-1.0549	0.15982	-0.00948	4.5	1	4.29
0.133	1.2692	1.3082	1.0135	1.2961	1.3395	-0.01135	-0.18792	5.67	-1.0545	0.15882	-0.0094	4.5	1	4.3
0.14	1.2883	1.327	1.036	1.3137	1.3162	-0.02471	-0.18566	5.7	-1.0537	0.15672	-0.00923	4.5	1	4.34
0.15	1.3095	1.3481	1.0648	1.3324	1.2844	-0.04207	-0.18234	5.74	-1.0532	0.15401	-0.00898	4.5	1	4.39
0.16	1.3235	1.3615	1.0876	1.3437	1.2541	-0.05759	-0.17853	5.78	-1.0533	0.15158	-0.00873	4.5	1	4.44
0.17	1.3306	1.3679	1.104	1.3487	1.2244	-0.07186	-0.17421	5.82	-1.0541	0.14948	-0.00847	4.5	1	4.49
0.18	1.3327	1.3689	1.1149	1.3492	1.1941	-0.08564	-0.16939	5.85	-1.0556	0.14768	-0.00822	4.5	1	4.53
0.19	1.3307	1.3656	1.1208	1.3463	1.1635	-0.09888	-0.16404	5.89	-1.0579	0.14616	-0.00797	4.5	1	4.57
0.2	1.3255	1.359	1.122	1.3414	1.1349	-0.11096	-0.15852	5.92	-1.0607	0.14489	-0.00772	4.5	1	4.61
0.22	1.3091	1.3394	1.1133	1.3281	1.0823	-0.133	-0.14704	5.97	-1.067	0.14263	-0.00722	4.5	1	4.68
0.24	1.2881	1.315	1.0945	1.3132	1.0366	-0.15299	-0.13445	6.03	-1.0737	0.14035	-0.00675	4.5	1	4.75
0.25	1.2766	1.3017	1.0828	1.3052	1.0166	-0.16213	-0.12784	6.05	-1.0773	0.13925	-0.00652	4.5	1	4.78

0.26	1.2651	1.2886	1.071	1.2972	0.99932	-0.17041	-0.12115	6.07	-1.0808	0.13818	-0.00629	4.5	1	4.82
0.28	1.2429	1.2635	1.0476	1.2815	0.97282	-0.18463	-0.10714	6.11	-1.0879	0.13604	-0.00587	4.5	1	4.88
0.29	1.2324	1.2517	1.0363	1.2736	0.96348	-0.19057	-0.10011	6.12	-1.0913	0.13499	-0.00567	4.5	1	4.9
0.3	1.2217	1.2401	1.0246	1.2653	0.95676	-0.1959	-0.09286	6.14	-1.0948	0.13388	-0.00548	4.5	1	4.93
0.32	1.2007	1.2177	1.0011	1.2479	0.95004	-0.20454	-0.07892	6.16	-1.1013	0.13179	-0.00512	4.5	1	4.98
0.34	1.179	1.1955	0.97677	1.2286	0.94956	-0.21134	-0.06513	6.18	-1.1074	0.12984	-0.00481	4.5	1	5.03
0.35	1.1674	1.1836	0.9638	1.2177	0.95077	-0.21446	-0.05792	6.18	-1.1105	0.1289	-0.00466	4.5	1	5.06
0.36	1.1558	1.172	0.9512	1.2066	0.95278	-0.21716	-0.05104	6.19	-1.1133	0.12806	-0.00453	4.5	1	5.08
0.38	1.1305	1.1468	0.9244	1.1816	0.95899	-0.22214	-0.03676	6.19	-1.119	0.12647	-0.00428	4.5	1	5.12
0.4	1.1046	1.1214	0.89765	1.1552	0.96766	-0.22608	-0.02319	6.2	-1.1243	0.12512	-0.00405	4.5	1	5.16
0.42	1.0782	1.0955	0.87067	1.1276	0.97862	-0.22924	-0.01042	6.2	-1.1291	0.12389	-0.00385	4.5	1	5.2
0.44	1.0515	1.0697	0.84355	1.0995	0.99144	-0.23166	0.001168	6.2	-1.1337	0.12278	-0.00367	4.5	1	5.24
0.45	1.0376	1.0562	0.82941	1.0847	0.99876	-0.23263	0.006589	6.2	-1.1359	0.12227	-0.00359	4.5	1	5.25
0.46	1.0234	1.0426	0.81509	1.0696	1.0064	-0.2335	0.011871	6.2	-1.1381	0.12177	-0.00351	4.5	1	5.27
0.48	0.99719	1.0172	0.7886	1.0415	1.0215	-0.23464	0.020767	6.2	-1.142	0.12093	-0.00336	4.5	1	5.3
0.5	0.96991	0.99106	0.7615	1.012	1.0384	-0.23522	0.029119	6.2	-1.1459	0.12015	-0.00322	4.5	1	5.34
0.55	0.9048	0.9283	0.6984	0.9417	1.0833	-0.23449	0.046932	6.2	-1.1543	0.11847	-0.0029	4.5	1	5.41
0.6	0.84165	0.86715	0.63875	0.87351	1.1336	-0.23128	0.062667	6.2	-1.1615	0.11671	-0.00261	4.5	1	5.48
0.65	0.78181	0.80876	0.58231	0.80948	1.1861	-0.22666	0.077997	6.2	-1.1676	0.11465	-0.00236	4.5	1	5.53
0.667	0.76262	0.78994	0.56422	0.78916	1.2035	-0.22497	0.083058	6.2	-1.1694	0.11394	-0.00228	4.5	1	5.54
0.7	0.72513	0.75302	0.52878	0.74985	1.2375	-0.22143	0.093185	6.2	-1.1728	0.11253	-0.00213	4.5	1	5.56
0.75	0.66903	0.69737	0.47523	0.69173	1.2871	-0.21591	0.10829	6.2	-1.1777	0.11054	-0.00193	4.5	1	5.6
0.8	0.61346	0.64196	0.42173	0.63519	1.3341	-0.21047	0.12256	6.2	-1.1819	0.10873	-0.00175	4.5	1	5.63
0.85	0.55853	0.58698	0.36813	0.57969	1.378	-0.20528	0.13608	6.2	-1.1854	0.10709	-0.0016	4.5	1	5.66
0.9	0.50296	0.53136	0.31376	0.52361	1.4208	-0.20011	0.14983	6.2	-1.1884	0.10548	-0.00146	4.5	1	5.69
0.95	0.44701	0.47541	0.25919	0.46706	1.4623	-0.1949	0.16432	6.2	-1.1909	0.10389	-0.00133	4.5	1	5.72
1	0.3932	0.4218	0.207	0.4124	1.5004	-0.18983	0.17895	6.2	-1.193	0.10248	-0.00121	4.5	1	5.74
1.1	0.28484	0.31374	0.10182	0.30209	1.569	-0.18001	0.21042	6.2	-1.1966	0.10016	-0.00099	4.5	1	5.82
1.2	0.1734	0.20259	-0.0062	0.18866	1.6282	-0.1709	0.2441	6.2	-1.1996	0.098482	-0.0008	4.5	1	5.92

1.3	0.06152	0.09106	-0.11345	0.07433	1.6794	-0.16233	0.27799	6.2	-1.2018	0.097375	-0.00064	4.5	1	6.01
1.4	-0.04575	-0.0157	-0.2155	-0.03607	1.7239	-0.15413	0.30956	6.2	-1.2039	0.096743	-0.00049	4.5	1	6.1
1.5	-0.14954	-0.11866	-0.3138	-0.1437	1.7622	-0.1467	0.33896	6.2	-1.2063	0.096445	-0.00037	4.5	1	6.18
1.6	-0.2486	-0.21672	-0.40682	-0.24708	1.7955	-0.13997	0.36616	6.2	-1.2086	0.096338	-0.00026	4.5	1	6.26
1.7	-0.34145	-0.3084	-0.49295	-0.34465	1.8259	-0.13361	0.39065	6.2	-1.2106	0.096254	-0.00017	4.5	1	6.33
1.8	-0.42975	-0.39558	-0.57388	-0.43818	1.8564	-0.12686	0.41244	6.2	-1.2123	0.096207	-9.9E-05	4.5	1	6.4
1.9	-0.51276	-0.47731	-0.64899	-0.52682	1.8868	-0.11959	0.43151	6.2	-1.2141	0.096255	-4.2E-05	4.5	1	6.48
2	-0.58669	-0.55003	-0.71466	-0.60658	1.9152	-0.11237	0.44788	6.2	-1.2159	0.096361	0	4.5	1	6.54
2.2	-0.72143	-0.6822	-0.83003	-0.75402	1.9681	-0.09802	0.48024	6.2	-1.219	0.096497	0	4.5	1	6.66
2.4	-0.8481	-0.8069	-0.9326	-0.8941	2.017	-0.08377	0.51873	6.2	-1.2202	0.096198	0	4.5	1	6.73
2.5	-0.90966	-0.86765	-0.98228	-0.96187	2.0406	-0.07631	0.53883	6.2	-1.2201	0.096106	0	4.5	1	6.77
2.6	-0.96863	-0.92577	-1.0313	-1.0266	2.0628	-0.06893	0.5581	6.2	-1.2198	0.096136	0	4.5	1	6.81
2.8	-1.0817	-1.0367	-1.1301	-1.1495	2.1014	-0.05523	0.59394	6.2	-1.2189	0.096667	0	4.5	1	6.87
3	-1.1898	-1.142	-1.23	-1.2664	2.1323	-0.04332	0.62694	6.2	-1.2179	0.097638	0	4.5	1	6.93
3.2	-1.2914	-1.2406	-1.3255	-1.376	2.1545	-0.03444	0.65811	6.2	-1.2169	0.098649	-2.3E-05	4.5	1	6.99
3.4	-1.386	-1.3322	-1.415	-1.4786	2.1704	-0.02789	0.68755	6.2	-1.216	0.099553	-0.00004	4.5	1	7.08
3.5	-1.4332	-1.3778	-1.4599	-1.5297	2.1775	-0.025	0.70216	6.2	-1.2156	0.099989	-4.5E-05	4.5	1	7.12
3.6	-1.4762	-1.4193	-1.5014	-1.5764	2.1834	-0.02258	0.71523	6.2	-1.2156	0.10043	-4.9E-05	4.5	1	7.16
3.8	-1.5617	-1.5014	-1.5865	-1.6685	2.1938	-0.01836	0.74028	6.2	-1.2158	0.10142	-5.3E-05	4.5	1	7.24
4	-1.6388	-1.5748	-1.6673	-1.7516	2.204	-0.01464	0.76303	6.2	-1.2162	0.10218	-5.2E-05	4.5	1	7.32
4.2	-1.7116	-1.6439	-1.7451	-1.829	2.2123	-0.01225	0.78552	6.2	-1.2165	0.10269	-4.7E-05	4.5	1	7.39
4.4	-1.7798	-1.7089	-1.8192	-1.9011	2.2181	-0.01146	0.80792	6.2	-1.2169	0.10304	-3.9E-05	4.5	1	7.46
4.6	-1.8469	-1.7731	-1.8923	-1.9712	2.223	-0.01176	0.83126	6.2	-1.2175	0.10324	-2.7E-05	4.5	1	7.52
4.8	-1.9063	-1.8303	-1.9573	-2.0326	2.2268	-0.01288	0.8524	6.2	-1.2182	0.10337	-1.4E-05	4.5	1	7.64
5	-1.966	-1.8882	-2.0245	-2.0928	2.2299	-0.01486	0.87314	6.2	-1.2189	0.10353	0	4.5	1	7.78
5.5	-2.1051	-2.0232	-2.1908	-2.2288	2.2389	-0.0195	0.91466	6.2	-1.2204	0.1046	0	4.5	1	8.07
6	-2.2421	-2.1563	-2.3659	-2.3579	2.2377	-0.02638	0.9487	6.2	-1.2232	0.1075	0	4.5	1	8.48
6.5	-2.3686	-2.2785	-2.5322	-2.477	2.215	-0.03951	0.97643	6.2	-1.2299	0.11231	0	4.5	1	8.9
7	-2.4827	-2.3881	-2.6818	-2.5854	2.172	-0.05914	0.99757	6.2	-1.2408	0.11853	0	4.5	1	9.2

7.5	-2.5865	-2.4874	-2.8176	-2.6854	2.1187	-0.08161	1.0121	6.2	-1.2543	0.12507	0	4.5	1	9.48
8	-2.6861	-2.5829	-2.9438	-2.7823	2.0613	-0.10382	1.0232	6.2	-1.2688	0.13146	0	4.5	1	9.57
8.5	-2.782	-2.6752	-3.0597	-2.8776	2.0084	-0.12114	1.0335	6.2	-1.2839	0.13742	0	4.5	1	9.62
9	-2.8792	-2.7687	-3.1713	-2.9759	1.9605	-0.13407	1.0453	6.2	-1.2989	0.14294	0	4.5	1	9.66
9.5	-2.9769	-2.8634	-3.2785	-3.076	1.9189	-0.14364	1.0567	6.2	-1.313	0.14781	0	4.5	1	9.66
10	-3.0702	-2.9537	-3.3776	-3.1726	1.8837	-0.15096	1.0651	6.2	-1.3253	0.15183	0	4.5	1	9.66

BSSA13	***Anelastic attenuation***			***Linear site term***			***Nonlinear site term***				***Basin depth***	
Period(sec)	**Δc_3 (globalCATW)**	**Δc_3 (ChinaTurkey)**	**Δc_3 (ItalyJapan)**	**c**	**V_c (m/s)**	**V_{ref} (m/s)**	**f_1**	**f_3**	**f_4**	**f_5**	**f_6 (1/km)**	**f_7**
-1	0.00000	0.00435	-0.00033	-0.8050	950.00	760	0	0.1	-0.1000	-0.00844	-9.9	-9.9
0	0.00000	0.00286	-0.00255	-0.5150	925.00	760	0	0.1	-0.1500	-0.00701	-9.9	-9.9
0.01	0.00000	0.00282	-0.00244	-0.5257	930.00	760	0	0.1	-0.1483	-0.00701	-9.9	-9.9
0.02	0.00000	0.00278	-0.00234	-0.5362	967.50	760	0	0.1	-0.1471	-0.00728	-9.9	-9.9
0.022	0.00000	0.00276	-0.00229	-0.5403	964.23	760	0	0.1	-0.1477	-0.00732	-9.9	-9.9
0.025	0.00000	0.00275	-0.00225	-0.5410	961.65	760	0	0.1	-0.1496	-0.00736	-9.9	-9.9
0.029	0.00000	0.00276	-0.00221	-0.5391	959.61	760	0	0.1	-0.1525	-0.00737	-9.9	-9.9
0.03	0.00000	0.00276	-0.00217	-0.5399	959.71	760	0	0.1	-0.1549	-0.00735	-9.9	-9.9
0.032	0.00000	0.00277	-0.00212	-0.5394	956.83	760	0	0.1	-0.1574	-0.00731	-9.9	-9.9
0.035	0.00000	0.00278	-0.00210	-0.5358	955.39	760	0	0.1	-0.1607	-0.00721	-9.9	-9.9
0.036	0.00000	0.00280	-0.00207	-0.5315	954.35	760	0	0.1	-0.1641	-0.00717	-9.9	-9.9
0.04	0.00000	0.00282	-0.00205	-0.5264	953.91	760	0	0.1	-0.1678	-0.00698	-9.9	-9.9
0.042	0.00000	0.00285	-0.00203	-0.5209	954.10	760	0	0.1	-0.1715	-0.00687	-9.9	-9.9
0.044	0.00000	0.00287	-0.00202	-0.5142	955.15	760	0	0.1	-0.1760	-0.00677	-9.9	-9.9
0.045	0.00000	0.00290	-0.00200	-0.5067	957.18	760	0	0.1	-0.1810	-0.00672	-9.9	-9.9
0.046	0.00000	0.00292	-0.00199	-0.4991	960.17	760	0	0.1	-0.1862	-0.00667	-9.9	-9.9
0.048	0.00000	0.00294	-0.00199	-0.4916	963.44	760	0	0.1	-0.1915	-0.00656	-9.9	-9.9

0.05	0.00000	0.00296	-0.00199	-0.4850	967.06	760	0	0.1	-0.1963	-0.00647	-9.9	-9.9
0.055	0.00000	0.00296	-0.00200	-0.4788	970.75	760	0	0.1	-0.2014	-0.00625	-9.9	-9.9
0.06	0.00000	0.00297	-0.00202	-0.4735	973.97	760	0	0.1	-0.2066	-0.00607	-9.9	-9.9
0.065	0.00000	0.00297	-0.00204	-0.4687	976.38	760	0	0.1	-0.2120	-0.00593	-9.9	-9.9
0.067	0.00000	0.00297	-0.00208	-0.4646	977.78	760	0	0.1	-0.2176	-0.00588	-9.9	-9.9
0.07	0.00000	0.00296	-0.00211	-0.4616	978.02	760	0	0.1	-0.2232	-0.00582	-9.9	-9.9
0.075	0.00000	0.00296	-0.00216	-0.4598	977.23	760	0	0.1	-0.2287	-0.00573	-9.9	-9.9
0.08	0.00000	0.00294	-0.00221	-0.4601	974.98	760	0	0.1	-0.2337	-0.00567	-9.9	-9.9
0.085	0.00000	0.00293	-0.00227	-0.4620	972.16	760	0	0.1	-0.2382	-0.00563	-9.9	-9.9
0.09	0.00000	0.00291	-0.00233	-0.4652	969.48	760	0	0.1	-0.2421	-0.00561	-9.9	-9.9
0.095	0.00000	0.00290	-0.00238	-0.4688	966.90	760	0	0.1	-0.2458	-0.00560	-9.9	-9.9
0.1	0.00000	0.00288	-0.00244	-0.4732	964.90	760	0	0.1	-0.2492	-0.00560	-9.9	-9.9
0.11	0.00000	0.00286	-0.00249	-0.4787	963.89	760	0	0.1	-0.2519	-0.00562	-9.9	-9.9
0.12	0.00000	0.00285	-0.00254	-0.4853	964.03	760	0	0.1	-0.2540	-0.00567	-9.9	-9.9
0.13	0.00000	0.00283	-0.00258	-0.4931	965.34	760	0	0.1	-0.2556	-0.00572	-9.9	-9.9
0.133	0.00000	0.00282	-0.00263	-0.5022	967.71	760	0	0.1	-0.2566	-0.00574	-9.9	-9.9
0.14	0.00000	0.00280	-0.00267	-0.5126	970.89	760	0	0.1	-0.2571	-0.00578	-9.9	-9.9
0.15	0.00000	0.00279	-0.00271	-0.5244	974.53	760	0	0.1	-0.2571	-0.00585	-9.9	-9.9
0.16	0.00000	0.00276	-0.00275	-0.5392	977.78	760	0	0.1	-0.2562	-0.00591	-9.9	-9.9
0.17	0.00000	0.00273	-0.00280	-0.5569	979.37	760	0	0.1	-0.2544	-0.00597	-9.9	-9.9
0.18	0.00000	0.00270	-0.00285	-0.5758	979.38	760	0	0.1	-0.2522	-0.00602	-9.9	-9.9
0.19	0.00000	0.00266	-0.00291	-0.5962	978.42	760	0	0.1	-0.2497	-0.00608	-9.9	-9.9
0.2	0.00000	0.00261	-0.00297	-0.6192	975.61	760	0	0.1	-0.2466	-0.00614	-9.9	-9.9
0.22	0.00000	0.00256	-0.00303	-0.6426	971.31	760	0	0.1	-0.2432	-0.00626	-9.9	-9.9
0.24	0.00000	0.00251	-0.00308	-0.6658	965.97	760	0	0.1	-0.2396	-0.00638	-9.9	-9.9
0.25	0.00000	0.00244	-0.00314	-0.6897	960.05	760	0	0.1	-0.2357	-0.00644	-9.9	-9.9
0.26	0.00000	0.00238	-0.00319	-0.7133	954.24	760	0	0.1	-0.2315	-0.00650	-9.9	-9.9
0.28	0.00000	0.00231	-0.00324	-0.7356	948.77	760	0	0.1	-0.2274	-0.00660	-9.9	-9.9
0.29	0.00000	0.00225	-0.00327	-0.7567	943.90	760	0	0.1	-0.2232	-0.00665	-9.9	-9.9

0.3	0.00000	0.00220	-0.00330	-0.7749	940.75	760	0	0.1	-0.2191	-0.00670	-9.9	-9.9
0.32	0.00000	0.00215	-0.00330	-0.7902	939.61	760	0	0.1	-0.2152	-0.00680	-9.9	-9.9
0.34	0.00000	0.00212	-0.00330	-0.8048	939.66	760	0	0.1	-0.2112	-0.00689	-9.9	-9.9
0.35	0.00000	0.00210	-0.00329	-0.8186	940.74	760	0	0.1	-0.2070	-0.00693	-9.9	-9.9
0.36	0.00000	0.00210	-0.00327	-0.8298	943.02	760	0	0.1	-0.2033	-0.00697	-9.9	-9.9
0.38	0.00000	0.00210	-0.00324	-0.8401	945.83	760	0	0.1	-0.1996	-0.00705	-9.9	-9.9
0.4	0.00000	0.00211	-0.00321	-0.8501	949.18	760	0	0.1	-0.1958	-0.00713	-9.9	-9.9
0.42	0.00000	0.00213	-0.00318	-0.8590	952.96	760	0	0.1	-0.1922	-0.00719	-9.9	-9.9
0.44	0.00000	0.00216	-0.00313	-0.8685	957.31	760	0	0.1	-0.1884	-0.00726	-9.9	-9.9
0.45	0.00000	0.00220	-0.00308	-0.8790	962.25	760	0	0.1	-0.1840	-0.00729	-9.9	-9.9
0.46	0.00000	0.00225	-0.00302	-0.8903	967.61	760	0	0.1	-0.1793	-0.00732	-9.9	-9.9
0.48	0.00000	0.00230	-0.00296	-0.9011	972.54	760	0	0.1	-0.1749	-0.00738	-9.9	-9.9
0.5	0.00000	0.00235	-0.00291	-0.9118	977.09	760	0	0.1	-0.1704	-0.00744	-9.9	-9.9
0.55	0.00000	0.00240	-0.00285	-0.9227	981.13	760	0	0.1	-0.1658	-0.00758	-9.9	-9.9
0.6	0.00000	0.00245	-0.00279	-0.9338	984.26	760	0	0.1	-0.1610	-0.00773	-9.9	-9.9
0.65	0.00000	0.00251	-0.00273	-0.9453	986.32	760	0	0.1	-0.1558	-0.00787	0.006	0.004
0.667	0.00000	0.00257	-0.00266	-0.9573	987.12	760	0	0.1	-0.1503	-0.00792	0.026	0.017
0.7	0.00000	0.00263	-0.00260	-0.9692	986.52	760	0	0.1	-0.1446	-0.00800	0.055	0.036
0.75	0.00000	0.00269	-0.00253	-0.9811	984.70	760	0	0.1	-0.1387	-0.00812	0.092	0.059
0.8	0.00000	0.00275	-0.00246	-0.9924	981.17	760	0	0.1	-0.1325	-0.00822	0.140	0.088
0.85	0.00000	0.00280	-0.00238	-1.0033	976.97	760	0	0.1	-0.1262	-0.00830	0.195	0.120
0.9	0.00000	0.00284	-0.00229	-1.0139	972.90	760	0	0.1	-0.1197	-0.00836	0.252	0.152
0.95	0.00000	0.00288	-0.00220	-1.0250	969.79	760	0	0.1	-0.1126	-0.00841	0.309	0.181
1	0.00000	0.00292	-0.00209	-1.0361	967.51	760	0	0.1	-0.1052	-0.00844	0.367	0.208
1.1	0.00000	0.00295	-0.00198	-1.0467	965.94	760	0	0.1	-0.0977	-0.00847	0.425	0.233
1.2	0.00000	0.00298	-0.00186	-1.0565	965.20	760	0	0.1	-0.0902	-0.00842	0.481	0.256
1.3	0.00000	0.00301	-0.00175	-1.0655	965.38	760	0	0.1	-0.0827	-0.00829	0.536	0.276
1.4	0.00000	0.00303	-0.00163	-1.0736	966.44	760	0	0.1	-0.0753	-0.00806	0.588	0.294
1.5	0.00000	0.00304	-0.00152	-1.0808	968.24	760	0	0.1	-0.0679	-0.00771	0.638	0.309

1.6	0.00000	0.00304	-0.00141	-1.0867	969.94	760	0	0.1	-0.0604	-0.00723	0.689	0.324
1.7	0.00000	0.00303	-0.00132	-1.0904	971.24	760	0	0.1	-0.0534	-0.00666	0.736	0.337
1.8	0.00000	0.00300	-0.00125	-1.0923	971.65	760	0	0.1	-0.0470	-0.00603	0.780	0.350
1.9	0.00000	0.00297	-0.00120	-1.0925	970.45	760	0	0.1	-0.0414	-0.00540	0.824	0.364
2	0.00000	0.00292	-0.00117	-1.0908	966.44	760	0	0.1	-0.0361	-0.00479	0.871	0.382
2.2	0.00000	0.00287	-0.00116	-1.0872	959.61	760	0	0.1	-0.0314	-0.00378	0.920	0.404
2.4	0.00000	0.00281	-0.00115	-1.0819	950.34	760	0	0.1	-0.0271	-0.00302	0.969	0.427
2.5	0.00000	0.00276	-0.00116	-1.0753	939.03	760	0	0.1	-0.0231	-0.00272	1.017	0.451
2.6	0.00000	0.00271	-0.00117	-1.0682	926.85	760	0	0.1	-0.0196	-0.00246	1.060	0.474
2.8	0.00000	0.00266	-0.00118	-1.0605	914.07	760	0	0.1	-0.0165	-0.00208	1.099	0.495
3	0.00000	0.00262	-0.00119	-1.0521	900.07	760	0	0.1	-0.0136	-0.00183	1.135	0.516
3.2	0.00000	0.00259	-0.00119	-1.0435	885.63	760	0	0.1	-0.0112	-0.00167	1.164	0.534
3.4	0.00000	0.00258	-0.00119	-1.0350	871.15	760	0	0.1	-0.0093	-0.00158	1.188	0.551
3.5	0.00000	0.00257	-0.00117	-1.0265	856.21	760	0	0.1	-0.0075	-0.00155	1.211	0.570
3.6	0.00000	0.00257	-0.00115	-1.0180	840.97	760	0	0.1	-0.0058	-0.00154	1.234	0.589
3.8	0.00000	0.00259	-0.00112	-1.0101	826.47	760	0	0.1	-0.0044	-0.00152	1.253	0.609
4	0.00000	0.00261	-0.00108	-1.0028	812.92	760	0	0.1	-0.0032	-0.00152	1.271	0.629
4.2	0.00000	0.00262	-0.00102	-0.9949	799.72	760	0	0.1	-0.0023	-0.00152	1.287	0.652
4.4	0.00000	0.00262	-0.00095	-0.9859	787.55	760	0	0.1	-0.0016	-0.00150	1.300	0.674
4.6	0.00000	0.00262	-0.00084	-0.9748	776.05	760	0	0.1	-0.0010	-0.00148	1.312	0.697
4.8	0.00000	0.00262	-0.00072	-0.9613	765.55	760	0	0.1	-0.0006	-0.00146	1.323	0.719
5	0.00000	0.00260	-0.00057	-0.9456	756.97	760	0	0.1	-0.0003	-0.00144	1.329	0.738
5.5	0.00000	0.00259	-0.00041	-0.9273	735.74	760	0	0.1	-0.0001	-0.00140	1.345	0.778
6	0.00000	0.00258	-0.00023	-0.9063	728.14	760	0	0.1	0.0000	-0.00138	1.350	0.803
6.5	0.00000	0.00259	-0.00004	-0.8822	726.30	760	0	0.1	0.0000	-0.00137	1.349	0.815
7	0.00000	0.00260	0.00017	-0.8551	728.24	760	0	0.1	0.0000	-0.00137	1.342	0.816
7.5	0.00000	0.00260	0.00038	-0.8249	731.96	760	0	0.1	-0.0001	-0.00137	1.329	0.809
8	0.00000	0.00263	0.00072	-0.7990	735.81	760	0	0.1	0.0001	-0.00137	1.308	0.795
8.5	0.00000	0.00267	0.00094	-0.7620	739.50	760	0	0.1	0.0001	-0.00137	1.282	0.777

9	0.00000	0.00276	0.00113	-0.7230	743.07	760	0	0.1	0.0001	-0.00137	1.252	0.754
9.5	0.00000	0.00289	0.00131	-0.6840	746.55	760	0	0.1	0.0001	-0.00136	1.218	0.729
10	0.00000	0.00303	0.00149	-0.6440	750.00	760	0	0.1	0.0000	-0.00136	1.183	0.703

BSSA13	***Aleatory Uncertainty***									
Period (sec)	**R_1 (km)**	**R_2 (km)**	**$\Delta\phi_R$**	**$\Delta\phi_V$**	**V_1 (m/s)**	**V_2 (m/s)**	**ϕ_1**	**ϕ_2**	**τ_1**	**τ_2**
-1	105.00	272.00	0.082	0.068	225	300	0.644	0.552	0.401	0.346
0	110.00	270.00	0.100	0.084	225	300	0.695	0.495	0.398	0.348
0.01	111.67	270.00	0.096	0.079	225	300	0.698	0.499	0.402	0.345
0.02	113.10	270.00	0.092	0.079	225	300	0.702	0.502	0.409	0.346
0.022	113.37	270.00	0.088	0.080	225	300	0.707	0.505	0.418	0.349
0.025	113.07	270.00	0.086	0.081	225	300	0.711	0.508	0.427	0.354
0.029	112.36	270.00	0.084	0.081	225	300	0.716	0.510	0.436	0.359
0.03	112.13	270.00	0.081	0.082	225	300	0.721	0.514	0.445	0.364
0.032	111.65	270.00	0.078	0.082	225	300	0.726	0.516	0.454	0.369
0.035	110.64	270.00	0.077	0.083	225	300	0.730	0.518	0.462	0.374
0.036	109.53	270.00	0.075	0.083	225	300	0.734	0.520	0.470	0.379
0.04	108.28	270.00	0.073	0.084	225	300	0.738	0.521	0.478	0.384
0.042	106.99	270.00	0.072	0.083	225	300	0.742	0.523	0.484	0.390
0.044	105.41	270.00	0.070	0.083	225	300	0.745	0.525	0.490	0.397
0.045	103.61	270.00	0.069	0.082	225	300	0.748	0.527	0.496	0.405
0.046	101.70	270.00	0.067	0.081	225	300	0.750	0.529	0.499	0.412
0.048	99.76	270.00	0.065	0.079	225	300	0.752	0.530	0.502	0.419
0.05	97.93	270.00	0.063	0.077	225	300	0.753	0.532	0.503	0.426
0.055	96.03	270.00	0.062	0.075	225	300	0.753	0.534	0.502	0.434
0.06	94.10	270.01	0.061	0.073	225	300	0.753	0.536	0.499	0.441

0.065	92.08	270.02	0.061	0.070	225	300	0.752	0.538	0.495	0.448
0.067	90.01	270.02	0.061	0.067	225	300	0.750	0.540	0.489	0.455
0.07	87.97	270.03	0.062	0.064	225	300	0.748	0.541	0.483	0.461
0.075	85.99	270.04	0.064	0.062	225	300	0.745	0.542	0.474	0.466
0.08	84.23	270.05	0.067	0.060	225	300	0.741	0.543	0.464	0.468
0.085	82.74	270.06	0.072	0.058	225	300	0.737	0.543	0.452	0.468
0.09	81.54	270.07	0.076	0.057	225	300	0.734	0.542	0.440	0.466
0.095	80.46	270.08	0.082	0.057	225	300	0.731	0.542	0.428	0.464
0.1	79.59	270.09	0.087	0.057	225	300	0.728	0.541	0.415	0.458
0.11	79.05	270.11	0.093	0.059	225	300	0.726	0.540	0.403	0.451
0.12	78.85	270.13	0.099	0.061	225	300	0.724	0.539	0.392	0.441
0.13	78.99	270.15	0.104	0.063	225	300	0.723	0.538	0.381	0.430
0.133	79.47	270.15	0.110	0.066	225	300	0.722	0.538	0.371	0.417
0.14	80.26	270.16	0.115	0.069	225	300	0.721	0.537	0.362	0.403
0.15	81.33	270.16	0.120	0.072	225	300	0.720	0.537	0.354	0.388
0.16	82.86	270.16	0.125	0.076	225	300	0.720	0.536	0.349	0.372
0.17	84.72	270.14	0.128	0.079	225	300	0.718	0.536	0.346	0.357
0.18	86.67	270.11	0.131	0.081	225	300	0.717	0.536	0.344	0.341
0.19	88.73	270.06	0.134	0.084	225	300	0.714	0.537	0.343	0.324
0.2	90.91	270.00	0.136	0.086	225	300	0.711	0.539	0.344	0.309
0.22	93.04	269.83	0.138	0.087	225	300	0.708	0.541	0.345	0.294
0.24	95.08	269.59	0.140	0.088	225	300	0.703	0.544	0.347	0.280
0.25	97.04	269.45	0.141	0.089	225	300	0.698	0.547	0.350	0.266
0.26	98.87	269.30	0.141	0.090	225	300	0.693	0.550	0.353	0.255
0.28	100.53	268.96	0.140	0.091	225	300	0.687	0.554	0.357	0.244
0.29	102.01	268.78	0.139	0.092	225	300	0.681	0.557	0.360	0.236
0.3	103.15	268.59	0.138	0.093	225	300	0.675	0.561	0.363	0.229
0.32	104.00	268.20	0.135	0.094	225	300	0.670	0.566	0.366	0.223
0.34	104.70	267.79	0.133	0.094	225	300	0.664	0.570	0.369	0.218

0.35	105.26	267.58	0.130	0.095	225	300	0.658	0.573	0.372	0.215
0.36	105.61	267.37	0.128	0.095	225	300	0.653	0.576	0.375	0.212
0.38	105.87	266.95	0.125	0.095	225	300	0.648	0.578	0.378	0.210
0.4	106.02	266.54	0.122	0.095	225	300	0.643	0.580	0.381	0.210
0.42	106.03	266.16	0.120	0.094	225	300	0.638	0.583	0.384	0.210
0.44	105.92	265.80	0.117	0.093	225	300	0.634	0.585	0.388	0.211
0.45	105.79	265.64	0.115	0.092	225	300	0.629	0.589	0.393	0.213
0.46	105.69	265.48	0.113	0.091	225	300	0.624	0.592	0.398	0.216
0.48	105.59	265.21	0.111	0.089	225	300	0.619	0.595	0.404	0.219
0.5	105.54	265.00	0.109	0.088	225	300	0.615	0.599	0.410	0.224
0.55	105.61	264.74	0.108	0.086	225	300	0.610	0.603	0.417	0.229
0.6	105.83	264.83	0.106	0.085	225	300	0.605	0.607	0.424	0.235
0.65	106.20	265.20	0.105	0.083	225	300	0.599	0.611	0.431	0.243
0.667	106.75	265.38	0.103	0.082	225	300	0.593	0.615	0.440	0.250
0.7	107.48	265.78	0.102	0.081	225	300	0.587	0.619	0.448	0.258
0.75	108.39	266.51	0.100	0.080	225	300	0.581	0.622	0.457	0.266
0.8	109.62	267.32	0.099	0.079	225	300	0.576	0.624	0.466	0.274
0.85	111.08	268.14	0.099	0.079	225	300	0.570	0.625	0.475	0.281
0.9	112.71	268.90	0.098	0.078	225	300	0.564	0.626	0.483	0.288
0.95	114.50	269.55	0.098	0.078	225	300	0.558	0.626	0.491	0.294
1	116.39	270.00	0.098	0.078	225	300	0.553	0.625	0.498	0.298
1.1	118.30	270.18	0.099	0.078	225	300	0.548	0.624	0.505	0.302
1.2	120.19	269.42	0.100	0.077	225	300	0.543	0.623	0.511	0.306
1.3	122.01	267.82	0.101	0.077	225	300	0.539	0.622	0.516	0.309
1.4	123.75	265.45	0.102	0.077	225	300	0.535	0.620	0.521	0.312
1.5	125.38	262.41	0.104	0.076	225	300	0.532	0.619	0.525	0.315
1.6	126.90	258.78	0.105	0.075	225	300	0.529	0.618	0.528	0.318
1.7	128.14	254.66	0.106	0.074	225	300	0.527	0.618	0.530	0.321
1.8	129.11	250.11	0.106	0.072	225	300	0.526	0.618	0.531	0.323

1.9	129.86	245.25	0.106	0.071	225	300	0.526	0.618	0.532	0.326
2	130.37	240.14	0.105	0.069	225	300	0.526	0.618	0.532	0.329
2.2	130.67	229.55	0.103	0.066	225	300	0.527	0.619	0.533	0.332
2.4	130.81	219.05	0.100	0.064	225	300	0.528	0.619	0.533	0.335
2.5	130.81	214.04	0.097	0.061	225	300	0.530	0.619	0.534	0.337
2.6	130.72	209.32	0.094	0.058	225	300	0.531	0.620	0.535	0.340
2.8	130.57	201.08	0.091	0.056	225	300	0.532	0.619	0.536	0.342
3	130.36	195.00	0.088	0.053	225	300	0.534	0.619	0.537	0.344
3.2	130.13	191.61	0.084	0.050	225	300	0.535	0.618	0.538	0.345
3.4	129.90	190.73	0.081	0.047	225	300	0.535	0.618	0.540	0.346
3.5	129.71	191.11	0.078	0.045	225	300	0.536	0.617	0.541	0.347
3.6	129.56	191.98	0.075	0.042	225	300	0.536	0.616	0.542	0.348
3.8	129.49	195.01	0.072	0.039	225	300	0.536	0.616	0.543	0.349
4	129.49	199.45	0.070	0.036	225	300	0.536	0.616	0.543	0.349
4.2	129.57	204.93	0.068	0.034	225	300	0.535	0.616	0.542	0.349
4.4	129.71	211.09	0.066	0.033	225	300	0.534	0.617	0.540	0.347
4.6	129.87	217.56	0.064	0.032	225	300	0.533	0.619	0.538	0.345
4.8	130.05	223.99	0.063	0.032	225	300	0.531	0.621	0.535	0.341
5	130.22	230.00	0.061	0.032	225	300	0.528	0.622	0.532	0.335
5.5	130.39	241.86	0.060	0.031	225	300	0.526	0.624	0.528	0.329
6	130.53	249.34	0.059	0.031	225	300	0.524	0.625	0.524	0.321
6.5	130.63	252.94	0.059	0.032	225	300	0.520	0.634	0.517	0.312
7	130.70	253.12	0.059	0.033	225	300	0.515	0.636	0.514	0.302
7.5	130.72	250.39	0.058	0.034	225	300	0.512	0.634	0.511	0.270
8	130.87	245.23	0.059	0.033	225	300	0.510	0.630	0.507	0.278
8.5	130.71	238.13	0.059	0.031	225	300	0.509	0.622	0.503	0.265
9	130.50	229.56	0.060	0.028	225	300	0.509	0.613	0.498	0.252
9.5	130.26	220.02	0.060	0.025	225	300	0.509	0.604	0.492	0.239
10	130.00	210.00	0.060	0.025	225	300	0.510	0.604	0.487	0.239

PEER REPORTS

PEER reports are available as a free PDF download from http://peer.berkeley.edu/publications/peer_reports_complete.html. Printed hard copies of PEER reports can be ordered directly from our printer by following the instructions at http://peer.berkeley.edu/publications/peer_reports.html. For other related questions about the PEER Report Series, contact the Pacific Earthquake Engineering Research Center, 325 Davis Hall mail code 1792, Berkeley, CA 94720. Tel.: (510) 642-3437; Fax: (510) 665-1655; Email: peer_editor@berkeley.edu

PEER 2013/05 *NGA-West2 Equations for Predicting Response Spectral Accelerations for Shallow Crustal Earthquakes.* David M. Boore, Jonathan P. Stewart, Emel Seyhan, Gail M. Atkinson. May 2013.

PEER 2013/04 *Update of the AS08 Ground-Motion Prediction Equations Based on the NGA-West2 Data Set.* Norman A. Abrahamson, Walter J. Silva, and Ronnie Kamai. May 2013.

PEER 2013/03 *PEER NGA-West2 Database.* Timothy D. Ancheta, Robert B. Darragh, Jonathan P. Stewart, Emel Seyhan, Walter J. Silva, Brian S.J. Chiou, Katie E. Wooddell, Robert W. Graves, Albert R. Kottke, David M. Boore, Tadahiro Kishida, and Jennifer L. Donahue. May 2013.

PEER 2013/02 *Hybrid Simulation of the Seismic Response of Squat Reinforced Concrete Shear Walls.* Catherine A. Whyte and Bozidar Stojadinovic. May 2013.

PEER 2013/01 *Housing Recovery in Chile: A Qualitative Mid-program Review.* Mary C. Comerio. February 2013.

PEER 2012/08 *Guidelines for Estimation of Shear Wave Velocity.* Bernard R. Wair, Jason T. DeJong, and Thomas Shantz. December 2012.

PEER 2012/07 *Earthquake Engineering for Resilient Communities: 2012 PEER Internship Program Research Report Collection.* Heidi Tremayne (Editor), Stephen A. Mahin (Editor), Collin Anderson, Dustin Cook, Michael Erceg, Carlos Esparza, Jose Jimenez, Dorian Krausz, Andrew Lo, Stephanie Lopez, Nicole McCurdy, Paul Shipman, Alexander Strum, Eduardo Vega. December 2012.

PEER 2012/06 *Fragilities for Precarious Rocks at Yucca Mountain.* Matthew D. Purvance, Rasool Anooshehpoor, and James N. Brune. December 2012.

PEER 2012/05 *Development of Simplified Analysis Procedure for Piles in Laterally Spreading Layered Soils.* Christopher R. McGann, Pedro Arduino, and Peter Mackenzie–Helnwein. December 2012.

PEER 2012/04 *Unbonded Pre-Tensioned Columns for Bridges in Seismic Regions.* Phillip M. Davis, Todd M. Janes, Marc O. Eberhard, and John F. Stanton. December 2012.

PEER 2012/03 *Experimental and Analytical Studies on Reinforced Concrete Buildings with Seismically Vulnerable Beam-Column Joints.* Sangjoon Park and Khalid M. Mosalam. October 2012.

PEER 2012/02 *Seismic Performance of Reinforced Concrete Bridges Allowed to Uplift during Multi-Directional Excitation.* Andres Oscar Espinoza and Stephen A. Mahin. July 2012.

PEER 2012/01 *Spectral Damping Scaling Factors for Shallow Crustal Earthquakes in Active Tectonic Regions.* Sanaz Rezaeian, Yousef Bozorgnia, I. M. Idriss, Kenneth Campbell, Norman Abrahamson, and Walter Silva. July 2012.

PEER 2011/10 *Earthquake Engineering for Resilient Communities: 2011 PEER Internship Program Research Report Collection.* Eds. Heidi Faison and Stephen A. Mahin. December 2011.

PEER 2011/09 *Calibration of Semi-Stochastic Procedure for Simulating High-Frequency Ground Motions.* Jonathan P. Stewart, Emel Seyhan, and Robert W. Graves. December 2011.

PEER 2011/08 *Water Supply in regard to Fire Following Earthquake.* Charles Scawthorn. November 2011.

PEER 2011/07 *Seismic Risk Management in Urban Areas. Proceedings of a U.S.-Iran-Turkey Seismic Workshop.* September 2011.

PEER 2011/06 *The Use of Base Isolation Systems to Achieve Complex Seismic Performance Objectives.* Troy A. Morgan and Stephen A. Mahin. July 2011.

PEER 2011/05 *Case Studies of the Seismic Performance of Tall Buildings Designed by Alternative Means.* Task 12 Report for the Tall Buildings Initiative. Jack Moehle, Yousef Bozorgnia, Nirmal Jayaram, Pierson Jones, Mohsen Rahnama, Nilesh Shome, Zeynep Tuna, John Wallace, Tony Yang, and Farzin Zareian. July 2011.

PEER 2011/04 *Recommended Design Practice for Pile Foundations in Laterally Spreading Ground.* Scott A. Ashford, Ross W. Boulanger, and Scott J. Brandenberg. June 2011.

PEER 2011/03 *New Ground Motion Selection Procedures and Selected Motions for the PEER Transportation Research Program.* Jack W. Baker, Ting Lin, Shrey K. Shahi, and Nirmal Jayaram. March 2011.

PEER 2011/02 *A Bayesian Network Methodology for Infrastructure Seismic Risk Assessment and Decision Support.* Michelle T. Bensi, Armen Der Kiureghian, and Daniel Straub. March 2011.

PEER 2011/01 *Demand Fragility Surfaces for Bridges in Liquefied and Laterally Spreading Ground.* Scott J. Brandenberg, Jian Zhang, Pirooz Kashighandi, Yili Huo, and Minxing Zhao. March 2011.

PEER 2010/05 *Guidelines for Performance-Based Seismic Design of Tall Buildings.* Developed by the Tall Buildings Initiative. November 2010.

PEER 2010/04 *Application Guide for the Design of Flexible and Rigid Bus Connections between Substation Equipment Subjected to Earthquakes.* Jean-Bernard Dastous and Armen Der Kiureghian. September 2010.

PEER 2010/03 *Shear Wave Velocity as a Statistical Function of Standard Penetration Test Resistance and Vertical Effective Stress at Caltrans Bridge Sites.* Scott J. Brandenberg, Naresh Bellana, and Thomas Shantz. June 2010.

PEER 2010/02 *Stochastic Modeling and Simulation of Ground Motions for Performance-Based Earthquake Engineering.* Sanaz Rezaeian and Armen Der Kiureghian. June 2010.

PEER 2010/01 *Structural Response and Cost Characterization of Bridge Construction Using Seismic Performance Enhancement Strategies.* Ady Aviram, Božidar Stojadinović, Gustavo J. Parra-Montesinos, and Kevin R. Mackie. March 2010.

PEER 2009/03 *The Integration of Experimental and Simulation Data in the Study of Reinforced Concrete Bridge Systems Including Soil-Foundation-Structure Interaction.* Matthew Dryden and Gregory L. Fenves. November 2009.

PEER 2009/02 *Improving Earthquake Mitigation through Innovations and Applications in Seismic Science, Engineering, Communication, and Response. Proceedings of a U.S.-Iran Seismic Workshop.* October 2009.

PEER 2009/01 *Evaluation of Ground Motion Selection and Modification Methods: Predicting Median Interstory Drift Response of Buildings.* Curt B. Haselton, Ed. June 2009.

PEER 2008/10 *Technical Manual for Strata.* Albert R. Kottke and Ellen M. Rathje. February 2009.

PEER 2008/09 *NGA Model for Average Horizontal Component of Peak Ground Motion and Response Spectra.* Brian S.-J. Chiou and Robert R. Youngs. November 2008.

PEER 2008/08 *Toward Earthquake-Resistant Design of Concentrically Braced Steel Structures.* Patxi Uriz and Stephen A. Mahin. November 2008.

PEER 2008/07 *Using OpenSees for Performance-Based Evaluation of Bridges on Liquefiable Soils.* Stephen L. Kramer, Pedro Arduino, and HyungSuk Shin. November 2008.

PEER 2008/06 *Shaking Table Tests and Numerical Investigation of Self-Centering Reinforced Concrete Bridge Columns.* Hyung IL Jeong, Junichi Sakai, and Stephen A. Mahin. September 2008.

PEER 2008/05 *Performance-Based Earthquake Engineering Design Evaluation Procedure for Bridge Foundations Undergoing Liquefaction-Induced Lateral Ground Displacement.* Christian A. Ledezma and Jonathan D. Bray. August 2008.

PEER 2008/04 *Benchmarking of Nonlinear Geotechnical Ground Response Analysis Procedures.* Jonathan P. Stewart, Annie On-Lei Kwok, Yousseff M. A. Hashash, Neven Matasovic, Robert Pyke, Zhiliang Wang, and Zhaohui Yang. August 2008.

PEER 2008/03 *Guidelines for Nonlinear Analysis of Bridge Structures in California.* Ady Aviram, Kevin R. Mackie, and Božidar Stojadinović. August 2008.

PEER 2008/02 *Treatment of Uncertainties in Seismic-Risk Analysis of Transportation Systems.* Evangelos Stergiou and Anne S. Kiremidjian. July 2008.

PEER 2008/01 *Seismic Performance Objectives for Tall Buildings.* William T. Holmes, Charles Kircher, William Petak, and Nabih Youssef. August 2008.

PEER 2007/12 *An Assessment to Benchmark the Seismic Performance of a Code-Conforming Reinforced Concrete Moment-Frame Building.* Curt Haselton, Christine A. Goulet, Judith Mitrani-Reiser, James L. Beck, Gregory G. Deierlein, Keith A. Porter, Jonathan P. Stewart, and Ertugrul Taciroglu. August 2008.

PEER 2007/11 *Bar Buckling in Reinforced Concrete Bridge Columns.* Wayne A. Brown, Dawn E. Lehman, and John F. Stanton. February 2008.

PEER 2007/10 *Computational Modeling of Progressive Collapse in Reinforced Concrete Frame Structures.* Mohamed M. Talaat and Khalid M. Mosalam. May 2008.

PEER 2007/09 *Integrated Probabilistic Performance-Based Evaluation of Benchmark Reinforced Concrete Bridges.* Kevin R. Mackie, John-Michael Wong, and Božidar Stojadinović. January 2008.

PEER 2007/08 *Assessing Seismic Collapse Safety of Modern Reinforced Concrete Moment-Frame Buildings.* Curt B. Haselton and Gregory G. Deierlein. February 2008.

PEER 2007/07 *Performance Modeling Strategies for Modern Reinforced Concrete Bridge Columns.* Michael P. Berry and Marc O. Eberhard. April 2008.

PEER 2007/06 *Development of Improved Procedures for Seismic Design of Buried and Partially Buried Structures.* Linda Al Atik and Nicholas Sitar. June 2007.

PEER 2007/05 *Uncertainty and Correlation in Seismic Risk Assessment of Transportation Systems.* Renee G. Lee and Anne S. Kiremidjian. July 2007.

PEER 2007/04 *Numerical Models for Analysis and Performance-Based Design of Shallow Foundations Subjected to Seismic Loading.* Sivapalan Gajan, Tara C. Hutchinson, Bruce L. Kutter, Prishati Raychowdhury, José A. Ugalde, and Jonathan P. Stewart. May 2008.

PEER 2007/03 *Beam-Column Element Model Calibrated for Predicting Flexural Response Leading to Global Collapse of RC Frame Buildings.* Curt B. Haselton, Abbie B. Liel, Sarah Taylor Lange, and Gregory G. Deierlein. May 2008.

PEER 2007/02 *Campbell-Bozorgnia NGA Ground Motion Relations for the Geometric Mean Horizontal Component of Peak and Spectral Ground Motion Parameters.* Kenneth W. Campbell and Yousef Bozorgnia. May 2007.

PEER 2007/01 *Boore-Atkinson NGA Ground Motion Relations for the Geometric Mean Horizontal Component of Peak and Spectral Ground Motion Parameters.* David M. Boore and Gail M. Atkinson. May. May 2007.

PEER 2006/12 *Societal Implications of Performance-Based Earthquake Engineering.* Peter J. May. May 2007.

PEER 2006/11 *Probabilistic Seismic Demand Analysis Using Advanced Ground Motion Intensity Measures, Attenuation Relationships, and Near-Fault Effects.* Polsak Tothong and C. Allin Cornell. March 2007.

PEER 2006/10 *Application of the PEER PBEE Methodology to the I-880 Viaduct.* Sashi Kunnath. February 2007.

PEER 2006/09 *Quantifying Economic Losses from Travel Forgone Following a Large Metropolitan Earthquake.* James Moore, Sungbin Cho, Yue Yue Fan, and Stuart Werner. November 2006.

PEER 2006/08 *Vector-Valued Ground Motion Intensity Measures for Probabilistic Seismic Demand Analysis.* Jack W. Baker and C. Allin Cornell. October 2006.

PEER 2006/07 *Analytical Modeling of Reinforced Concrete Walls for Predicting Flexural and Coupled–Shear-Flexural Responses.* Kutay Orakcal, Leonardo M. Massone, and John W. Wallace. October 2006.

PEER 2006/06 *Nonlinear Analysis of a Soil-Drilled Pier System under Static and Dynamic Axial Loading.* Gang Wang and Nicholas Sitar. November 2006.

PEER 2006/05 *Advanced Seismic Assessment Guidelines.* Paolo Bazzurro, C. Allin Cornell, Charles Menun, Maziar Motahari, and Nicolas Luco. September 2006.

PEER 2006/04 *Probabilistic Seismic Evaluation of Reinforced Concrete Structural Components and Systems.* Tae Hyung Lee and Khalid M. Mosalam. August 2006.

PEER 2006/03 *Performance of Lifelines Subjected to Lateral Spreading.* Scott A. Ashford and Teerawut Juirnarongrit. July 2006.

PEER 2006/02 *Pacific Earthquake Engineering Research Center Highway Demonstration Project.* Anne Kiremidjian, James Moore, Yue Yue Fan, Nesrin Basoz, Ozgur Yazali, and Meredith Williams. April 2006.

PEER 2006/01 *Bracing Berkeley. A Guide to Seismic Safety on the UC Berkeley Campus.* Mary C. Comerio, Stephen Tobriner, and Ariane Fehrenkamp. January 2006.

PEER 2005/16 *Seismic Response and Reliability of Electrical Substation Equipment and Systems.* Junho Song, Armen Der Kiureghian, and Jerome L. Sackman. April 2006.

PEER 2005/15 *CPT-Based Probabilistic Assessment of Seismic Soil Liquefaction Initiation.* R. E. S. Moss, R. B. Seed, R. E. Kayen, J. P. Stewart, and A. Der Kiureghian. April 2006.

PEER 2005/14 *Workshop on Modeling of Nonlinear Cyclic Load-Deformation Behavior of Shallow Foundations.* Bruce L. Kutter, Geoffrey Martin, Tara Hutchinson, Chad Harden, Sivapalan Gajan, and Justin Phalen. March 2006.

PEER 2005/13 *Stochastic Characterization and Decision Bases under Time-Dependent Aftershock Risk in Performance-Based Earthquake Engineering.* Gee Liek Yeo and C. Allin Cornell. July 2005.

PEER 2005/12 *PEER Testbed Study on a Laboratory Building: Exercising Seismic Performance Assessment.* Mary C. Comerio, editor. November 2005.

PEER 2005/11 *Van Nuys Hotel Building Testbed Report: Exercising Seismic Performance Assessment.* Helmut Krawinkler, editor. October 2005.

PEER 2005/10 *First NEES/E-Defense Workshop on Collapse Simulation of Reinforced Concrete Building Structures.* September 2005.

PEER 2005/09 *Test Applications of Advanced Seismic Assessment Guidelines.* Joe Maffei, Karl Telleen, Danya Mohr, William Holmes, and Yuki Nakayama. August 2006.

PEER 2005/08 *Damage Accumulation in Lightly Confined Reinforced Concrete Bridge Columns.* R. Tyler Ranf, Jared M. Nelson, Zach Price, Marc O. Eberhard, and John F. Stanton. April 2006.

PEER 2005/07 *Experimental and Analytical Studies on the Seismic Response of Freestanding and Anchored Laboratory Equipment.* Dimitrios Konstantinidis and Nicos Makris. January 2005.

PEER 2005/06 *Global Collapse of Frame Structures under Seismic Excitations*. Luis F. Ibarra and Helmut Krawinkler. September 2005.

PEER 2005//05 *Performance Characterization of Bench- and Shelf-Mounted Equipment.* Samit Ray Chaudhuri and Tara C. Hutchinson. May 2006.

PEER 2005/04 *Numerical Modeling of the Nonlinear Cyclic Response of Shallow Foundations.* Chad Harden, Tara Hutchinson, Geoffrey R. Martin, and Bruce L. Kutter. August 2005.

PEER 2005/03 *A Taxonomy of Building Components for Performance-Based Earthquake Engineering.* Keith A. Porter. September 2005.

PEER 2005/02 *Fragility Basis for California Highway Overpass Bridge Seismic Decision Making*. Kevin R. Mackie and Božidar Stojadinović. June 2005.

PEER 2005/01 *Empirical Characterization of Site Conditions on Strong Ground Motion.* Jonathan P. Stewart, Yoojoong Choi, and Robert W. Graves. June 2005.

PEER 2004/09 *Electrical Substation Equipment Interaction: Experimental Rigid Conductor Studies.* Christopher Stearns and André Filiatrault. February 2005.

PEER 2004/08 *Seismic Qualification and Fragility Testing of Line Break 550-kV Disconnect Switches.* Shakhzod M. Takhirov, Gregory L. Fenves, and Eric Fujisaki. January 2005.

PEER 2004/07 *Ground Motions for Earthquake Simulator Qualification of Electrical Substation Equipment.* Shakhzod M. Takhirov, Gregory L. Fenves, Eric Fujisaki, and Don Clyde. January 2005.

PEER 2004/06 *Performance-Based Regulation and Regulatory Regimes.* Peter J. May and Chris Koski. September 2004.

PEER 2004/05 *Performance-Based Seismic Design Concepts and Implementation: Proceedings of an International Workshop.* Peter Fajfar and Helmut Krawinkler, editors. September 2004.

PEER 2004/04 *Seismic Performance of an Instrumented Tilt-up Wall Building.* James C. Anderson and Vitelmo V. Bertero. July 2004.

PEER 2004/03 *Evaluation and Application of Concrete Tilt-up Assessment Methodologies.* Timothy Graf and James O. Malley. October 2004.

PEER 2004/02 *Analytical Investigations of New Methods for Reducing Residual Displacements of Reinforced Concrete Bridge Columns.* Junichi Sakai and Stephen A. Mahin. August 2004.

PEER 2004/01 *Seismic Performance of Masonry Buildings and Design Implications.* Kerri Anne Taeko Tokoro, James C. Anderson, and Vitelmo V. Bertero. February 2004.

PEER 2003/18 *Performance Models for Flexural Damage in Reinforced Concrete Columns.* Michael Berry and Marc Eberhard. August 2003.

PEER 2003/17 *Predicting Earthquake Damage in Older Reinforced Concrete Beam-Column Joints.* Catherine Pagni and Laura Lowes. October 2004.

PEER 2003/16 *Seismic Demands for Performance-Based Design of Bridges.* Kevin Mackie and Božidar Stojadinović. August 2003.

PEER 2003/15 *Seismic Demands for Nondeteriorating Frame Structures and Their Dependence on Ground Motions.* Ricardo Antonio Medina and Helmut Krawinkler. May 2004.

PEER 2003/14 *Finite Element Reliability and Sensitivity Methods for Performance-Based Earthquake Engineering.* Terje Haukaas and Armen Der Kiureghian. April 2004.

PEER 2003/13 *Effects of Connection Hysteretic Degradation on the Seismic Behavior of Steel Moment-Resisting Frames.* Janise E. Rodgers and Stephen A. Mahin. March 2004.

PEER 2003/12 *Implementation Manual for the Seismic Protection of Laboratory Contents: Format and Case Studies.* William T. Holmes and Mary C. Comerio. October 2003.

PEER 2003/11 *Fifth U.S.-Japan Workshop on Performance-Based Earthquake Engineering Methodology for Reinforced Concrete Building Structures.* February 2004.

PEER 2003/10 *A Beam-Column Joint Model for Simulating the Earthquake Response of Reinforced Concrete Frames.* Laura N. Lowes, Nilanjan Mitra, and Arash Altoontash. February 2004.

PEER 2003/09 *Sequencing Repairs after an Earthquake: An Economic Approach.* Marco Casari and Simon J. Wilkie. April 2004.

PEER 2003/08 *A Technical Framework for Probability-Based Demand and Capacity Factor Design (DCFD) Seismic Formats*. Fatemeh Jalayer and C. Allin Cornell. November 2003.

PEER 2003/07 *Uncertainty Specification and Propagation for Loss Estimation Using FOSM Methods.* Jack W. Baker and C. Allin Cornell. September 2003.

PEER 2003/06 *Performance of Circular Reinforced Concrete Bridge Columns under Bidirectional Earthquake Loading*. Mahmoud M. Hachem, Stephen A. Mahin, and Jack P. Moehle. February 2003.

PEER 2003/05 *Response Assessment for Building-Specific Loss Estimation.* Eduardo Miranda and Shahram Taghavi. September 2003.

PEER 2003/04 *Experimental Assessment of Columns with Short Lap Splices Subjected to Cyclic Loads.* Murat Melek, John W. Wallace, and Joel Conte. April 2003.

PEER 2003/03 *Probabilistic Response Assessment for Building-Specific Loss Estimation.* Eduardo Miranda and Hesameddin Aslani. September 2003.

PEER 2003/02 *Software Framework for Collaborative Development of Nonlinear Dynamic Analysis Program.* Jun Peng and Kincho H. Law. September 2003.

PEER 2003/01 *Shake Table Tests and Analytical Studies on the Gravity Load Collapse of Reinforced Concrete Frames.* Kenneth John Elwood and Jack P. Moehle. November 2003.

PEER 2002/24 *Performance of Beam to Column Bridge Joints Subjected to a Large Velocity Pulse.* Natalie Gibson, André Filiatrault, and Scott A. Ashford. April 2002.

PEER 2002/23 *Effects of Large Velocity Pulses on Reinforced Concrete Bridge Columns.* Greg L. Orozco and Scott A. Ashford. April 2002.

PEER 2002/22 *Characterization of Large Velocity Pulses for Laboratory Testing.* Kenneth E. Cox and Scott A. Ashford. April 2002.

PEER 2002/21 *Fourth U.S.-Japan Workshop on Performance-Based Earthquake Engineering Methodology for Reinforced Concrete Building Structures*. December 2002.

PEER 2002/20 *Barriers to Adoption and Implementation of PBEE Innovations.* Peter J. May. August 2002.

PEER 2002/19 *Economic-Engineered Integrated Models for Earthquakes: Socioeconomic Impacts.* Peter Gordon, James E. Moore II, and Harry W. Richardson. July 2002.

PEER 2002/18 *Assessment of Reinforced Concrete Building Exterior Joints with Substandard Details.* Chris P. Pantelides, Jon Hansen, Justin Nadauld, and Lawrence D. Reaveley. May 2002.

PEER 2002/17 *Structural Characterization and Seismic Response Analysis of a Highway Overcrossing Equipped with Elastomeric Bearings and Fluid Dampers: A Case Study.* Nicos Makris and Jian Zhang. November 2002.

PEER 2002/16 *Estimation of Uncertainty in Geotechnical Properties for Performance-Based Earthquake Engineering.* Allen L. Jones, Steven L. Kramer, and Pedro Arduino. December 2002.

PEER 2002/15 *Seismic Behavior of Bridge Columns Subjected to Various Loading Patterns.* Asadollah Esmaeily-Gh. and Yan Xiao. December 2002.

PEER 2002/14 *Inelastic Seismic Response of Extended Pile Shaft Supported Bridge Structures.* T.C. Hutchinson, R.W. Boulanger, Y.H. Chai, and I.M. Idriss. December 2002.

PEER 2002/13 *Probabilistic Models and Fragility Estimates for Bridge Components and Systems.* Paolo Gardoni, Armen Der Kiureghian, and Khalid M. Mosalam. June 2002.

PEER 2002/12 *Effects of Fault Dip and Slip Rake on Near-Source Ground Motions: Why Chi-Chi Was a Relatively Mild M7.6 Earthquake.* Brad T. Aagaard, John F. Hall, and Thomas H. Heaton. December 2002.

PEER 2002/11 *Analytical and Experimental Study of Fiber-Reinforced Strip Isolators*. James M. Kelly and Shakhzod M. Takhirov. September 2002.

PEER 2002/10 *Centrifuge Modeling of Settlement and Lateral Spreading with Comparisons to Numerical Analyses***.** Sivapalan Gajan and Bruce L. Kutter. January 2003.

PEER 2002/09 *Documentation and Analysis of Field Case Histories of Seismic Compression during the 1994 Northridge, California, Earthquake.* Jonathan P. Stewart, Patrick M. Smith, Daniel H. Whang, and Jonathan D. Bray. October 2002.

PEER 2002/08 *Component Testing, Stability Analysis and Characterization of Buckling-Restrained Unbonded Braces™.* Cameron Black, Nicos Makris, and Ian Aiken. September 2002.

PEER 2002/07 *Seismic Performance of Pile-Wharf Connections.* Charles W. Roeder, Robert Graff, Jennifer Soderstrom, and Jun Han Yoo. December 2001.

PEER 2002/06 *The Use of Benefit-Cost Analysis for Evaluation of Performance-Based Earthquake Engineering Decisions*. Richard O. Zerbe and Anthony Falit-Baiamonte. September 2001.

PEER 2002/05 *Guidelines, Specifications, and Seismic Performance Characterization of Nonstructural Building Components and Equipment*. André Filiatrault, Constantin Christopoulos, and Christopher Stearns. September 2001.

PEER 2002/04 *Consortium of Organizations for Strong-Motion Observation Systems and the Pacific Earthquake Engineering Research Center Lifelines Program: Invited Workshop on Archiving and Web Dissemination of Geotechnical Data, 4–5 October 2001*. September 2002.

PEER 2002/03 *Investigation of Sensitivity of Building Loss Estimates to Major Uncertain Variables for the Van Nuys Testbed.* Keith A. Porter, James L. Beck, and Rustem V. Shaikhutdinov. August 2002.

PEER 2002/02 *The Third U.S.-Japan Workshop on Performance-Based Earthquake Engineering Methodology for Reinforced Concrete Building Structures*. July 2002.

PEER 2002/01 *Nonstructural Loss Estimation: The UC Berkeley Case Study.* Mary C. Comerio and John C. Stallmeyer. December 2001.

PEER 2001/16 *Statistics of SDF-System Estimate of Roof Displacement for Pushover Analysis of Buildings.* Anil K. Chopra, Rakesh K. Goel, and Chatpan Chintanapakdee. December 2001.

PEER 2001/15 *Damage to Bridges during the 2001 Nisqually Earthquake.* R. Tyler Ranf, Marc O. Eberhard, and Michael P. Berry. November 2001.

PEER 2001/14 *Rocking Response of Equipment Anchored to a Base Foundation.* Nicos Makris and Cameron J. Black. September 2001.

PEER 2001/13 *Modeling Soil Liquefaction Hazards for Performance-Based Earthquake Engineering.* Steven L. Kramer and Ahmed-W. Elgamal. February 2001.

PEER 2001/12 *Development of Geotechnical Capabilities in OpenSees.* Boris Jeremić. September 2001.

PEER 2001/11 *Analytical and Experimental Study of Fiber-Reinforced Elastomeric Isolators*. James M. Kelly and Shakhzod M. Takhirov. September 2001.

PEER 2001/10 *Amplification Factors for Spectral Acceleration in Active Regions.* Jonathan P. Stewart, Andrew H. Liu, Yoojoong Choi, and Mehmet B. Baturay. December 2001.

PEER 2001/09 *Ground Motion Evaluation Procedures for Performance-Based Design.* Jonathan P. Stewart, Shyh-Jeng Chiou, Jonathan D. Bray, Robert W. Graves, Paul G. Somerville, and Norman A. Abrahamson. September 2001.

PEER 2001/08 *Experimental and Computational Evaluation of Reinforced Concrete Bridge Beam-Column Connections for Seismic Performance*. Clay J. Naito, Jack P. Moehle, and Khalid M. Mosalam. November 2001.

PEER 2001/07 *The Rocking Spectrum and the Shortcomings of Design Guidelines.* Nicos Makris and Dimitrios Konstantinidis. August 2001.

PEER 2001/06 *Development of an Electrical Substation Equipment Performance Database for Evaluation of Equipment Fragilities*. Thalia Agnanos. April 1999.

PEER 2001/05 *Stiffness Analysis of Fiber-Reinforced Elastomeric Isolators.* Hsiang-Chuan Tsai and James M. Kelly. May 2001.

PEER 2001/04 *Organizational and Societal Considerations for Performance-Based Earthquake Engineering.* Peter J. May. April 2001.

PEER 2001/03 *A Modal Pushover Analysis Procedure to Estimate Seismic Demands for Buildings: Theory and Preliminary Evaluation.* Anil K. Chopra and Rakesh K. Goel. January 2001.

PEER 2001/02 *Seismic Response Analysis of Highway Overcrossings Including Soil-Structure Interaction.* Jian Zhang and Nicos Makris. March 2001.

PEER 2001/01 *Experimental Study of Large Seismic Steel Beam-to-Column Connections.* Egor P. Popov and Shakhzod M. Takhirov. November 2000.

PEER 2000/10 *The Second U.S.-Japan Workshop on Performance-Based Earthquake Engineering Methodology for Reinforced Concrete Building Structures.* March 2000.

PEER 2000/09 *Structural Engineering Reconnaissance of the August 17, 1999 Earthquake: Kocaeli (Izmit), Turkey.* Halil Sezen, Kenneth J. Elwood, Andrew S. Whittaker, Khalid Mosalam, John J. Wallace, and John F. Stanton. December 2000.

PEER 2000/08 *Behavior of Reinforced Concrete Bridge Columns Having Varying Aspect Ratios and Varying Lengths of Confinement.* Anthony J. Calderone, Dawn E. Lehman, and Jack P. Moehle. January 2001.

PEER 2000/07 *Cover-Plate and Flange-Plate Reinforced Steel Moment-Resisting Connections.* Taejin Kim, Andrew S. Whittaker, Amir S. Gilani, Vitelmo V. Bertero, and Shakhzod M. Takhirov. September 2000.

PEER 2000/06 *Seismic Evaluation and Analysis of 230-kV Disconnect Switches.* Amir S. J. Gilani, Andrew S. Whittaker, Gregory L. Fenves, Chun-Hao Chen, Henry Ho, and Eric Fujisaki. July 2000.

PEER 2000/05 *Performance-Based Evaluation of Exterior Reinforced Concrete Building Joints for Seismic Excitation.* Chandra Clyde, Chris P. Pantelides, and Lawrence D. Reaveley. July 2000.

PEER 2000/04 *An Evaluation of Seismic Energy Demand: An Attenuation Approach.* Chung-Che Chou and Chia-Ming Uang. July 1999.

PEER 2000/03 *Framing Earthquake Retrofitting Decisions: The Case of Hillside Homes in Los Angeles.* Detlof von Winterfeldt, Nels Roselund, and Alicia Kitsuse. March 2000.

PEER 2000/02 *U.S.-Japan Workshop on the Effects of Near-Field Earthquake Shaking.* Andrew Whittaker, ed. July 2000.

PEER 2000/01 *Further Studies on Seismic Interaction in Interconnected Electrical Substation Equipment.* Armen Der Kiureghian, Kee-Jeung Hong, and Jerome L. Sackman. November 1999.

PEER 1999/14 *Seismic Evaluation and Retrofit of 230-kV Porcelain Transformer Bushings.* Amir S. Gilani, Andrew S. Whittaker, Gregory L. Fenves, and Eric Fujisaki. December 1999.

PEER 1999/13 *Building Vulnerability Studies: Modeling and Evaluation of Tilt-up and Steel Reinforced Concrete Buildings.* John W. Wallace, Jonathan P. Stewart, and Andrew S. Whittaker, editors. December 1999.

PEER 1999/12 *Rehabilitation of Nonductile RC Frame Building Using Encasement Plates and Energy-Dissipating Devices.* Mehrdad Sasani, Vitelmo V. Bertero, James C. Anderson. December 1999.

PEER 1999/11 *Performance Evaluation Database for Concrete Bridge Components and Systems under Simulated Seismic Loads.* Yael D. Hose and Frieder Seible. November 1999.

PEER 1999/10 *U.S.-Japan Workshop on Performance-Based Earthquake Engineering Methodology for Reinforced Concrete Building Structures.* December 1999.

PEER 1999/09 *Performance Improvement of Long Period Building Structures Subjected to Severe Pulse-Type Ground Motions.* James C. Anderson, Vitelmo V. Bertero, and Raul Bertero. October 1999.

PEER 1999/08 *Envelopes for Seismic Response Vectors.* Charles Menun and Armen Der Kiureghian. July 1999.

PEER 1999/07 *Documentation of Strengths and Weaknesses of Current Computer Analysis Methods for Seismic Performance of Reinforced Concrete Members.* William F. Cofer. November 1999.

PEER 1999/06 *Rocking Response and Overturning of Anchored Equipment under Seismic Excitations.* Nicos Makris and Jian Zhang. November 1999.

PEER 1999/05 *Seismic Evaluation of 550 kV Porcelain Transformer Bushings.* Amir S. Gilani, Andrew S. Whittaker, Gregory L. Fenves, and Eric Fujisaki. October 1999.

PEER 1999/04 *Adoption and Enforcement of Earthquake Risk-Reduction Measures.* Peter J. May, Raymond J. Burby, T. Jens Feeley, and Robert Wood.

PEER 1999/03 *Task 3 Characterization of Site Response General Site Categories.* Adrian Rodriguez-Marek, Jonathan D. Bray, and Norman Abrahamson. February 1999.

PEER 1999/02 *Capacity-Demand-Diagram Methods for Estimating Seismic Deformation of Inelastic Structures: SDF Systems.* Anil K. Chopra and Rakesh Goel. April 1999.

PEER 1999/01 *Interaction in Interconnected Electrical Substation Equipment Subjected to Earthquake Ground Motions.* Armen Der Kiureghian, Jerome L. Sackman, and Kee-Jeung Hong. February 1999.

PEER 1998/08 *Behavior and Failure Analysis of a Multiple-Frame Highway Bridge in the 1994 Northridge Earthquake.* Gregory L. Fenves and Michael Ellery. December 1998.

PEER 1998/07 *Empirical Evaluation of Inertial Soil-Structure Interaction Effects.* Jonathan P. Stewart, Raymond B. Seed, and Gregory L. Fenves. November 1998.

PEER 1998/06 *Effect of Damping Mechanisms on the Response of Seismic Isolated Structures.* Nicos Makris and Shih-Po Chang. November 1998.

PEER 1998/05 *Rocking Response and Overturning of Equipment under Horizontal Pulse-Type Motions.* Nicos Makris and Yiannis Roussos. October 1998.

PEER 1998/04 *Pacific Earthquake Engineering Research Invitational Workshop Proceedings, May 14–15, 1998: Defining the Links between Planning, Policy Analysis, Economics and Earthquake Engineering.* Mary Comerio and Peter Gordon. September 1998.

PEER 1998/03 *Repair/Upgrade Procedures for Welded Beam to Column Connections.* James C. Anderson and Xiaojing Duan. May 1998.

PEER 1998/02 *Seismic Evaluation of 196 kV Porcelain Transformer Bushings.* Amir S. Gilani, Juan W. Chavez, Gregory L. Fenves, and Andrew S. Whittaker. May 1998.

PEER 1998/01 *Seismic Performance of Well-Confined Concrete Bridge Columns.* Dawn E. Lehman and Jack P. Moehle. December 2000.

ONLINE PEER REPORTS

The following PEER reports are available by Internet only at http://peer.berkeley.edu/publications/peer_reports_complete.html.

PEER 2012/103 *Performance-Based Seismic Demand Assessment of Concentrically Braced Steel Frame Buildings.* Chui-Hsin Chen and Stephen A. Mahin. December 2012.

PEER 2012/102 *Procedure to Restart an Interrupted Hybrid Simulation: Addendum to PEER Report 2010/103.* Vesna Terzic and Bozidar Stojadinovic. October 2012.

PEER 2012/101 *Mechanics of Fiber Reinforced Bearings.* James M. Kelly and Andrea Calabrese. February 2012.

PEER 2011/107 *Nonlinear Site Response and Seismic Compression at Vertical Array Strongly Shaken by 2007 Niigata-ken Chuetsu-oki Earthquake.* Eric Yee, Jonathan P. Stewart, and Kohji Tokimatsu. December 2011.

PEER 2011/106 *Self Compacting Hybrid Fiber Reinforced Concrete Composites for Bridge Columns.* Pardeep Kumar, Gabriel Jen, William Trono, Marios Panagiotou, and Claudia Ostertag. September 2011.

PEER 2011/105 *Stochastic Dynamic Analysis of Bridges Subjected to Spacially Varying Ground Motions.* Katerina Konakli and Armen Der Kiureghian. August 2011.

PEER 2011/104 *Design and Instrumentation of the 2010 E-Defense Four-Story Reinforced Concrete and Post-Tensioned Concrete Buildings.* Takuya Nagae, Kenichi Tahara, Taizo Matsumori, Hitoshi Shiohara, Toshimi Kabeyasawa, Susumu Kono, Minehiro Nishiyama (Japanese Research Team) and John Wallace, Wassim Ghannoum, Jack Moehle, Richard Sause, Wesley Keller, Zeynep Tuna (U.S. Research Team). June 2011.

PEER 2011/103 *In-Situ Monitoring of the Force Output of Fluid Dampers: Experimental Investigation.* Dimitrios Konstantinidis, James M. Kelly, and Nicos Makris. April 2011.

PEER 2011/102 *Ground-motion prediction equations 1964 - 2010.* John Douglas. April 2011.

PEER 2011/101 *Report of the Eighth Planning Meeting of NEES/E-Defense Collaborative Research on Earthquake Engineering.* Convened by the Hyogo Earthquake Engineering Research Center (NIED), NEES Consortium, Inc. February 2011.

PEER 2010/111 *Modeling and Acceptance Criteria for Seismic Design and Analysis of Tall Buildings.* Task 7 Report for the Tall Buildings Initiative - Published jointly by the Applied Technology Council. October 2010.

PEER 2010/110 *Seismic Performance Assessment and Probabilistic Repair Cost Analysis of Precast Concrete Cladding Systems for Multistory Buildlings.* Jeffrey P. Hunt and Božidar Stojadinovic. November 2010.

PEER 2010/109 *Report of the Seventh Joint Planning Meeting of NEES/E-Defense Collaboration on Earthquake Engineering. Held at the E-Defense, Miki, and Shin-Kobe, Japan, September 18–19, 2009.* August 2010.

PEER 2010/108 *Probabilistic Tsunami Hazard in California.* Hong Kie Thio, Paul Somerville, and Jascha Polet, preparers. October 2010.

PEER 2010/107 *Performance and Reliability of Exposed Column Base Plate Connections for Steel Moment-Resisting Frames.* Ady Aviram, Božidar Stojadinovic, and Armen Der Kiureghian. August 2010.

PEER 2010/106 *Verification of Probabilistic Seismic Hazard Analysis Computer Programs.* Patricia Thomas, Ivan Wong, and Norman Abrahamson. May 2010.

PEER 2010/105 *Structural Engineering Reconnaissance of the April 6, 2009, Abruzzo, Italy, Earthquake, and Lessons Learned.* M. Selim Günay and Khalid M. Mosalam. April 2010.

PEER 2010/104 *Simulating the Inelastic Seismic Behavior of Steel Braced Frames, Including the Effects of Low-Cycle Fatigue.* Yuli Huang and Stephen A. Mahin. April 2010.

PEER 2010/103 *Post-Earthquake Traffic Capacity of Modern Bridges in California.* Vesna Terzic and Božidar Stojadinović. March 2010.

PEER 2010/102 *Analysis of Cumulative Absolute Velocity (CAV) and JMA Instrumental Seismic Intensity (I_{JMA}) Using the PEER–NGA Strong Motion Database.* Kenneth W. Campbell and Yousef Bozorgnia. February 2010.

PEER 2010/101 *Rocking Response of Bridges on Shallow Foundations.* Jose A. Ugalde, Bruce L. Kutter, and Boris Jeremic. April 2010.

PEER 2009/109 *Simulation and Performance-Based Earthquake Engineering Assessment of Self-Centering Post-Tensioned Concrete Bridge Systems.* Won K. Lee and Sarah L. Billington. December 2009.

PEER 2009/108 *PEER Lifelines Geotechnical Virtual Data Center.* J. Carl Stepp, Daniel J. Ponti, Loren L. Turner, Jennifer N. Swift, Sean Devlin, Yang Zhu, Jean Benoit, and John Bobbitt. September 2009.

PEER 2009/107 *Experimental and Computational Evaluation of Current and Innovative In-Span Hinge Details in Reinforced Concrete Box-Girder Bridges: Part 2: Post-Test Analysis and Design Recommendations.* Matias A. Hube and Khalid M. Mosalam. December 2009.

PEER 2009/106 *Shear Strength Models of Exterior Beam-Column Joints without Transverse Reinforcement.* Sangjoon Park and Khalid M. Mosalam. November 2009.

PEER 2009/105 *Reduced Uncertainty of Ground Motion Prediction Equations through Bayesian Variance Analysis.* Robb Eric S. Moss. November 2009.

PEER 2009/104 *Advanced Implementation of Hybrid Simulation.* Andreas H. Schellenberg, Stephen A. Mahin, Gregory L. Fenves. November 2009.

PEER 2009/103 *Performance Evaluation of Innovative Steel Braced Frames.* T. Y. Yang, Jack P. Moehle, and Božidar Stojadinovic. August 2009.

PEER 2009/102 *Reinvestigation of Liquefaction and Nonliquefaction Case Histories from the 1976 Tangshan Earthquake.* Robb Eric Moss, Robert E. Kayen, Liyuan Tong, Songyu Liu, Guojun Cai, and Jiaer Wu. August 2009.

PEER 2009/101 *Report of the First Joint Planning Meeting for the Second Phase of NEES/E-Defense Collaborative Research on Earthquake Engineering.* Stephen A. Mahin et al. July 2009.

PEER 2008/104 *Experimental and Analytical Study of the Seismic Performance of Retaining Structures.* Linda Al Atik and Nicholas Sitar. January 2009.

PEER 2008/103 *Experimental and Computational Evaluation of Current and Innovative In-Span Hinge Details in Reinforced Concrete Box-Girder Bridges. Part 1: Experimental Findings and Pre-Test Analysis.* Matias A. Hube and Khalid M. Mosalam. January 2009.

PEER 2008/102 *Modeling of Unreinforced Masonry Infill Walls Considering In-Plane and Out-of-Plane Interaction.* Stephen Kadysiewski and Khalid M. Mosalam. January 2009.

PEER 2008/101 *Seismic Performance Objectives for Tall Buildings.* William T. Holmes, Charles Kircher, William Petak, and Nabih Youssef. August 2008.

PEER 2007/101 *Generalized Hybrid Simulation Framework for Structural Systems Subjected to Seismic Loading.* Tarek Elkhoraibi and Khalid M. Mosalam. July 2007.

PEER 2007/100 *Seismic Evaluation of Reinforced Concrete Buildings Including Effects of Masonry Infill Walls.* Alidad Hashemi and Khalid M. Mosalam. July 2007.

The Pacific Earthquake Engineering Research Center (PEER) is a multi-institutional research and education center with headquarters at the University of California, Berkeley. Investigators from over 20 universities, several consulting companies, and researchers at various state and federal government agencies contribute to research programs focused on performance-based earthquake engineering.

These research programs aim to identify and reduce the risks from major earthquakes to life safety and to the economy by including research in a wide variety of disciplines including structural and geotechnical engineering, geology/seismology, lifelines, transportation, architecture, economics, risk management, and public policy.

PEER is supported by federal, state, local, and regional agencies, together with industry partners.

PEER Core Institutions:
University of California, Berkeley (Lead Institution)
California Institute of Technology
Oregon State University
Stanford University
University of California, Davis
University of California, Irvine
University of California, Los Angeles
University of California, San Diego
University of Southern California
University of Washington

PEER reports can be ordered at http://peer.berkeley.edu/publications/peer_reports.html or by contacting

Pacific Earthquake Engineering Research Center
University of California, Berkeley
325 Davis Hall, mail code 1792
Berkeley, CA 94720-1792
Tel: 510-642-3437
Fax: 510-642-1655
Email: peer_editor@berkeley.edu

ISSN 1547-0587X